Gastroenterology Research and Practice

Imaging in Gastroenterology

Guest Editors: Radu Badea, Iwona Sudoł-Szopińska, Sebastian Mueller, Horia Ştefănescu, and Monica Lupsor Platon

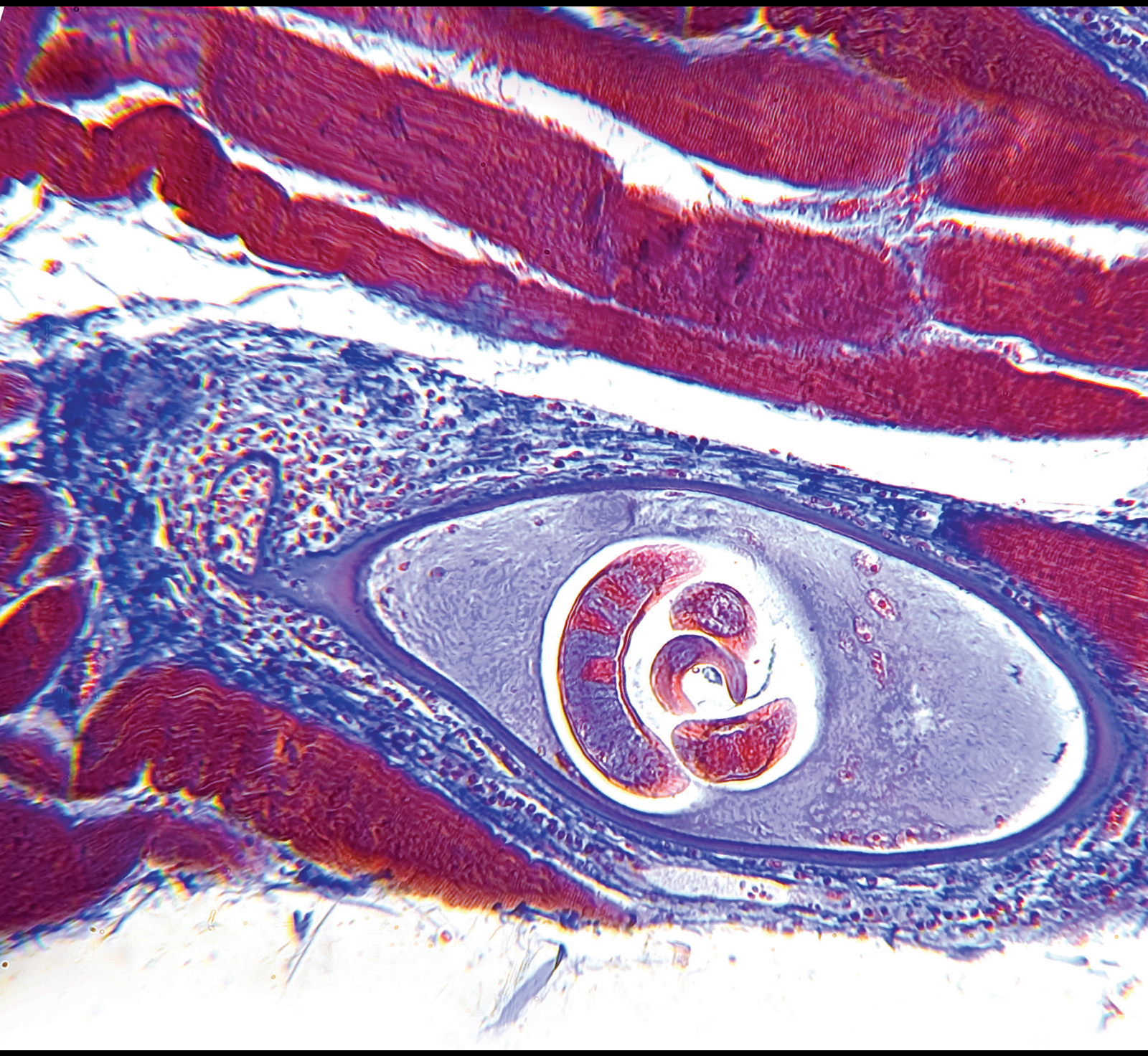

Imaging in Gastroenterology

Gastroenterology Research and Practice

Imaging in Gastroenterology

Guest Editors: Radu Badea, Iwona Sudoł-Szopińska,
Sebastian Mueller, Horia Ştefănescu,
and Monica Lupsor Platon

Copyright © 2014 Hindawi Publishing Corporation. All rights reserved.

This is a special issue published in "Gastroenterology Research and Practice." All articles are open access articles distributed under the Creative Commons Attribution License, which permits unrestricted use, distribution, and reproduction in any medium, provided the original work is properly cited.

Editorial Board

Firas H. Al-Kawas, USA
Gianfranco D. Alpini, USA
Akira Andoh, Japan
Everson Artifon, Brazil
Mala Banerjee, India
Ramón Bataller, Spain
Edmund J. Bini, USA
E. Björnssön, Sweden
Sedat Boyacioglu, Turkey
David A. A. Brenner, USA
Peter Bytzer, Denmark
Antoni Castells, Spain
Vito D. Corleto, Italy
Gianfranco F. Delle Fave, Italy
Cataldo Doria, USA
Peter V. Draganov, USA
R. Eliakim, Israel
Paul Enck, Germany
Maria Eugenicos, UK
D. Fan, China
Fabio Farinati, Italy
R. Fass, USA
Davide Festi, Italy
Alfred Gangl, Austria
Edoardo Giovanni Giannini, Italy
Paolo Gionchetti, Italy
Guillermo A. Gomez, USA
B. J. Hoffman, USA
Michel Kahaleh, USA
Vikram Kate, India
John Kellow, Australia
Spiros D. Ladas, Greece
Greger Lindberg, Sweden
Lawrence L. Lumeng, USA
Ariane Mallat, France
Nirmal S. Mann, USA
Gerassimos Mantzaris, Greece
Fabio Marra, Italy
Sergio Morini, Italy
Bjrn Moum, Norway
Zeynel Mungan, Turkey
Robert Odze, USA
Stephen O'Keefe, USA
John N. Plevris, UK
Massimo Raimondo, USA
J. F. Rey, France
Lorenzo Rossaro, USA
Muhammad Wasif Saif, USA
Hirozumi Sawai, Japan
Hakan Senturk, Turkey
Orhan Sezgin, Turkey
Eldon A. Shaffer, Canada
Matthew Shale, UK
Prateek Sharma, USA
Bo Shen, USA
Stuart Sherman, USA
Davor Stimac, Croatia
M. Storr, Canada
Andrew Thillainayagam, UK
Vasundhara Tolia, USA
keith Tolman, USA
Dino Vaira, Italy
David Hoffman Van Thiel, USA
Takuya Watanabe, Japan
Peter James Whorwell, UK
Yoshio Yamaoka, USA

Contents

Hindawi Publishing Corporation
Gastroenterology Research and Practice
Volume 2014, Article ID 963498, 2 pages
http://dx.doi.org/10.1155/2014/963498

Editorial
Imaging in Gastroenterology

Radu Badea,[1] Iwona Sudoł-Szopińska,[2] Sebastian Mueller,[3] Horia Ştefănescu,[4] and Monica Lupsor Platon[1]

[1] *Department of Clinical Imaging, "Octavian Fodor" Regional Institute of Gastroenterology and Hepatology and "Iuliu Hatieganu" University of Medicine & Pharmacy Cluj Napoca, Romania*
[2] *Department of Radiology, Institute of Rheumatology, Warsaw and Department of Diagnostic Imaging, Warsaw Medical University, Poland*
[3] *Department of Medicine, Salem Medical Center and Center for Alcohol Research, University of Heidelberg, Germany*
[4] *Department of Hepatology, "Octavian Fodor" Regional Institute of Gastroenterology and Hepatology, Cluj Napoca, Romania*

Correspondence should be addressed to Radu Badea; rbadea@umfcluj.ro

Received 22 April 2014; Accepted 22 April 2014; Published 11 May 2014

Copyright © 2014 Radu Badea et al. This is an open access article distributed under the Creative Commons Attribution License, which permits unrestricted use, distribution, and reproduction in any medium, provided the original work is properly cited.

Imaging becomes more and more important for all clinical specialities, including gastroenterology. This issue is focusing on some very interesting and new applications of imaging procedures in liver, biliary tract, and digestive tube pathology. The content is representative for this "new era" of visual diagnosis that we live.

In the article entitled "*Preliminary study on hepatocyte-targeted phosphorus-31 MRS using ATP-loaded galactosylated chitosan oligosaccharide nanoparticles*" R.-S. Yu et al. are describing their preliminary work on MR spectroscopy for evaluating the hepatocyte uptake of ATP-loaded Gal-CSO (Gal-CSO/ATP) nanoparticles. They show significant targeting efficiency in hepatic cells in vitro and enhancement efficiency of ATP peaks in HepG-2 cells. Furthermore, they demonstrate that phosphorus-31 MR spectroscopy could be applied in the research of hepatic molecular imaging.

V. Granata et al. in the article "*Surveillance of HCC patients after liver RFA: role of MRI with hepatospecific contrast versus three-phase CT scan—experience of high volume oncologic institute*" compare the diagnostic accuracy of hepatospecific contrast-enhanced MRI versus triple-phase CT scan after radiofrequency ablation (RFA) in hepatocellular carcinoma (HCC) patients. This is an excellent paper with a very good design. The authors examine a cohort of thirty-four consecutive HCC patients (42 hepatic nodules), treated with percutaneous RFA, who underwent MR and CT scan. All patients were enrolled in a research protocol that included CT with iodized contrast medium injection and MR with hepatospecific contrast medium injection and restaged within four weeks and at 3 months after ablation. Following this work, hepatospecific contrast-enhanced MRI seems to be more effective than multiphase CT in assessment of HCC treated with RFA.

T. Gorycki et al. in the article entitled "*Bile duct strictures caused by solid masses: MR in differential diagnosis and as a prognostic tool to plan the endoscopic treatment*" assess the meaning of qualitative parameters counted from magnetic resonance (MR) plane images as well as from cholangiopancreatography (MRCP) including cases of bile duct obstructions caused by solid masses in differential diagnosis between benign and malignant conditions and as the prognostic factors for endoscopic treatment. They conclude that the probability of malignancy of solid lesions obstructing biliary duct is increasing with higher SIR in T2W images and with longer strictures. Passing the stricture during ERCP treatment was easier and more probable in cases of shorter strictures caused by lesions with higher SIR in STIR T2W images.

B. Małkowski et al. make a study entitled "^{18}*F-FLT PET/CT in patients with gastric carcinoma*" focused on gastric carcinoma. Gastric cancer is a neoplasm presenting different types, frequently containing mucus. Cellularity of this tumor

type can be limited and ^{18}F-glucose uptake is not high enough to be seen in PET. The aim of the study was to evaluate the usefulness of ^{18}F-FLT PET/CT in the detection and differentiation of gastric cancers. The work suggests that there is a good accumulation of fluorothymidine in such a tumor which enabled the visualization and evaluation. Simultaneously to neoplastic cells fluorothymidine was accumulated in normal mucosa, so the authors analyzed optimal cut-off value for SUVmax in normal and neoplastic tissue. Ultrasonography (especially EUS) plays the important role in gastric cancer staging but it should be used together with other imaging modalities (e.g., PET) indicating possible invasion of any anatomical and pathological structures.

The enterovesical fistulas (the paper entitled "*Enterovesical fistulae: aetiology, imaging, and management*") are discussed in the report made by T. Golabek et al. The study provides a state-of-the-art overview of the clinical and radiological diagnosis of enterovesical fistulae. The treatment of fistulae is also briefly discussed. The diagnosis of EVF can be challenging and is often delayed for several months after the symptoms begin. Computed tomography and magnetic resonance imaging remain ideal modality options in establishing the site, course, and complexity of fistulae and in identifying an aetiological factor. Management of fistulae is mainly dependent on the underlying pathology, site of the bowel lesion, and patient's preoperative performance status and may involve conservative or invasive treatment. However, surgical one-stage strategy is a preferred option in most of the cases.

Dr. W. Memon et al. in the paper entitled "*MDCT of small bowel obstruction: how reliable are oblique reformatted images in localizing point of transition?*" evaluate prospectively the additional value of oblique reformations from isotropic voxels obtained using a 64-slice MDCT (multidetector row CT) to localize POT (point of transition), having surgery as a reference standard. Early diagnosis of SBO (small bowel obstruction) is essential to prevent bowel ischemia. Although plain X-ray abdominal evaluation still remains the investigation of first choice in cases of suspected SBO due to its low cost and wide availability, it cannot reliably diagnose the exact level of obstruction and thus can only serve as a basis for triage for further imaging workup. With the ongoing developments in imaging techniques overtime, computed tomography (CT) has emerged as an excellent modality in the diagnosis of SBO. CT scan is not only reliably diagnose SBO but also can be of great help in determining the cause, severity, and the precise point of obstruction. Localizing the point of transition (POT) is empirical as it increases confidence in diagnosis, guides patient care, and thus helps in further management. The authors found that although the oblique MPR increases the image load and is time consuming it surely represents a development and new perspective of utilizing the available information whereby it can significantly prove as a powerful adjunct in diagnosis and management of SBO.

Dr. T. S. Kirtane and M. S. Wagh in the work entitled "*Endoscopic optical coherence tomography (OCT): advances in gastrointestinal imaging*" present the current status of OCT and its practical applications in imaging normal and abnormal mucosa in the esophagus, stomach, small and large intestines, and biliary and pancreatic ducts. They also highlight technical aspects and principles of imaging, assess published data, and suggest future directions for OCT-guided evaluation and therapy.

Finally, the group of Dr. A. Gebesce et al. (in the work entitled "*Importance of the ultrasonography in diagnosis of ileal duplication cyst*") are presenting an interesting case of intestinal duplication cyst and are discussing the role of ultrasonography for the diagnosis of this rare condition, both ante- and postpartum.

In conclusion, the present issue represents a holistic approach of the visual diagnosis in modern gastroenterology.

Radu Badea
Iwona Sudoł-Szopińsk
Sebastian Mueller
Horia Ştefănescu
Monica Lupsor Platon

Hindawi Publishing Corporation
Gastroenterology Research and Practice
Volume 2014, Article ID 815802, 7 pages
http://dx.doi.org/10.1155/2014/815802

Research Article

MDCT of Small Bowel Obstruction: How Reliable Are Oblique Reformatted Images in Localizing Point of Transition?

Wasim Memon,[1] Yasir Jamil Khattak,[1] Tariq Alam,[1] Luca Maria Sconfienza,[2] Muhammad Awais,[1] and Shayan Sirat Maheen Anwar[1]

[1] *Aga khan University, Karachi, Pakistan*
[2] *Division Servizio di Radiologia, IRCCS Policlinico San Donato, Organization Università degli Studi di Milano, Milano, Italy*

Correspondence should be addressed to Tariq Alam; drtariqalam@gmail.com

Received 29 September 2013; Revised 17 December 2013; Accepted 25 December 2013; Published 6 May 2014

Academic Editor: Monica Lupsor Platon

Copyright © 2014 Wasim Memon et al. This is an open access article distributed under the Creative Commons Attribution License, which permits unrestricted use, distribution, and reproduction in any medium, provided the original work is properly cited.

The goal of this study is to prospectively assess the additional value of oblique reformatted images for localizing POT, having surgery as a reference standard. *Materials and Methods*. 102 consecutive patients with suspected small bowel obstruction (SBO) underwent 64-slice multidetector row CT (MDCT) using surgical findings as reference standard. Two independent GI radiologists reviewed the CT scans to localize the exact POT by evaluating axial images (data set A) followed by axial, coronal, and oblique MPR images. CT findings were compared to surgical findings in terms of diagnostic performance. McNemar's test was used to detect any statistical difference in POT evaluation between datasets A and B. Kappa statistics were applied for measuring agreement between two readers. *Results*. There was a diagnostic improvement of 9.9% in the case of the less experienced radiologist in localizing POT by using oblique reformatted images. The more experienced radiologist showed diagnostic improvement by 12.9%.

1. Introduction

Small bowel obstruction (SBO) is a common clinical condition as a cause of abdominal pain, accounting for approximately 20% of all emergency admissions for acute abdomen. It is also amongst one of the commonest bowel pathologies leading to surgical consultation [1–3].

Early diagnosis of SBO obstruction is essential to prevent bowel ischemia. In the past, the paradigm was to "never let the sun set or rise on an obstructed bowel." This probably was an evidence of limitations regarding availability of various imaging modalities for diagnosing the exact site of SBO [4].

Although plain X-ray abdominal evaluation still remains the investigation of first choice in cases of suspected SBO due to its low cost and wide availability, it cannot reliably diagnose the exact level of obstruction and thus can only serve as a basis for triage for further imaging workup [5, 6].

With the ongoing developments in imaging techniques overtime, computed tomography (CT) has emerged as an excellent modality in the diagnosis of SBO. CT scan not only reliably diagnoses SBO but can also be of great help in determining the cause, severity, and the precise point of obstruction [7–10]. Localizing the point of transition (POT) is empirical as it increases confidence in diagnosis, guides patient care, and thus helps in further management.

Ongoing dilation of the intestine increases luminal pressures. When luminal pressures exceed venous pressures, loss of venous drainage causes increasing edema and hyperemia of the bowel. This may eventually lead to compromised arterial flow to the bowel, causing ischemia, necrosis, and perforation. One such example is closed-loop obstruction, in which a section of bowel is obstructed proximally and distally. In such cases there may be few presenting symptoms with rapid progression to ischemia. Localizing the point of transition is imperative to pick the diagnosis in these patients.

Another important reason for finding the discrete transition point is that it helps guide operative planning. The number of points of transition being either one or more is also helpful in deciding between laparotomy and laparoscopic surgery.

In certain cases of extensively dilated bowel loops or lean and thin patients in whom interfaces between bowel loops are

very thin due to paucity of intraperitoneal adipose tissue, it may be challenging to localize the POT reliably using axial slices alone [11, 12].

With the currently available multidetector CT (MDCT) scanners, we can get near-isotropic voxels, which can be less than a millimeter in dimension and thus can produce multiplanar reformations with spatial resolution similar to axial sections. This may potentially enhance the role of reformatted images in localizing POT.

Thus, the purpose of this study was to prospectively assess the additional value of oblique reformations from isotropic voxels obtained using a 64-slice MDCT to localize POT, having surgery as a reference standard [13–16].

2. Materials and Methods

This was a cross-sectional study carried out between January, 2008, and July, 2011, at Aga Khan University Hospital, Karachi. All patients who entered the emergency department with strong suspicion of SBO on plain radiographs and underwent a CT examination for evaluation of SBO were included in the study. A total of 187 consecutive patients were considered for inclusion in our work. Among these 187 patients, 102 underwent surgery. The remaining 85 patients were conservatively managed and were therefore excluded. CT examinations were performed using a 64-slice MDCT (Toshiba Aquilion 64) without oral contrast administration unless specifically requested by the surgical team. Images were acquired starting from the diaphragmatic dome extending to the pubic symphysis with section thickness of 5 mm at 5 mm interval with beam pitch of 1.5, rotation time of 5 seconds using 120 kV, and 350 mA and 175 mAs and WL = 340/40. All patients received 1.5–2 mL/kg body weight of nonionic contrast (name, brand) warmed to body temperature, injected at a rate of 3-4 mL/s using a mechanical power injector (name, brand) through a 20 G cannula inserted into an antecubital vein. Images were acquired in arterial and portovenous phases using 10-second delay for arterial and 65 seconds for delayed phases. After the raw data was acquired, reconstructions were performed.

The axial sections, that is, the raw data, were reconstructed in two steps: first with 5 mm-thick sections at 5 mm intervals in the transverse plane followed by 0.5 mm thick sections at 1.5 mm intervals.

This second dataset of reconstructed axial sections scans was then used to acquire coronal reformations in the coronal plane with a thickness of 3 mm at 1.5 mm intervals using soft tissue algorithm. The acquisition of reformations is part of the routine MDCT protocol in our department. All these reconstructions were performed by the technologist at the CT console with a commercially available console system devoted to rapid reconstruction and later sent to picture archive and communication system (PACS). Oblique reformations were performed by the readers at the Vitrea station from available data. We were able to get near-isotropic voxels, producing multiplanar reformations with spatial resolution similar to axial sections. This potentially enhanced the role of reformatted images in localizing POT. Two independent radiologists with 10 and 12 years of experience in abdominal imaging reviewed the images. Both observers were blinded to surgical findings and reviewed two different datasets (A, including axial and coronal images only; B, volume data for oblique reconstructions in addition to dataset A) with an 8-week interval to prevent recall bias. Reviewing radiologists were blinded to surgical findings of the level of obstruction. CT was evaluated to localize the exact location of the point of transition (POT) and etiology of obstruction. Also, readers were asked to rate the confidence of localizing and reporting the POT after use of data set B using a semiquantitative scale (increased, not changed, and decreased). CT findings were compared to surgical findings in terms of diagnostic performance. Interpretations were compared with surgical findings by primary researcher to evaluate for accuracy. McNemar's test was used to detect any statistical difference in POT evaluation between datasets A and B. Kappa statistics were applied for measuring agreement between two readers for their findings of localizing the POT. SPSS version 11 was used for statistical analysis. A P value <0.05 was considered significant.

Table 1: Cause of small bowel obstruction in the study group.

Cause	Frequency	Percent	Valid percent
Adhesions	59	57.8	57.8
Hernia	17	16.7	16.7
Volvulus	1	1.0	1.0
Tuberculosis	16	15.7	15.7
Tumour	2	2.0	2.0
Abscess formation	1	1.0	1.0
Foreign body or bezoars	1	1.0	1.0
Post radiation	3	2.9	2.9
Gall stone ileus	2	2.0	2.0
Total	102	100.0	100.0

3. Results

The commonest cause of SBO in the study group was adhesions found on laparotomy ($n = 59$), followed by hernias ($n = 17$) and small bowel obstruction secondary to tuberculosis ($n = 16$). Other causes included postradiation stricture formation, gall stone ileus, tumor, volvulus, abscess formation, and foreign body/bezoars. (Table 1).

3.1. Cause of Small Bowel Obstruction in the Study Group. A total of 102 cases of surgically proven SBO were included in the study. Among these 102 patients, the less experienced radiologist correctly localized the transition zone in 85 cases (84.2%) using data set A and 95 cases when using data set B (94.15%), with a 9.9% diagnostic improvement (95% CI 2.7%–11.6%).

The more experienced radiologist correctly localized the transition zone in 83 cases (82.2%) using data set A, versus 96

Table 2: Improvement in accuracy of detecting point of transition after using data set B.

	Improvement in accuracy				
Readers	Data set A	Data set B	Improvement	McNemar values	Cl values
Experienced radiologist	82.2%	95%	12.9%	0.002	6.5%–12.9%
Less experienced radiologist	84.2%	94.15%	9.9%	0.006	2.7%–11.6%

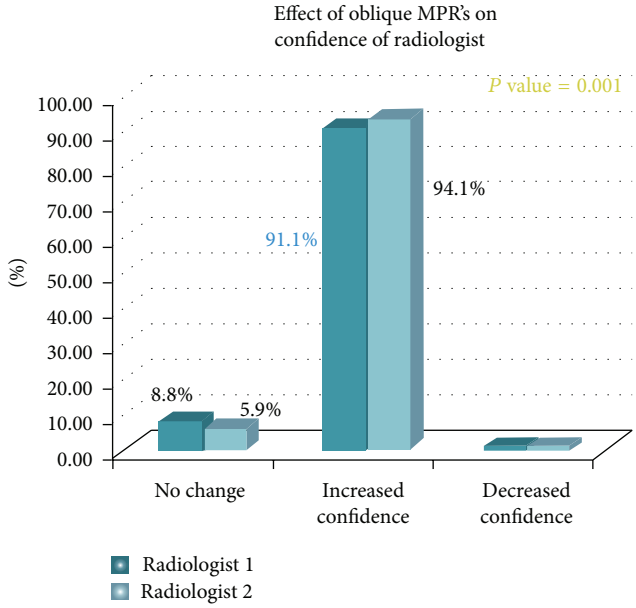

Figure 1: Effect of oblique MPRs on confidence of radiologist in diagnosing point of transition.

cases (95.0%) using data set B, improving by 12.9% with 95% CI of 6.5% to 12.9% (Table 2).

3.2. Improvement in and Accuracy of Detecting Point of Transition after Using Data Set B. When evaluating dataset B, the less experienced radiologist reported increased confidence in diagnosis of POT in 93 cases and similar confidence in 83 cases compared to the evaluation of dataset A. The more experienced radiologist reported increased confidence in diagnosis of POT in 95 cases and similar confidence in 82 cases compared to the evaluation of dataset A. The confidence scores for the presence of point of transition for both radiologists were higher after using data set B (axial, coronal, and oblique reformatted images) as compared to data set A (only axial and coronal images). Thus use of oblique reconstructions enhanced confidence in localizing POT ($P = 0.001$) (Figures 1, 2, and 3).

Kappa statistics for the measurement of agreement were found between readers for both sets A and B. For the data set A, there was good agreement between both radiologists (value = 0.51). For the data set B, the value was even higher, 0.71, indicating a higher level of agreement after using MPRs (Figure 4).

4. Discussion

Small bowel obstruction is one of the commonest reasons for presentation to the emergency department. Even today with the recent advances in imaging the diagnosis is made on the basis of clinical signs and symptoms, with plain radiography as the initial approach. However regarding the management of SBO, it is imperative not only to diagnose its severity but also to localize the exact site of obstruction which is an important determinant of the prognosis and help to the surgeon [17, 18].

With CT it has now become possible to not only reliably diagnose SBO but also acquire multiplanar reformations. Technological advances have crept up the ladder with time, making us available scanners like 64-slice MDCT and above. This paradigm shift has negotiated the problems like limited z-axis resolution, longer acquisition times allowing submillimeter isotropic data which not only is of great diagnostic help in cardiac, pulmonary, and musculoskeletal pathologies by facilitating better evaluation of anatomy but also has applications with respect to the abdomen and pelvis like pancreatic and gastric cancers as described by Prokesch et al. and Kim et al. in their respective studies [19–22].

Coronal reformatted images have also proved to be helpful in increasing confidence level of readers for the diagnosis of acute appendicitis [23].

In the literature several studies have evaluated the role of multiplanar reconstructions in SBO. Lazarus et al., Caoili and Paulson, and Furukawa et al. in their studies suggested that multiplanar reformations are helpful in the localization of the transitional zone. Jaffe et al. proved isotropic coronal multiplanar reformatted images to have additional diagnostic value in cases of bowel obstruction showing better agreement among independent observers especially for the diagnosis of level and cause. A recent study by Hodel et al. specifically evaluated the role of CT reformatted images in small bowel obstruction using 16-slice MDCT and reported an increase in both accuracy and confidence in the localization of the transition zone in CT of mechanical SBO [11, 13, 24–26].

Compared to the study by Hodel et al., the cases included in this study were all surgically proven with perioperative findings taken as the gold standard for point of transition. Moreover the study was performed with a 64-slice MDCT as opposed to a 16-slice MDCT.

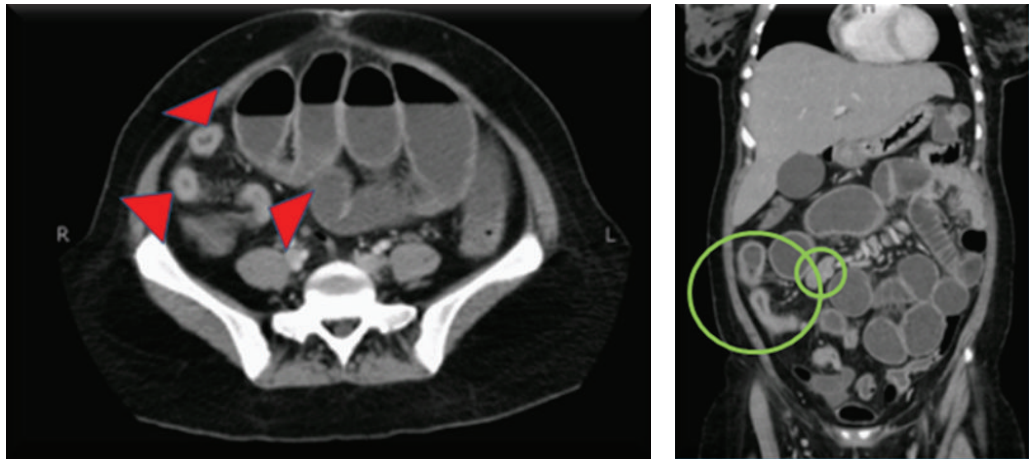

(a) Multiple dilated small-bowel loops collapsed thickened loops in right iliac fossa (red arrow and green circles)

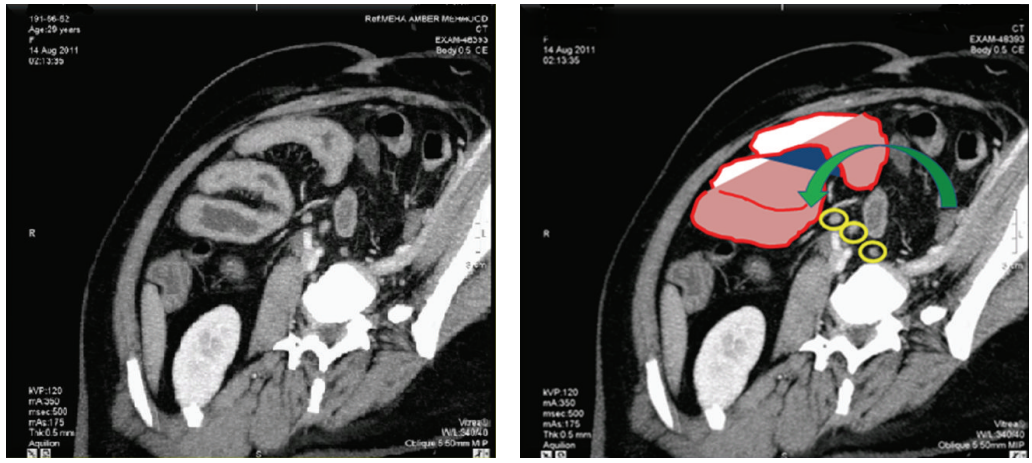

(b)

Figure 2: CT scan of 48-year-old female with acute abdominal pain. (a) Axial and coronal CT images obtained with intravenous contrast agents show dilated small-bowel loops (red arrow heads and green circles). (b) Oblique reformation shows dilated small-bowel loops with a transition point (green arrow) in the midabdomen. Multiple small mesenteric lymph nodes also visualized (yellow circles).

Although some radiologists and surgeons would consider coronal sections to be a better view regarding display of bowel since Coronal view is almost analogous to the frontal view of an abdominal radiograph and is synonymous to the plane learned in surgical training, Coronal view cannot be employed alone in cases of SBO since all the parts of bowel are not included on an isolated reformatted view. This could lead to confusion of narrowed part with an adjacent structure [27].

We thus included both the axial and coronal images in data set A, to make both data sets as similar as possible. This would also help to more correctly elucidate the additional value of oblique MPRs. Sagittal sections were however excluded from the data sets since they do not display more bowel loops in a single image and additionally it is difficult to localize the bowel loop anatomically as compared to axial and coronal images making it more time-consuming with little potential improvement in diagnosis.

Since the study went on for duration of more than 4 years, image grid overload with volume data was one of the prime challenges the researchers were confronted with. To deal with this all the available volume data was saved in compact discs while removing it from the image grid every 3 months and then reloading it onto the workstation for making oblique reconstructions at the time of recording the findings. To reduce the image load the axial data was presented on the PACS as 5 mm-thick sections. Reconstructions were performed from the available source images which were 1.5 mm thick.

We had in the study group myriad causes of SBO proven either by surgery or histopathology, amongst which adhesions were the commonest cause followed by abdominal hernias and tuberculosis. Although SBO was studied in different data sets, the radiologist was not asked to record the probable cause of obstruction on available images since it was not the prime objective for the study.

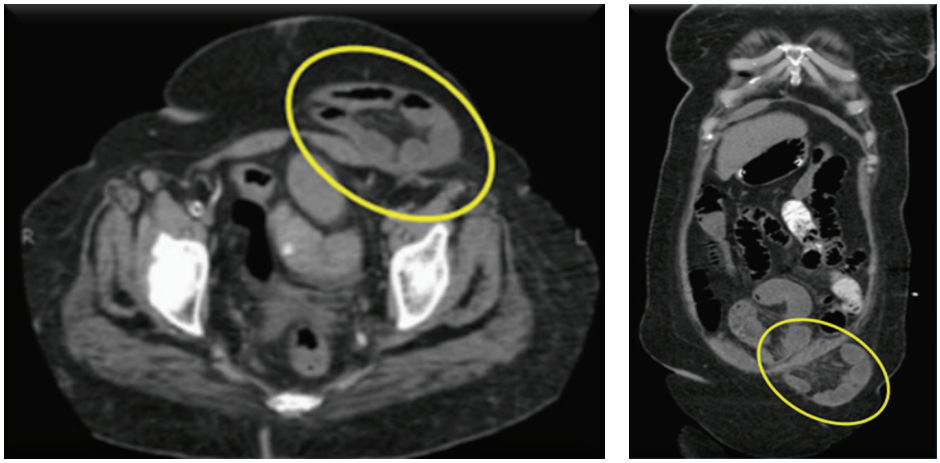

(a) Herniated loop of bowel through anterior abdominal wall (yellow circles)

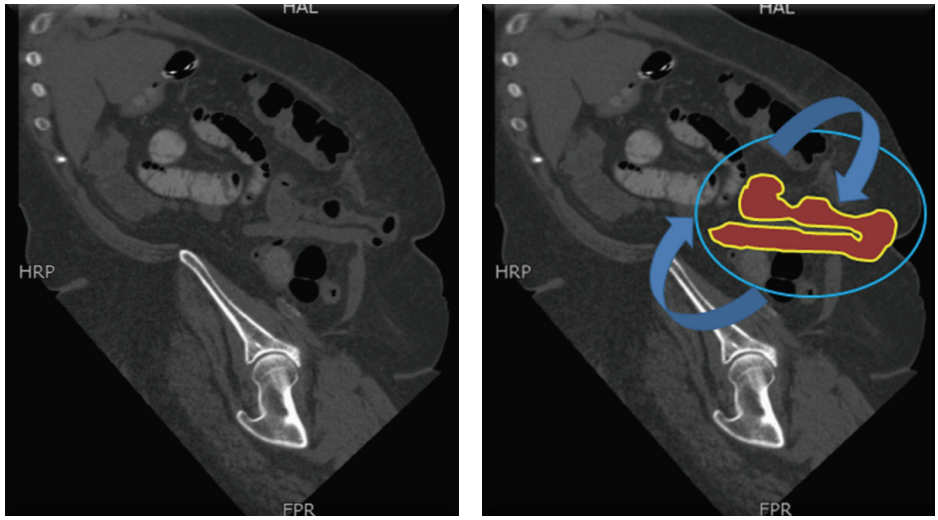

(b) Using oblique MPRs both the outgoing and incoming bowel loops are well delineated

Figure 3: CT scans in a 54-year-old woman with a two-month history of nausea and vomiting acutely presenting with worsening of symptoms. (a) Axial and coronal CT images obtained with intravenous contrast agent show herniated loops of small-bowel loops through a defect in anterior abdominal wall; however, the tract of bowel could not be completely elucidated on axial and coronal sections alone (yellow circles). (b) Oblique reformation exactly shows the outgoing and incoming loops of bowel with proximal dilated segments of bowel representing partial obstruction (blue circles and curved arrows).

We were able to achieve significantly improved accuracy in localization of transitional zone following use of MPRs by both radiologists with good agreement between the two. Although there was a difference between the two radiologists regarding experience, in our study no significant difference was found with respect to the results for both data sets A and B. We were also able to find that MPR enhances radiologist's confidence in calling a particular level point of obstruction which corroborates results given in studies by Jaffe et al., Paulson et al., and Hodel et al.

All the 102 patients included in our study underwent surgery, amongst which 19 patients had multiple levels of obstruction mostly due to adhesions. It was difficult to pick all the transition in cases where there was more than a single point of obstruction. This factor together with cases with extensive dilatation of bowel loops (high grade obstruction) could have been the reason for reduced CT accuracy in the first data set (84.1% and 82.1%) [3, 7, 14, 28].

One of the limitations of our study is that we did not classify the bowel obstruction into its grades of severity. By classifying the obstruction into various grades we could correlate the accuracy rates for various grades using MPRs as well.

5. Conclusion

In conclusion it was found that although the oblique MPR increases the image load and is time-consuming it surely is

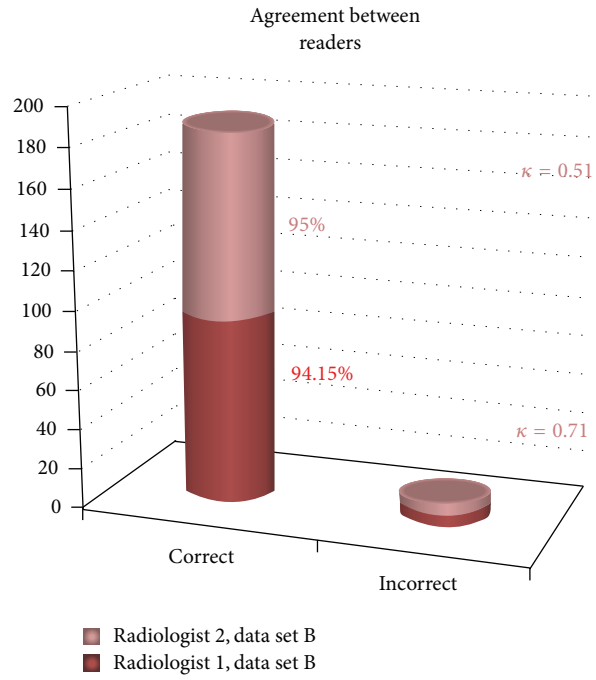

Figure 4: Agreement between readers.

a development and a new perspective of utilizing the available information whereby it can significantly prove as a powerful adjunct in diagnosis and management of SBO.

Conflict of Interests

The authors declare that there is no conflict of interests regarding the publication of this paper.

References

[1] N. M. Foster, M. L. McGory, D. S. Zingmond, and C. Y. Ko, "Small bowel obstruction: a population-based appraisal," *Journal of the American College of Surgeons*, vol. 203, no. 2, pp. 170–176, 2006.

[2] M. P. Rosen, B. Siewert, D. Z. Sands, R. Bromberg, J. Edlow, and V. Raptopoulos, "Value of abdominal CT in the emergency department for patients with abdominal pain," *European Radiology*, vol. 13, no. 2, pp. 418–424, 2003.

[3] D. Frager, S. W. Medwid, J. W. Baer, B. Mollinelli, and M. Friedman, "CT of small-bowel obstruction: value in establishing the diagnosis and determining the degree and cause," *American Journal of Roentgenology*, vol. 162, no. 1, pp. 37–41, 1994.

[4] W. Silen, M. F. Hein, and L. Goldman, "Strangulation obstruction of the small intestine," *Archives of Surgery*, vol. 85, pp. 121–129, 1962.

[5] J. C. Lappas, B. L. Reyes, and D. D. T. Maglinte, "Abdominal radiography findings in small-bowel obstruction: relevance to triage for additional diagnostic imaging," *American Journal of Roentgenology*, vol. 176, no. 1, pp. 167–174, 2001.

[6] W. M. Thompson, R. K. Kilani, B. B. Smith et al., "Accuracy of abdominal radiography in acute small-bowel obstruction: does reviewer experience matter?" *American Journal of Roentgenology*, vol. 188, no. 3, pp. W233–W238, 2007.

[7] E. J. Balthazar and W. George, "Holmes lecture CT of SBO," *American Journal of Roentgenology*, vol. 162, pp. 255–261, 1994.

[8] A. J. Megibow, E. J. Balthazar, K. C. Cho, S. W. Medwid, B. A. Birnbaum, and M. E. Noz, "Bowel obstruction: evaluation with CT," *Radiology*, vol. 180, no. 2, pp. 313–318, 1991.

[9] P. G. Taourel, J.-M. Fabre, J. A. Pradel, E. J. Seneterre, A. J. Megibow, and J. M. Bruel -, "Value of CT in the diagnosis and management of patients with suspected acute small-bowel obstruction," *American Journal of Roentgenology*, vol. 165, no. 5, pp. 1187–1192, 1995.

[10] M. Boudiaf, P. Soyer, C. Terem, J. P. Pelage, E. Maissiat, and R. Rymer, "CT evaluation of small bowel obstruction," *Radiographics*, vol. 21, no. 3, pp. 613–624, 2001.

[11] D. E. Lazarus, C. Slywotsky, G. L. Bennett, A. J. Megibow, and M. Macari, "Frequency and relevance of the "small-bowel feces" sign on CT in patients with small-bowel obstruction," *American Journal of Roentgenology*, vol. 183, no. 5, pp. 1361–1366, 2004.

[12] B. Khurana, S. Ledbetter, J. McTavish, W. Wiesner, and P. R. Ros, "Pictorial essay: bowel obstruction revealed by multidetector CT," *American Journal of Roentgenology*, vol. 178, no. 5, pp. 1139–1144, 2002.

[13] T. A. Jaffe, R. C. Nelson, G. A. Johnson et al., "Optimization of multiplanar reformations from isotropic data sets acquired with 16-detector row helical CT scanner," *Radiology*, vol. 238, no. 1, pp. 292–299, 2006.

[14] H. Hu, H. D. He, W. D. Foley, and S. H. Fox, "Four multidetector-row helical CT: image quality and volume coverage speed," *Radiology*, vol. 215, no. 1, pp. 55–62, 2000.

[15] P. R. Ros and J. E. Huprich, "Appropriateness Criteria on suspected small-bowel obstruction," *Journal of the American College of Radiology*, vol. 3, no. 11, pp. 838–841, 2006.

[16] J. Rydberg, K. A. Buckwalter, K. S. Caldemeyer et al., "Multisection CT: scanning techniques and clinical applications," *Radiographics*, vol. 20, no. 6, pp. 1787–1806, 2000.

[17] V. Donckier, J. Closset, D. van Gansbeke et al., "Contribution of computed tomography to decision making in the management of adhesive small bowel obstruction," *British Journal of Surgery*, vol. 85, no. 8, pp. 1071–1074, 1998.

[18] S. Daneshmand, C. G. Hedley, and S. C. Stain, "The utility and reliability of computed tomography scan in the diagnosis of small bowel obstruction," *American Surgeon*, vol. 65, no. 10, pp. 922–926, 1999.

[19] M. Dewey, A. Lembcke, C. Enzweiler, B. Hamm, and P. Rogalla, "Isotropic half-millimeter angiography of coronary artery bypass grafts with 16-slice computed tomography," *Annals of Thoracic Surgery*, vol. 77, no. 3, pp. 800–804, 2004.

[20] O. Honda, T. Johkoh, S. Yamamoto et al., "Comparison of quality of multiplanar reconstructions and direct coronal multidetector CT scans of the lung," *American Journal of Roentgenology*, vol. 179, no. 4, pp. 875–879, 2002.

[21] M. Noroozian, R. H. Cohan, E. M. Caoili, N. C. Cowan, and J. H. Ellis, "Multislice CT urography: state of the art," *British Journal of Radiology*, vol. 77, no. 1, pp. S74–S86, 2004.

[22] H. J. Kim, A. Y. Kim, S. T. Oh et al., "Gastric cancer staging at multi-detector row CT gastrography: comparison of transverse and volumetric CT scanning," *Radiology*, vol. 236, no. 3, pp. 879–885, 2005.

[23] E. K. Paulson, J. P. Harris, T. A. Jaffe, P. A. Haugan, and R. C. Nelson, "Acute appendicitis: added diagnostic value of coronal

reformations from isotropic voxels at multi-detector row CT," *Radiology*, vol. 235, no. 3, pp. 879–885, 2005.

[24] E. M. Caoili and E. K. Paulson, "CT of small-bowel obstruction: another perspective using multiplanar reformations," *American Journal of Roentgenology*, vol. 174, no. 4, pp. 993–998, 2000.

[25] A. Furukawa, M. Yamasaki, K. Furuichi et al., "Helical CT in the diagnosis of small bowel obstruction," *Radiographics*, vol. 21, no. 2, pp. 341–355, 2001.

[26] J. Hodel, M. Zins, L. Desmottes et al., "Location of the transition zone in CT of small-bowel obstruction: added value of multiplanar reformations," *Abdominal Imaging*, vol. 34, no. 1, pp. 35–41, 2009.

[27] R. W. Prokesch, L. C. Chow, C. F. Beaulia et al., "Local staging of pancreatic carcinomawith multi-detector row CT: use of curved planar reformations—initial experience," *Radiology*, vol. 225, no. 3, pp. 759–765, 2002.

[28] D. D. T. Maglinte, S. N. Gage, B. H. Harmon et al., "Obstruction of the small intestine: accuracy and role of CT in diagnosis," *Radiology*, vol. 188, no. 1, pp. 61–64, 1993.

Hindawi Publishing Corporation
Gastroenterology Research and Practice
Volume 2014, Article ID 376367, 7 pages
http://dx.doi.org/10.1155/2014/376367

Review Article

Endoscopic Optical Coherence Tomography (OCT): Advances in Gastrointestinal Imaging

Tejas S. Kirtane[1] and Mihir S. Wagh[2]

[1] *Department of Medicine, Washington Hospital Center, 110 Irving St NW, Washington, DC 20010, USA*
[2] *Division of Gastroenterology, University of Florida, 1600 SW Archer Road, P.O. Box 100214, Gainesville, FL 32610, USA*

Correspondence should be addressed to Mihir S. Wagh; mihir.wagh@medicine.ufl.edu

Received 27 September 2013; Accepted 21 December 2013; Published 26 February 2014

Academic Editor: Horia Stefănescu

Copyright © 2014 T. S. Kirtane and M. S. Wagh. This is an open access article distributed under the Creative Commons Attribution License, which permits unrestricted use, distribution, and reproduction in any medium, provided the original work is properly cited.

In the rapidly evolving field of endoscopic gastrointestinal imaging, Optical Coherence Tomography (OCT) has found many diverse applications. We present the current status of OCT and its practical applications in imaging normal and abnormal mucosa in the esophagus, stomach, small and large intestines, and biliary and pancreatic ducts. We highlight technical aspects and principles of imaging, assess published data, and suggest future directions for OCT-guided evaluation and therapy.

1. Introduction

Endoluminal imaging in gastrointestinal endoscopy has seen the advent of rapidly evolving new modalities over the last decade. Narrow band imaging [1], confocal laser endomicroscopy [2], and Optical Coherence Tomography (OCT or VLE: Volumetric Laser Endomicroscopy) [3] are some of the newer imaging techniques that have shown promise in the early detection of dysplasia and mucosal cancers and surveillance of cancers after endoscopic therapy. We present a practical assessment of OCT and its clinical applications focusing on recent advances in OCT in the diagnosis and management of gastrointestinal diseases.

2. OCT Technology

Conceptually, OCT (or Volumetric Laser Endomicroscopy/VLE) is analogous to B-mode ultrasonography, with the exception that near infrared light in the 700 to 1500 nm range of wavelength is used instead of sound waves to generate an image of the mucosal structure and its abnormalities using an interferometer device setup. Initially described in 1999 [4], OCT has evolved over the years to allow for higher resolution and rapid imaging. Time domain OCT was described initially but could not achieve high scanning rates. Subsequently, Fourier domain OCT was developed which allows for rapid image acquisition and generation of real time *in vivo* 2-dimensional and 3-dimensional mucosal renditions [5].

An OCT probe can be passed through the accessory channel of an endoscope and can be kept in contact with the mucosa of interest which allows for a resolution of 7–10 micrometers and an imaging depth of 2-3 mm depending on the wavelength of light used and the type of tissue being imaged [6, 7]. This allows visualization of histologic morphology in real time, especially the epithelial structures such as villi, crypts, and squamous and intestinal epithelium. In depth technical details and principles of optics involved in OCT have been discussed extensively elsewhere [8, 9].

Some of the more recent commercially available or custom-made OCT probes are Nvision VLE Imaging System (Nine Point Medical, Cambridge, MA) and probes from Lightlab Imaging (Westford, MA).

3. Gastrointestinal Applications

In the gastrointestinal tract, OCT has been used for imaging of the esophagus, stomach, small and large intestine, and biliary and pancreatic ducts. However, much of the experience and practical utility with OCT has been with esophageal, biliary, and pancreatic duct imaging.

Salient *in vivo* studies in the human gastrointestinal tract using OCT are summarized in Table 1.

Table 1: *In vivo* OCT studies in the human gastrointestinal tract.

Year	Author	Number of patients	Anatomic location/pathology
1997	A. M. Sergeev	3	Esophagus, stomach
2000	B. E. Bouma	32	Barrett's esophagus
2000	S. Jäckle	22	Esophagus, stomach, colon
2000	M. V. Sivak Jr.	72	Esophagus, stomach, duodenum terminal ileum, colon, rectum
2000	X. D. Li	8	Esophagus
2001	U. Seitz	4	Bile ducts
2001	J. M. Poneros	121	Barrett's esophagus
2001	G. Zuccaro	69	Esophagus, stomach
2002	J. M. Poneros	5	Bile ducts
2004	B. Shen	70	Crohn's disease and ulcerative colitis
2005	Isenberg	33	Barrett's esophagus
2005	V. X. Yang	22	Esophagus, stomach, duodenum
2006	J. A. Evans	55	High grade dysplasia/intramucosal carcinoma in Barrett's esophagus
2006	P. A. Testoni	15	Pancreatic duct
2006	E. Masci	40	Celiac disease
2007	Y. Chen	50	Barrett's esophagus
2008	P. Consolo	35	Ulcerative colitis and Crohn's disease
2009	M. Arvanitakis	37	Biliary strictures
2009	D. C. Adler	4	Colon, ulcerative colitis, radiation proctitis
2010	W. Hatta	62	Superficial squamous cell esophageal cancer
2012	T. H. Tsai	13	Barrett's esophagus
2012	C. Zhou	1	Cervical inlet patch

4. Esophageal Imaging with OCT

OCT has been shown to demonstrate the five-layered esophageal wall with good correlation with histologic structures [10]. With newer advances in techniques for endoscopic mucosal resection (EMR) [11] and ablation (radiofrequency and cryotherapy), assessing the depth of invasion of mucosal cancers is vital, with a pivotal role for OCT. Indeed, studies have shown superiority of resolution for OCT compared to EUS specifically for visualization of the mucosa and submucosa [12].

OCT is of particular importance in imaging patients with Barrett's esophagus (BE). Patients with BE are at an increased risk for development of esophageal adenocarcinoma [13] and the incidence of esophageal adenocarcinoma has increased by 300–500% in white men in the last 30 years [14, 15].

The feasibility of OCT for carrying out *in vivo* real time imaging of Barrett's esophagus, high grade dysplasia and esophageal adenocarcinoma has been well demonstrated (Figures 1, 2, and 3). In their study using ultra-high resolution OCT, Chen and colleagues [16] demonstrated characteristic layered epithelium in a normal esophagus with normal architecture, while images of Barrett's esophagus corresponded to crypt-like glandular structures. High grade dysplasia and esophageal adenocarcinoma images exhibited more heterogeneous structures corresponding to irregular, heterogeneous tissue morphology from distorted and cribriform or villiform glandular architecture. A prospective study showed that OCT had a sensitivity of 68% and specificity of 82% with a diagnostic accuracy of 78% for detection of dysplasia in Barrett's esophagus [17]. In this study, Isenberg et al. used 314 pairs of OCT images and biopsy specimens from 33 patients and blinded four endoscopists and one pathologist to the histology results/real time OCT images and arrived at their findings using histology as a gold standard.

The current Seattle Protocol for surveillance for Barrett's esophagus recommends random 4 quadrant biopsies and leaves room for sampling error due to missed areas of dysplasia at random biopsies. OCT can be useful in guiding biopsies or eventually acquiring optical biopsies *in lieu* of standard biopsies. Each 3D-OCT data set provides approximately 160 mm^2 (8 mm circumference × 20 mm pullback) coverage of the esophagus if the tissue is fully wrapped around the probe. This is approximately 30 to 60 times larger than the area sampled by jumbo biopsy forceps (~6 mm^2) and standard biopsy forceps (~2.5 mm^2) [18], thus, reducing sampling error.

OCT has also been used to show the surface morphology of rarer entities such as heterotopic gastric mucosa in the upper esophagus, also known as cervical inlet patch [19, 20].

An emerging utility of OCT can be in detecting Subsquamous Intestinal Metaplasia at the Gastroesophageal junction. Subsquamous Intestinal Metaplasia (SSIM) which has also been variably described as buried Barrett's glands or buried glands or subsquamous glands are areas of metaplastic columnar tissue present below normal appearing squamous mucosa (Figure 4). SSIM has been known to be present *de novo* [21, 22] in patients with BE and can persist in patients with BE after acid suppressive therapy and ablative therapies for Barrett's esophagus such as radiofrequency ablation, cryotherapy, or photodynamic therapy. Although the true

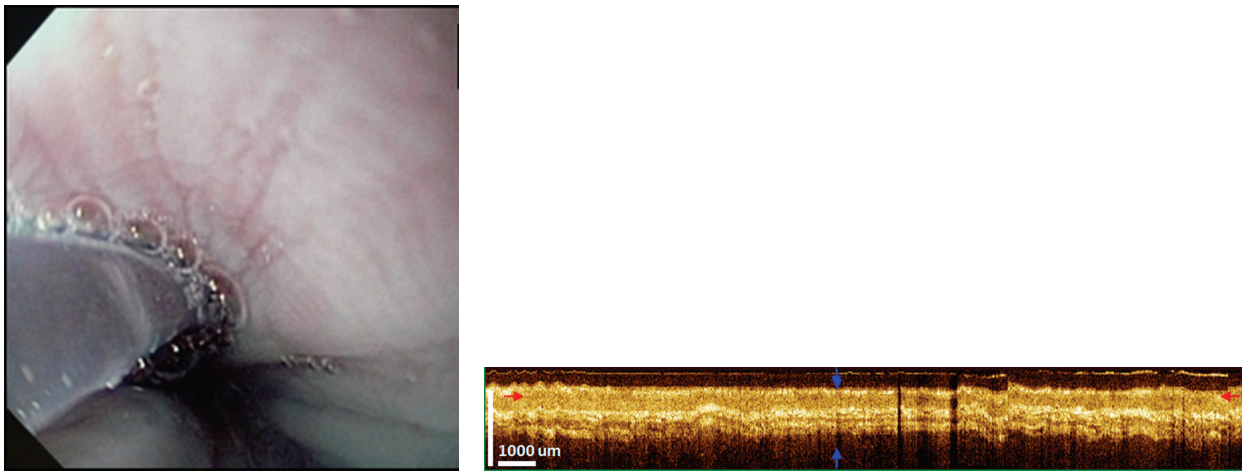

(a) (b)

Figure 1: OCT imaging of normal esophagus. (a) Conventional endoscopy of the esophagus showing smooth pale mucosa. (b) Corresponding OCT image showing a well-defined, layered architecture. The epithelium, lamina propria, muscularis mucosa, submucosa, and muscularis propria are seen as distinct layers with alternating hypo- and hyperintensity.

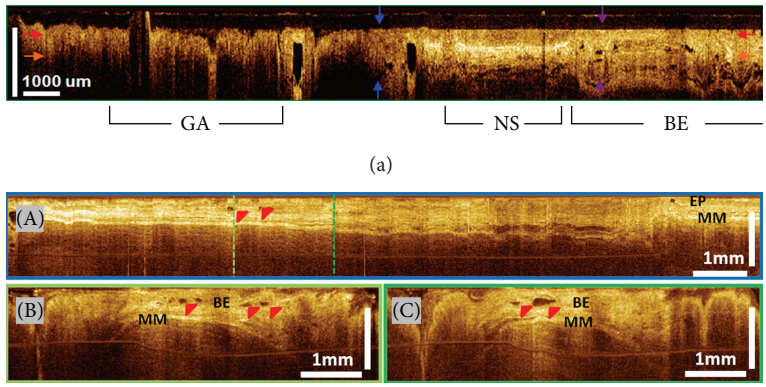

(a)

(b)

Figure 2: Barrett's esophagus (BE) without dysplasia. (a) Cross-sectional OCT imaging showing clear differences in layered architecture between gastric (GA), normal squamous (NS), and BE regions. BE regions exhibit distortion of the layered architecture and abnormal glandular features. (b) Cross-sectional OCT images around GEJ. BE glands (red arrows) are clearly observed (EP: epithelium; MM: muscularis mucosae in photos A–C).

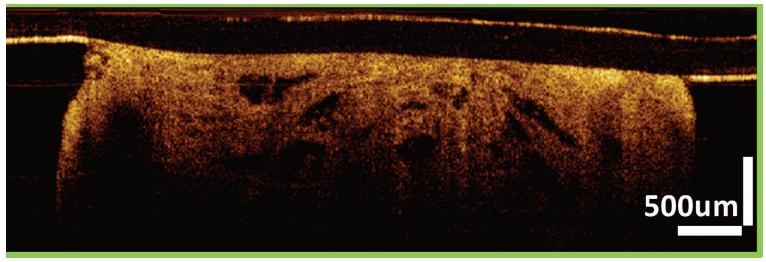

Figure 3: Intramucosal esophageal adenocarcinoma. OCT image showing dense large glands within the specimen. Lamina propria and muscularis mucosae (MM) layers are not clearly visible due to the infiltration of metaplasia into the MM layer.

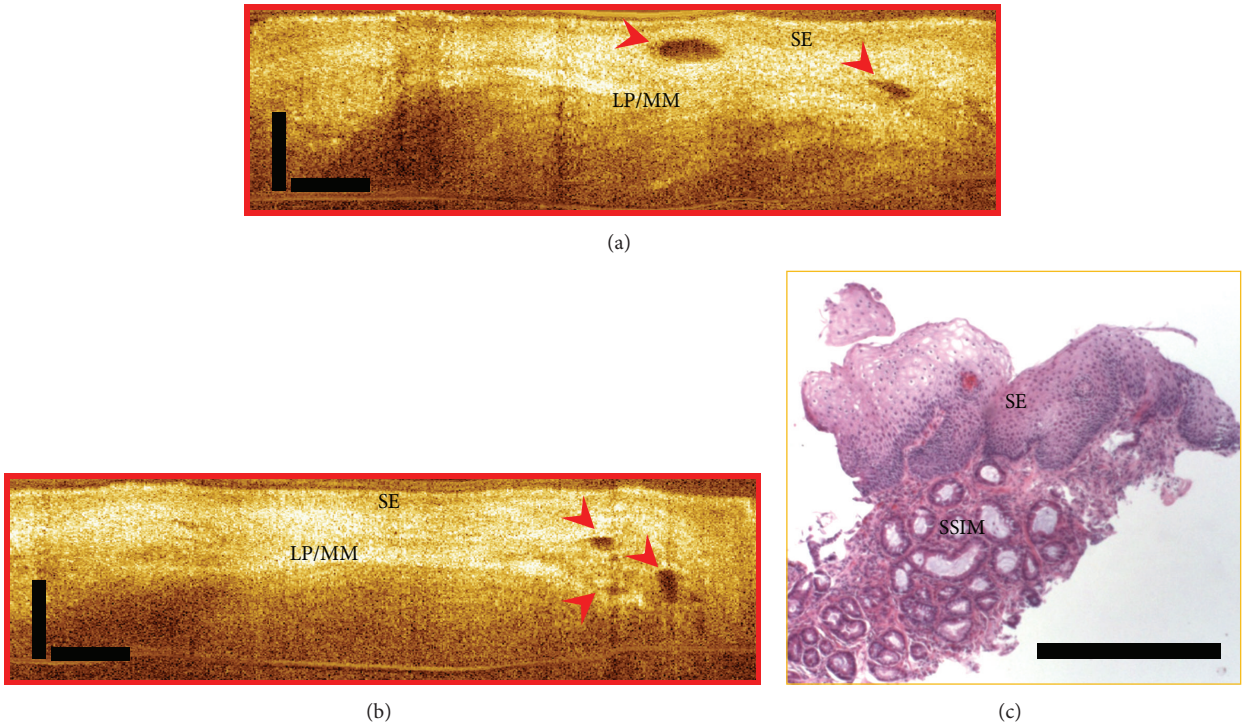

Figure 4: Subsquamous Intestinal Metaplasia (SSIM). (a-b): OCT images showing "buried glands" (red arrows). SE: squamous epithelium; LP/MM: lamina propria/muscularis mucosae. (c) Corresponding pathology showing subsquamous intestinal metaplasia under squamous epithelium.

malignant potential of residual SSIM is not known, concerns regarding identification and surveillance of SSIM are genuine owing to reports of progression to dysplasia and adenocarcinoma [23, 24]. Also, SSIM evades detection on conventional white light and narrow band endoscopy and can be missed even on biopsy using standard forceps due to sampling error and insufficient depth as shown by Gupta et al. [25]. Recently, one group working with OCT has demonstrated the existence of subsquamous intestinal metaplasia after radiofrequency ablation of Barrett's esophagus using OCT technology [18, 26]. This study showed regular flat squamous mucosa with small subepithelial vessels and glands in the normal esophagus. In contrast, BE showed large, densely packed glands with distortion of mucosal architecture. In post-RFA BE, findings were of a small number of isolated glands buried beneath 300–500 microns of neosquamous epithelium and lamina propria.

Going further, using OCT, it has been shown that the thickness of BE mucosa immediately after radiofrequency ablation predicts the response to RFA [27]. This study showed that BE mucosa was significantly thinner in patients who achieved complete eradication of intestinal metaplasia compared to those who did not achieve complete eradication of intestinal metaplasia at follow-up ($257 \pm 60\ \mu$m versus $403 \pm 86\ \mu$m; $P < 0.0001$). A threshold thickness of $333\ \mu$m derived from receiver operating characteristic curves corresponded to a 92.3% sensitivity, 85% specificity, and 87.9% accuracy in predicting the presence of BE at follow-up. These findings may have important implications for the need for more RFA sessions.

OCT has also been used to delineate the difference in architectural changes after different endoluminal ablative therapies for Barrett's esophagus. Radiofrequency ablation was observed to induce 230~260 micrometer depth of architectural changes after each set of ablations over a particular region, while cryotherapy was observed to induce edema-like spongiform changes to ~640 μm depth [28].

5. OCT in the Small Intestine

There is limited data on the use of OCT in the small bowel. OCT has been used to image small intestinal mucosa and demonstrated 100% agreement with histology in a blinded study for differentiating between no atrophy and mild and marked atrophy of villous architecture [29]. This finding can be important to differentiate celiac disease from iron deficiency anemia in which villous architecture is typically preserved. An endoscopic doppler OCT has been used to show increased microvascularity in villi in duodenal adenomas [30].

6. OCT in the Colon

A number of studies have used OCT for evaluation of the large bowel. A study by Pfau et al. [31] showed that adenomas had significantly less structure and scattered light to a lesser degree than hyperplastic polyps and that hyperplastic polyps were significantly closer in organization and light scattering to normal mucosa as compared with adenomas.

Other studies have characterized OCT findings in the normal colon, ulcerative colitis (UC), Crohn's disease (CD), and radiation proctitis [32–36]. The ability of OCT to image all the layers of the gastrointestinal wall can find utility in diagnosing the transmural inflammation of Crohn's disease (CD) and enable differentiating this from ulcerative colitis (UC). A prospective, blinded study by Shen and colleagues [37] showed a sensitivity of 90.0% and specificity of 83.3% for OCT in detecting the disrupted layered structure of the colon wall indicative of transmural inflammation, providing a valuable tool to distinguish CD from UC. This is especially relevant since biopsies are insufficient to assess for transmural inflammation.

7. OCT in the Biliary and Pancreatic Ducts

With the miniaturization of OCT probes, it is possible to use this technology for imaging the biliary and pancreatic ducts and evaluate strictures for neoplasia during ERCP. This was first demonstrated *in vivo* in the bile ducts by Seitz and colleagues in 2001 [38]. Their study demonstrated the layered architecture of the bile ducts similar to that found on histologic sections as well as underlying retroperitoneal structures with less backscattering. Similarly, OCT can recognize a differentiated three-layered architecture of the pancreatic duct in all cases with normal main pancreatic duct or chronic pancreatitis, whereas the layered architecture appears subverted in neoplastic lesions, with heterogeneous backscattering of the signal [39].

Given the low sensitivity (65%) of brush cytology for detection of malignancy in biliary strictures even in combination with other sampling techniques such as biopsy forceps [40], OCT offers a promising alternative. OCT has indeed been shown to enhance the yield of brush cytology for detection of malignant biliary strictures. Arvanitakis and colleagues [41] showed that the diagnostic sensitivity for biliary strictures could be increased to 84% by combining biliary brushings with 2 OCT criteria which were a disorganized and subverted layer structure and large hypo- or nonreflective areas considered as tumor vessels.

Testoni and colleagues performed a prospective study in 12 patients using OCT imaging with ERCP [42]. Twelve consecutive patients with documented main pancreatic duct stricture were investigated by endoscopic ultrasonography (EUS) and ERCP, followed by brush cytology and OCT scanning. OCT recognized a differentiated three-layer architecture in all cases with normal main pancreatic duct or chronic pancreatitis, while in all the neoplastic lesions the layer architecture appeared totally subverted, with heterogeneous backscattering of the signal. The accuracy of OCT for detection of neoplastic tissue was 100% compared with 66.7% for brush cytology.

8. Current Hurdles and Future Directions

At present, different OCT probes differ in their scanning speed, resolution, and depth penetration. There is a an unmet need for establishment of uniform objective and subjective criteria which can be used by the endoscopist for real time assessment of mucosal characteristics which can aid in differentiating normal from neoplastic tissue and identify varying grades of dysplasia. While OCT can easily identify intestinal metaplasia within a normal esophagus, its ability to identify dysplasia within Barrett's esophagus is relatively poor as shown in a prospective study by Isenberg and colleagues [17] and it calls for further improvements in imaging technique, such as involving computer aided image analysis which can identify textures and patterns indicative of dysplasia which may be underappreciated by the human eye. Efforts are underway in using computer aided image analysis for detection of dysplasia in Barrett's esophagus [43]. A consensus on the various terminologies used for imaging technologies would help standardize methods and findings and avoid ambiguity. Comparison of OCT with other imaging technologies is needed, and, most importantly, larger prospective data assessing clinical outcomes with OCT imaging is crucial which can identify niche areas where OCT can be sensitive, reliable, and have a high impact with respect to determining further therapy for patients. There are limitations to every new technology and identifying specific high yield applications for OCT will be required before it can be routinely used by practicing gastroenterologists.

9. Conclusions

OCT is a promising noninvasive imaging technology easily accessible through the working channel of an endoscope. OCT imaging has been performed in various parts of the GI tract, though mainly restricted to major academic and research institutions. Limitations of OCT include relatively high costs, need for standardized terminology and criteria for normal and neoplastic tissues, and lack of prospective data on clinical outcomes. With further refinement of this technology, OCT may allow "true optical biopsies" in the future.

Conflict of Interests

The authors declare that there is no conflict of interests regarding the publication of this paper.

Acknowledgments

The authors are thankful to Hsiang-Chieh Lee from the Massachusetts Institute of Technology and Dr. Hiroshi Mashimo from the Boston VA Medical Center and Harvard Medical School for contributing figures used in this paper.

References

[1] L. M. Song, D. G. Adler, J. D. Conway et al., "Narrow band imaging and multiband imaging," *Gastrointestinal Endoscopy*, vol. 67, no. 4, pp. 581–589, 2008.

[2] H. Neumann, R. Kiesslich, M. B. Wallace, and M. F. Neurath, "Confocal laser endomicroscopy: technical advances and clinical applications," *Gastroenterology*, vol. 139, no. 2, pp. 388.e2–392.e2, 2010.

[3] G. J. Tearney, M. E. Brezinski, J. F. Southern, B. E. Bouma, S. A. Boppart, and J. G. Fujimoto, "Optical biopsy in human gastrointestinal tissue using optical coherence tomography," *American Journal of Gastroenterology*, vol. 92, no. 10, pp. 1800–1804, 1997.

[4] D. Huang, E. A. Swanson, C. P. Lin et al., "Optical coherence tomography," *Science*, vol. 254, no. 5035, pp. 1178–1181, 1991.

[5] D. C. Adler, C. Zhou, T. Tsai et al., "Three-dimensional endomicroscopy of the human colon using optical coherence tomography," *Optics Express*, vol. 17, no. 2, pp. 784–786, 2009.

[6] Y. Wang, J. S. Nelson, Z. Chen, B. J. Reiser, R. S. Chuck, and R. S. Windeler, "Optimal wavelength for ultrahigh-resolution optical coherence tomography," *Optics Express*, vol. 11, no. 12, pp. 1411–1417, 2003.

[7] M. E. Brezinski and J. G. Fujimoto, "Optical coherence tomography: high-resolution imaging in nontransparent tissue," *IEEE Journal on Selected Topics in Quantum Electronics*, vol. 5, no. 4, pp. 1185–1192, 1999.

[8] J. G. Fujimoto, C. Pitris, S. A. Boppart, and M. E. Brezinski, "Optical coherence tomography: an emerging technology for biomedical imaging and optical biopsy," *Neoplasia*, vol. 2, no. 1-2, pp. 9–25, 2000.

[9] J. G. Fujimoto, "Optical coherence tomography for ultrahigh resolution in vivo imaging," *Nature Biotechnology*, vol. 21, no. 11, pp. 1361–1367, 2003.

[10] A. M. Sergeev, V. M. Gelikonov, G. V. Gelikonov et al., "In vivo endoscopic OCT imaging of precancer and cancer states of human mucosa," *Optics Express*, vol. 1, no. 13, pp. 432–440, 1997.

[11] J. Ortiz-Fernandez-Sordo, A. Parra-Blanco, A. Garcia-Varona et al., "Endoscopic resection techniques and ablative therapies for Barrett's neoplasia," *World Journal of Gastrointestinal Endoscopy*, vol. 3, no. 9, pp. 171–182, 2011.

[12] A. Das, M. V. Sivak Jr., A. Chak et al., "High-resolution endoscopic imaging of the GI tract: a comparative study of optical coherence tomography versus high-frequency catheter probe EUS," *Gastrointestinal Endoscopy*, vol. 54, no. 2, pp. 219–224, 2001.

[13] J.-F. Fléjou, "Barrett's oesophagus: from metaplasia to dysplasia and cancer," *Gut*, vol. 54, supplement 1, pp. i6–i12, 2005.

[14] S. S. Devesa, W. J. Blot, and J. F. Fraumeni Jr., "Changing patterns in the incidence of esophageal and gastric carcinoma in the United States," *Cancer*, vol. 83, no. 10, pp. 2049–2053, 1998.

[15] N. Shaheen and D. F. Ransohoff, "Gastroesophageal reflux, Barrett esophagus, and esophageal cancer: clinical applications," *Journal of the American Medical Association*, vol. 287, no. 15, pp. 1982–1986, 2002.

[16] Y. Chen, A. D. Aguirre, P.-L. Hsiung et al., "Ultrahigh resolution optical coherence tomography of Barrett's esophagus: preliminary descriptive clinical study correlating images with histology," *Endoscopy*, vol. 39, no. 7, pp. 599–605, 2007.

[17] G. Isenberg, M. V. Sivak Jr., A. Chak et al., "Accuracy of endoscopic optical coherence tomography in the detection of dysplasia in Barrett's esophagus: a prospective, double-blinded study," *Gastrointestinal Endoscopy*, vol. 62, no. 6, pp. 825–831, 2005.

[18] C. Zhou, T. Tsai, H. Lee et al., "Characterization of buried glands before and after radiofrequency ablation by using 3-dimensional optical coherence tomography (with videos)," *Gastrointestinal Endoscopy*, vol. 76, no. 1, pp. 32–40, 2012.

[19] C. Zhou, T. Kirtane, T. Tsai et al., "Three-dimensional endoscopic optical coherence tomography imaging of cervical inlet patch," *Gastrointestinal Endoscopy*, vol. 75, no. 3, pp. 675–677, 2012.

[20] C. Zhou, T. Kirtane, T. H. Tsai et al., "Cervical inlet patch-optical coherence tomography imaging and clinical significance," *World Journal of Gastroenterology*, vol. 18, no. 20, pp. 2502–2510, 2012.

[21] J. Chennat, A. S. Ross, V. J. A. Konda et al., "Advanced pathology under squamous epithelium on initial EMR specimens in patients with Barrett's esophagus and high-grade dysplasia or intramucosal carcinoma: implications for surveillance and endotherapy management," *Gastrointestinal Endoscopy*, vol. 70, no. 3, pp. 417–421, 2009.

[22] M. Anders, Y. Lucks, M. A. El-Masry et al., "Subsquamous extension of intestinal metaplasia is detected in 98% of cases of neoplastic Barrett's esophagus," *Clinical Gastroenterology and Hepatology*, 2013.

[23] N. A. Gray, R. D. Odze, and S. J. Spechler, "Buried metaplasia after endoscopic ablation of Barrett's esophagus: a systematic review," *American Journal of Gastroenterology*, vol. 106, no. 11, pp. 1899–1909, 2011.

[24] M. Titi, A. Overhiser, O. Ulusarac et al., "Development of subsquamous high-grade dysplasia and adenocarcinoma after successful radiofrequency ablation of Barrett's esophagus," *Gastroenterology*, vol. 143, no. 3, pp. 564.e1–566.e1, 2012.

[25] N. Gupta, S. C. Mathur, J. A. Dumot et al., "Adequacy of esophageal squamous mucosa specimens obtained during endoscopy: are standard biopsies sufficient for postablation surveillance in Barrett's esophagus?" *Gastrointestinal Endoscopy*, vol. 75, no. 1, pp. 11–18, 2012.

[26] D. C. Adler, C. Zhou, T.-H. Tsai et al., "Three-dimensional optical coherence tomography of Barretts esophagus and buried glands beneath neosquamous epithelium following radiofrequency ablation," *Endoscopy*, vol. 41, no. 9, pp. 773–776, 2009.

[27] T. H. Tsai, C. Zhou, Y. K. Tao et al., "Structural markers observed with endoscopic 3-dimensional optical coherence tomography correlating with Barrett's esophagus radiofrequency ablation treatment response (with videos)," *Gastrointestinal Endoscopy*, vol. 76, no. 6, pp. 1104–1112, 2012.

[28] T. H. Tsai, C. Zhou, H. C. Lee et al., "Comparison of tissue architectural changes between radiofrequency ablation and cryospray ablation in Barrett's esophagus using endoscopic three-dimensional optical coherence tomography," *Gastroenterology Research and Practice*, vol. 2012, Article ID 684832, 8 pages, 2012.

[29] E. Masci, B. Mangiavillano, L. Albarello, A. Mariani, C. Doglioni, and P. A. Testoni, "Optical coherence tomography in the diagnosis of coeliac disease: a preliminary report," *Gut*, vol. 55, no. 4, p. 579, 2006.

[30] V. X. D. Yang, S. Tang, M. L. Gordon et al., "Endoscopic Doppler optical coherence tomography in the human GI tract: initial experience," *Gastrointestinal Endoscopy*, vol. 61, no. 7, pp. 879–890, 2005.

[31] P. R. Pfau, M. V. Sivak Jr., A. Chak et al., "Criteria for the diagnosis of dysplasia by endoscopic optical coherence tomography," *Gastrointestinal Endoscopy*, vol. 58, no. 2, pp. 196–202, 2003.

[32] P. Consolo, G. Strangio, C. Luigiano, G. Giacobbe, S. Pallio, and L. Familiari, "Optical coherence tomography in inflammatory bowel disease: prospective evaluation of 35 patients," *Diseases of the Colon and Rectum*, vol. 51, no. 9, pp. 1374–1380, 2008.

[33] L. Familiari, G. Strangio, P. Consolo et al., "Optical coherence tomography evaluation of ulcerative colitis: the patterns and the comparison with histology," *American Journal of Gastroenterology*, vol. 101, no. 12, pp. 2833–2840, 2006.

[34] B. Shen and G. Zuccaro Jr., "Optical coherence tomography in the gastrointestinal tract," *Gastrointestinal Endoscopy Clinics of North America*, vol. 14, no. 3, pp. 555–571, 2004.

[35] D. C. Adler, C. Zhou, T. Tsai et al., "Three-dimensional endomicroscopy of the human colon using optical coherence tomography," *Optics Express*, vol. 17, no. 2, pp. 784–796, 2009.

[36] C. Zhou, D. C. Adler, L. Becker et al., "Effective treatment of chronic radiation proctitis using radiofrequency ablation," *Therapeutic Advances in Gastroenterology*, vol. 2, no. 3, pp. 149–156, 2009.

[37] B. Shen, G. Zuccaro Jr., T. L. Gramlich et al., "In vivo colonoscopic optical coherence tomography for transmural inflammation in inflammatory bowel disease," *Clinical Gastroenterology and Hepatology*, vol. 2, no. 12, pp. 1080–1087, 2004.

[38] U. Seitz, J. Freund, S. Jaeckle et al., "First in vivo optical coherence tomography in the human bile duct," *Endoscopy*, vol. 33, no. 12, pp. 1018–1021, 2001.

[39] P. A. Testoni and B. Mangiavillano, "Optical coherence tomography for bile and pancreatic duct imaging," *Gastrointestinal Endoscopy Clinics of North America*, vol. 19, no. 4, pp. 637–653, 2009.

[40] M. de Bellis, S. Sherman, E. L. Fogel et al., "Tissue sampling at ERCP in suspected malignant biliary strictures (Part 2)," *Gastrointestinal Endoscopy*, vol. 56, no. 5, pp. 720–730, 2002.

[41] M. Arvanitakis, L. Hookey, G. Tessier et al., "Intraductal optical coherence tomography during endoscopic retrograde cholangiopancreatography for investigation of biliary strictures," *Endoscopy*, vol. 41, no. 8, pp. 696–701, 2009.

[42] P. A. Testoni, A. Mariani, B. Mangiavillano, P. G. Arcidiacono, S. Di Pietro, and E. Masci, "Intraductal optical coherence tomography for investigating main pancreatic duct strictures," *American Journal of Gastroenterology*, vol. 102, no. 2, pp. 269–274, 2007.

[43] X. Qi, Y. Pan, M. V. Sivak, J. E. Willis, G. Isenberg, and A. M. Rollins, "Image analysis for classification of dysplasia in Barrett's esophagus using endoscopic optical coherence tomography," *Biomedical Optics Express*, vol. 1, no. 3, pp. 825–847, 2010.

Hindawi Publishing Corporation
Gastroenterology Research and Practice
Volume 2013, Article ID 696423, 6 pages
http://dx.doi.org/10.1155/2013/696423

Clinical Study

^{18}F-FLT PET/CT in Patients with Gastric Carcinoma

Bogdan Małkowski,[1,2] Tomasz Staniuk,[3] Ewa Śrutek,[4] Tomasz Gorycki,[5] Wojciech Zegarski,[3] and Michał Studniarek[5]

[1] *Department of Nuclear Medicine, Oncological Centre, Bydgoszcz, Poland*
[2] *Department of Positron Emission Tomography and Molecular Diagnostics, Collegium Medicum, Nicolaus Copernicus University, 85-796 Bydgoszcz, Poland*
[3] *Department of Oncological Surgery, Oncological Centre, 85-796 Bydgoszcz, Poland*
[4] *Department of Cancer Pathology and Pathomorphology, Collegium Medicum, Nicolaus Copernicus University, 85-796 Bydgoszcz, Poland*
[5] *Department of Radiology, Medical University of Gdańsk, 80-952 Gdańsk, Poland*

Correspondence should be addressed to Bogdan Małkowski; malkowskib@co.bydgoszcz.pl

Received 16 September 2013; Accepted 24 November 2013

Academic Editor: Iwona Sudoł-Szopinska

Copyright © 2013 Bogdan Małkowski et al. This is an open access article distributed under the Creative Commons Attribution License, which permits unrestricted use, distribution, and reproduction in any medium, provided the original work is properly cited.

The aim of the study was to evaluate the usefulness of 18F-FLT PET/CT in the detection and differentiation of gastric cancers (GC). 104 consecutive patients (57 cases of adenocarcinoma tubulare (G2 and G3), 17 cases of mucinous adenocarcinoma, 6 cases of undifferentiated carcinoma, 14 cases of adenocarcinoma partim mucocellulare, and 10 cases of end stage gastric cancer) with newly diagnosed advanced gastric cancer were examined with FLT PET/CT. For quantitative and comparative analyses, the maximal standardized uptake value (SUV_{max}) was calculated for both the tumors and noninvaded gastric wall. *Results.* There were found, in the group of adenocarcinoma tubulare, SUV_{max} 1.5–23.1 (7.46 ± 4.57), in mucinous adenocarcinoma, SUV_{max} 2.3–10.3 (5.5 ± 2.4), in undifferentiated carcinoma, SUV_{max} 3.1–13.6 (7.2 ± 3.25), in adenocarcinoma partim mucocellulare, SUV_{max} 2–25.3 (7.7 ± 6.99), and, in normal gastric wall, SUV_{max} 1.01–2.55 (1.84 ± 0.35). For the level of 2.6 cut-off value between the normal wall and neoplasm FLT uptake from ROC analysis, all but five gastric cancers showed higher accumulation of FLT than noninfiltrated mucosa. *Conclusion.* Gastric cancer presents higher accumulation of 18F-FLT than normal, distended gastric mucosa. Significantly higher accumulation was shown in cancers better differentiated and with higher cellular density.

1. Introduction

Gastric cancer (GC) is an aggressive neoplasm with very poor prognosis. In Poland, in 2010, a number of 5364 people died (3486 men and 1878 women) due to gastric cancer. During the last 4 decades, both morbidity and mortality have dropped significantly in Poland from the 1st place at the beginning of the 1970s to the 4th most common cancer related death in men and the 7th in females [1]. The treatment of choice for GC is complete tumor resection. Early detection and surgery have improved the results of treatment. However, many patients are still diagnosed with advanced-stage disease. Accurate determination of local invasion, tumor size and location, lymph node involvement, and distant metastases is of great importance in the qualification of patients to adequate treatment.

Detection of early-stage GC by ^{18}F-FDG PET is not successful, as FDG uptake is strongly related to tumor size, location, and histopathology, for example, a content of mucus [2, 3]. In 1998, ^{18}F-FLT (FLT)—a new radiotracer with the potential ability to be captured by fast proliferating cells—was reported [4]. The authors found that FLT is accumulated in proliferating tissues by the action of thymidine kinase and is resistant to degradation. In PET, it produces high-contrast images of normal marrow and tumors in human. Gastric mucosa is also proliferating tissue, so it can be important whether mucosal FLT uptake can affect the detection of gastric cancer. Choice of unaffected gastric mucosa on

the basis of PET only is doubtful, so in this work the PET/CT method was used to measure the FLT uptake within the normal gastric mucosa.

The purpose of the study was to verify the high potential to diagnose and differentiate GC using ^{18}F-FLT and to elaborate real cut-off value for SUV_{max} between the cancer tissue and normal gastric mucosa.

2. Material and Methods

104 consecutive patients (65 men and 39 women; mean age: 63 years) with the diagnosis of gastric tumor (biopsy-proven cancers) were included in this prospective study. They were enrolled to our department to diagnose the stage of the GC using FLT PET/CT. Written informed consent was obtained from all patients. The study protocol was approved by the local ethics committee of the Medical University Nicolaus Copernicus of Torun. In 10 patients with end-stage gastric cancer, the full verification of cancer type was not available.

The staging was not the issue of this paper. The aim of this evaluation was to compare uptake in normal and cancerous tissue in the stomach. The staging was described in our initial report published in June 2013 [5].

On the basis of histopathological evaluation of biopsy samples and/or removed specimens, the microscopic growth type in 94 patients was diagnosed and presented in Table 1. In some cases, there was no possibility to achieve full information about specific pathological classification. For example, there was group of patients in whom the surgery was canceled because of too advanced stage. In these patients, we have no full pathological information apart coming from endoscopy's specimens. Some frequently used classifications of diagnosed GC are presented in Table 1.

In order to assess the [^{18}F]FLT uptake in the normal gastric wall the SUV_{max} was measured in the area of normal gastric wall indicated on the basis of gastroscopy in 25 out of 104 patients in the study. The number of patients was limited to 25, as it was sufficient to further statistical analysis.

[^{18}F]FLT was synthesized in our laboratory using R&D Syncrom module (Raytest) following the standard operating procedure (SOP). Radiosynthesis of [^{18}F]FLT is based on [^{18}F]fluoride displacement of a protected nosylate precursor. A simple three-step synthesis was used to prepare radiochemically pure [^{18}F]FLT—98% ± 0.98%, at the end of synthesis within 45 min and with a 15% ± 7.6% radiochemical yield.

Patients fasted for at least 6 hours before the PET/CT scan. They were given antiperistalsis drug Buscopan (10 mg p.o.) 1 h before FLT injection.

Imaging was performed on the whole-body high-resolution PET/CT scanner Biograph 6. The images were acquired 60 min after administration of 350 ± 20 MBq of radiotracer. Standard CT scans were undertaken at 120 kV, 100 mAs, and 0.8 s rotation with a 1.25 mm slice width with no contrast injection. Pitch was 0.9. PET data were acquired in 3D mode for 3 min/bed. Acquisition of PET/CT was performed in two steps. Just before acquisition, patient drunk a glass (300 mL) of water to fulfill stomach. First, whole-body CT for attenuation correction and anatomical localization without contrast media was done. Immediately after CT, PET acquisition of two beds of placed on upper and mild abdomen was performed. As we tested before, this acquisition enables showing distended stomach without wall movement. The PET and CT parts of the image were exactly in the same position. Next, (without patient's position change) whole-body PET was performed. For attenuation correction and localization, the first whole-body CT was used.

Emission data were corrected for randomness, dead time, scatter, and attenuation.

Table 1: Histopathology of diagnosed gastric cancers.

Histopathology	*N*	Total
AdenoCa tubulare	57	94
Mucinous adenoCa	17	
Undifferentiated carcinoma	6	
AdenoCa partim mucocellulare	14	
Lauren type intestinal	38	88
Lauren type nonintestinal	50	
G2	28	78
G3	50	

3. Image Interpretation

To assure the proper interpretation, nuclear medicine and radiology specialists read the examination. They analyzed the image of the stomach using ^{18}F FLT PET/CT and knowledge from gastroscopy. Any discrepancies in the interpretation were solved by consensus. They selected the tumor localization according to the CT. In the tumor, increased focal uptake was detected and assessed by measurements of the maximum standardized uptake value (SUV_{max}). The normal stomach wall was chosen in the area of thin stomach wall (CT) and uniform FLT uptake. Then, we assessed the physiological FLT uptake in the stomach wall having knowledge about localization of the cancer from gastroscopy descriptions (files). These areas were omitted in physiological FLT uptake analysis. The images from the first two beds covering only upper abdomen with distended stomach were taken into consideration in this analysis. The ellipsoidal (circular) VOIs with the diameter of 10 mm were placed in the chosen areas which were the most active (the highest uptake) in the areas affected by gastric cancer and free of disease. The SUV_{max} from these VOI-s was calculated according to the standard formula (Bq/g × body weight (g)/injected activity in Bq).

The FLT uptake within the normal gastric wall was compared to accumulation within the tumor and the optimal cut-off value was estimated on the basis of ROC curve analysis.

The mean SUV_{max} values were compared to cancer type (according to histopathological evaluation) and the differences were statistically tested in order to measure the capability of cancer differentiation.

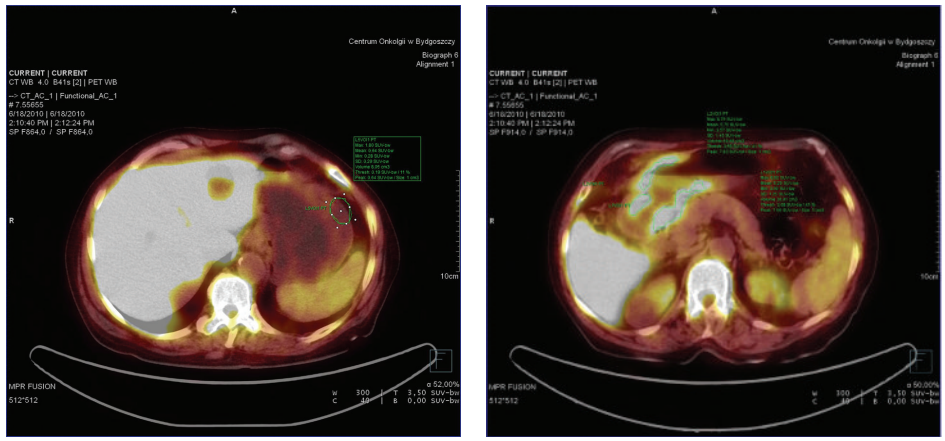

(a) (b)

Figure 1: (a) ^{18}FLT-PET in patient with undifferentiated adenocarcinoma. SUV_{max} in normal gastric wall was 1.8. (b) ^{18}FLT-PET in patient with undifferentiated adenocarcinoma. SUV_{max} = 8.9.

4. Statistical Analysis

(i) SUV_{max} values and the patients' age distribution were analyzed using Student's *t*-, Pearson, and Spearman tests. The age analysis was performed to assure lack of differences in the FLT uptake related to the age of patients.

(ii) Differences in FLT accumulation were analyzed by the Mann-Whitney *U*-test.

(iii) The changes of the sensitivities and specificities related to different thresholds between the SUV_{max} values in normal gastric wall and cancer tissue were performed on the basis of ROC curve analysis.

(iv) Differences were considered statistically significant at the $P < 0.05$ level.

5. Results

5.1. FLT Uptake in Normal Gastric Wall. In 25 out of 104 patients in the study, the SUV_{max} was measured in normal gastric wall. On the basis of endoscopic evaluation and surgical estimation, the gastric wall with no infiltration was chosen (CT), and the SUV_{max} was calculated. It has reached mean value and standard deviation of 1.84±0.35, respectively (from 1.01 to 2.55) (Figure 1). There were no statistical differences in the FLT uptake in normal gastric mucosa related to age. The FLT uptake was significantly lower than that in the cancer tissue (mean SUV_{max}—7.27 ± 4.73) and the optimal cut-off value differentiating tumor versus nontumor SUV_{max} was found at the level of 2.3 (sensitivity—97% and specificity—92%). For the threshold 2.6, the respective values were 94.7% and 100%, but in 5 patients with cancer the SUV_{max} was below this value (false negative ratio—5.3%).

All the 5% of false negative cases but one were mucus containing cancers. To achieve the specificity, we have compared cancerous localization as described in the endoscopy and confirmed in the pathology report and normal gastric wall. There were no additional foci of increased uptake apart from true GC localizations. It means that we had no FP results.

5.2. FLT Uptake in Different Types of Gastric Cancer. SUV_{max} of mucinous carcinoma presented in Table 2 was significantly different from other types of GC (Figures 2 and 3).

When the patients were divided according to Lauren classification into two groups and according to grading on G2 and G3 groups, other statistically significant differences of FLT uptake were found only for the G-grading. The results are presented in Table 3.

6. Discussion

6.1. Cancer Detection. Detection of gastric cancer is typically by endoscopy, and imaging is used to stage the disease rather than screening. In small tumors, usually endoscopic ultrasound is applied to stage cancer, but in larger ones it can be limited. Percutaneous ultrasound after careful preparation can be very valuable method in detection and characterization of digestive tract tumors, but assessment of whole stomach wall is extremely difficult [6, 7]. Computed tomography and MR imaging are used in locoregional nodal staging, but the full postsurgical verification is needed, not only the presence of lymph nodes on CT/MR images. After positive pathomorphological evaluation of tissue samples taken during endoscopy, there is a need to assess the real limits of tumor. ^{18}F-FDG was found to have extremely different accumulation in different gastric cancer. It is believed that ^{18}F-FLT can help in the problem, but further careful evaluation of its uptake in gastric cancer and additionally gastric nonneoplastic pathologies is still needed.

94 analyzed cases form the large group of patients with gastric cancer examined with ^{18}F-FLT PET when compared to other publications. The quantitative measurements of SUV_{max} are less dependent on ROI or VOI choice than the measurements of mean SUV value. Gastric mucosa is

Table 2: The mean value of SUV_{max} (SD) in normal mucosa and different cancer types.

Type	*N*	Min SUV_{max}	Max SUV_{max}	Mean (SD)
Normal mucosa	25*	1.01	2.55	1.84 (0.35)**
AdenoCa tubulare	57	1.5	23.1	7.46 (4.57)
Mucinous adenoCa	17	2.3	10.3	5.50 (2.40)**
Undifferentiated carcinoma	6	3.1	13.6	7.28 (3.25)
Adenocarcinoma partim mucocellulare	14	2	25.3	7.7 (6.99)
All	94	2.0	25.3	7.27 ± 4.73

*The patients were the same.
**Significantly differs from other cancer types ($P < 0.05$).

Table 3: The mean value of SUV_{max} (SD) in different cancer types, as divided according to Lauren classification and grading, compared to whole population studied and between the individual groups.

No.	Type	*N*	Mean (SD) SUV_{max}	Between groups
1	Lauren intestinal	38	7.69 (4.95)	$P = 0.16$
2	Lauren non-intestinal	50	6.84 (4.64)	1 versus 2
3	G2	28	8.2 (5.41)	$P = 0.026$*
4	G3	50	6.57 (4.59)	3 versus 4

*In G3 cancers the mean SUV_{max} value was significantly lower than in G2 tumors.

the tissue with very high proliferation. In normal conditions, its thickness can reach more than 10 mm, so, to avoid the false positive results, it should be significantly distended. The method of gastric wall distention is common and is realized by water or water-based contrast agents [8] or gas after ingestion of effervescent granules with a small amount of water [9]. Additionally, the digestive track peristalsis is suppressed by antiperistaltic drugs [8, 9]. In our group, there was the Buscopan tablet (10 mg) taken 1 hour before FLT injection. The SUV_{max} of FLT within the distended normal gastric mucosa was found within the range of 1.01–2.55 (mean: 1.84). It was high enough to create 5% of FN results, when we put the cut-off value at the level of 2.6 (to avoid FP results). One can suppose that it is acceptable price for the possibility to use FLT PET in TNM staging; however, in five gastric cancers, SUV_{max} was lower than 2.6. All of these cases but one were diagnosed as adenocarcinoma mucocellulare or partim mucocellulare.

6.2. Cancer Differentiation. The ^{18}F-FDG PET is the most frequently used radiopharmaceutical for diagnosing the cancer. But it is well known that FDG uptake depends on some tissue properties, not specific for the malignant neoplasm only [10]. Kawamura et al. [11] analyzed GLUT1 protein expression in 617 carcinomas and 50 tubular adenomas of the stomach. None of the adenomas expressed GLUT1, whereas 182 of the 617 carcinomas (30%) were positive for GLUT1 expression. Furthermore, signet-ring cell carcinoma and mucinous adenocarcinoma showed very low positive values for GLUT1 expression (2 and 6%, resp.). Among the other histological types, papillary adenocarcinoma (44%) showed slightly higher positive values for GLUT1 expression than tubular (32%) or poorly differentiated adenocarcinoma (28%). Yamada et al. [12] evaluated the association between FDG uptake and histopathological type in

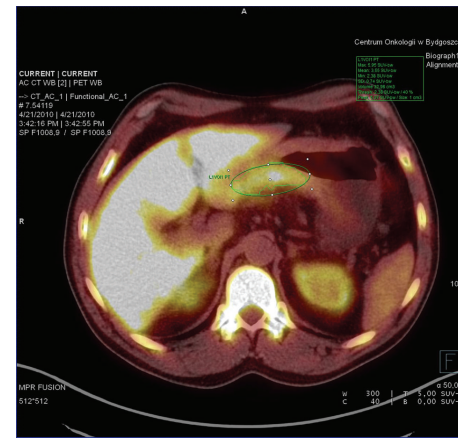

Figure 2: ^{18}FLT-PET in patient with mucinous adenocarcinoma. SUV_{max} = 5.9.

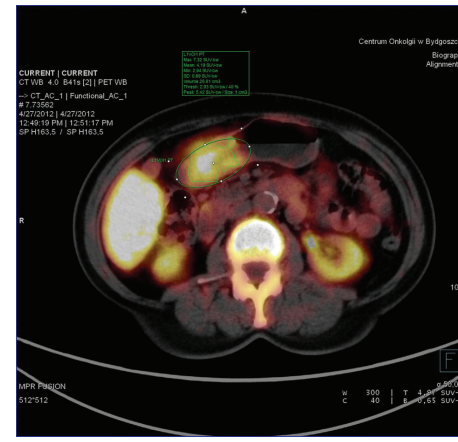

Figure 3: ^{18}FLT-PET in patient with adenocarcinoma tubulare G2 (G3). SUV_{max} = 7.32.

40 patients with gastric carcinoma among whom only 19 patients (48%) showed detectable FDG uptake. Cohesive carcinomas (papillary adenocarcinoma, tubular adenocarcinoma, and solid-type poorly differentiated adenocarcinoma) were significantly better detectable than noncohesive carcinomas (signet-ring cell carcinoma and nonsolid type poorly differentiated carcinoma −65% versus 14%, resp.). In 2007, Herrmann et al. [13] published paper in which they found 100% sensitivity in the diagnosis of gastric cancer with [^{18}F]FLT (3′-Fluoro-3′deoxythymidine-) PET. They have compared the accumulation of FLT and FDG in gastric cancer and showed that FLT PET was more sensitive than FDG PET, especially in tumors with no or low FDG uptake. This publication opened the new era in the stomach cancer PET diagnostics, but the authors concentrated only on the primary advanced tumors. Presented above data and results of other studies suggest that FDG is not ideal tracer for this type of cancers.

Analyzing the pathomorphological cancer structure, we compared independently some present or absent features within the cancer types. Stahl et al. [3] in publication on usefulness of ^{18}F-FDG PET in the diagnosis of gastric cancer concluded that FDG uptake is lower in nonintestinal than in intestinal Lauren type tumors. They described that only 60% of locally advanced GC were detected by FDG PET, but even 83% of intestinal type tumors were PET positive, when only 41% of diffused ones were seen. We found also lower accumulation of ^{18}F-FLT in nonintestinal gastric cancers—mean SUV_{max} = 6.84 versus 7.69 found in intestinal type tumors, but the difference was not statistically significant. It can suggest that cell proliferation is higher in intestinal GC Lauren type. The results Stahl et al. described for FDG PET were the same as those we found for FLT PET, showing higher uptake in nonmucus-containing GC with FLT SUV_{max} = 7.27 versus 5.50 in mucinous adenocarcinoma. In this work, FDG SUV_{max} was 7.2 in nonmucinous neoplasms versus 3.9 in mucus-containing ones. It can show that not only metabolic increase characterizes solid GC but higher cell proliferation as well. The uptake of both FDG and FLT was also higher in low-grade GC than in high-grade cancers. The differences were statistically significant for both radiopharmaceuticals (SUV 7.4 versus 5.2 for FDG and SUV_{max} 8.2 versus 6.57 in G2 and G3 tumors, resp.). We showed that detection of GC using ^{18}F-FLT PET was successful in 89 out of 94 patients (95% sensitivity) with 5 false negative cases (i.e., below SUV_{max} threshold of 2.6). In these 5 cases, the FLT uptake was within the range of noninvaded gastric wall, while, in all others, there was a great variety of SUV_{max} values. Only tumors with relatively lower cellular density (mucinous type) accumulated FLT significantly less than other ones. Histopathological types of gastric cancer donot reflect their ability to FLT accumulation which was supposed to be strongly related to cellular proliferation within the tumors. Kameyama et al. [14] in his study performed prospectively in 21 patients with advanced gastric cancer showed that the sensitivity in the diagnosis of gastric cancer with FLT and FDG was similar, but the mean SUV_{max} for FLT (7 ± 3.3) was significantly lower than that for FDG (9.4 ± 6.3) (similar to results of Kim et al. [9]). The accumulation of FLT was significantly higher in high-grade gastric tumors (SUV_{max} 8.5 versus 5.3 in low-grade ones) even if it did not correlate with KI-67 index. This was not the case in FDG uptake, but the number of patients enrolled into the study counted only 21 patients. High-grade tumors are frequently necrotic, so the mean cellularity can be lower in low-grade cancers. In our paper, we showed that FLT SUV_{max} was significantly lower in cancers with lower cellular density—similar to results of Kameyama group. FLT uptake has been shown to be lower in cancer with higher mucinous content and probably lower cellularity (18.1% of patients with mucinous adenocarcinoma) but simultaneously higher in better differentiated tumors. It is suspected that FLT uptake is not a simple result of proliferation alone, but can use an additional mechanism related to nucleoside transporters. It should be carefully studied in further works. Due to possibility to indicate a low cohesive cancer type, we hope it can be useful in predicting prognosis, planning treatment, and monitoring response in patients with gastric cancer.

7. Conclusions

We found that all gastric cancer types presented higher mean accumulation of FLT when compared to noninfiltrated gastric wall as measured by SUV_{max}. The optimal cut-off value between the cancer and mucosal accumulation was found at the level of 2.6 with sensitivity of 95% and an acceptable FN ratio of 5%. FLT PET/CT accumulation is significantly higher in regions of higher cellular density and cellular proliferation as well as in better differentiated neoplasm.

References

[1] U. Wojciechowska, J. Didkowska, and W. Zatoński, *Cancer in Poland in 2010*, Centrum Onkologii, Warsaw, Poland, 2012.

[2] E. Mochiki, H. Kuwano, H. Katoh, T. Asao, N. Oriuchi, and K. Endo, "Evaluation of 18F-2-deoxy-2-fluoro-D-glucose positron emission tomography for gastric cancer," *World Journal of Surgery*, vol. 28, no. 3, pp. 247–253, 2004.

[3] A. Stahl, K. Ott, W. A. Weber et al., "FDG PET imaging of locally advanced gastric carcinomas: correlation with endoscopic and histopathological findings," *European Journal of Nuclear Medicine and Molecular Imaging*, vol. 30, no. 2, pp. 288–295, 2003.

[4] A. F. Shields, J. R. Grierson, B. M. Dohmen et al., "Imaging proliferation in vivo with [F-18]FLT and positron emission tomography," *Nature Medicine*, vol. 4, no. 11, pp. 1334–1336, 1998.

[5] T. Staniuk, W. Zegarski, B. Malkowski, M. Jankowski, M. Klag, and T. Pietrzak, "Evaluation of 18F-FLT PET/CT usefulness in diagnosis and qualification for surgical treatment of gastric cancer," *Współczesna Onkologia*, no. 2, pp. 165–170, 2013.

[6] A. Smereczynski, T. Starzynska, and K. Kolaczyk, "Ultrasound of selected pathologies of small intestines," *Journal of Ultrasound*, vol. 13, pp. 155–166, 2013.

[7] G. Cwik and I. Gierblinski, "Errors and mistakes in the ultrasound diagnosis of the pancreas.," *Journal of Ultrasound*, vol. 13, pp. 178–191, 2013.

[8] A. Y. Kim, J. K. Han, T. K. Kim, S. J. Park, and B. I. Choi, "MR imaging of advanced gastric cancer: comparison of various MR

pulse sequences using water and gadopentetate dimeglumine as oral contrast agents," *Abdominal Imaging*, vol. 25, no. 1, pp. 7–13, 2000.

[9] J. W. Kim, S. S. Shin, S. H. Heo et al., "Diagnostic performance of 64-section CT using CT gastrography in preoperative T staging of gastric cancer according to 7th edition of AJCC cancer staging manual," *European Radiology*, vol. 22, no. 3, pp. 654–662, 2012.

[10] H. Takahashi, K. Ukawa, N. Ohkawa et al., "Significance of 18F-2-deoxy-2-fluoro-glucose accumulation in the stomach on positron emission tomography," *Annals of Nuclear Medicine*, vol. 23, no. 4, pp. 391–397, 2009.

[11] T. Kawamura, T. Kusakabe, T. Sugino et al., "Expression of glucose transporter-1 in human gastrin carcinoma: association with tumor aggressiveness, metastases, and patient survival," *Cancer*, vol. 92, no. 3, pp. 634–641, 2001.

[12] A. Yamada, K. Oguchi, M. Fukushima, Y. Imai, and M. Kadoya, "Evaluation of 2-deoxy-2-[18F]fluoro-D-glucose positron emission tomography in gastric carcinoma: relation to histological subtypes, depth of tumor invasion, and glucose transporter-1 expression," *Annals of Nuclear Medicine*, vol. 20, no. 9, pp. 597–604, 2006.

[13] K. Herrmann, K. Ott, A. K. Buck et al., "Imaging gastric cancer with PET and the radiotracers 18F-FLT and 18F-FDG: a comparative analysis," *Journal of Nuclear Medicine*, vol. 48, no. 12, pp. 1945–1950, 2007.

[14] R. Kameyama, Y. Yamamoto, K. Izuishi et al., "Detection of gastric cancer using 18F-FLT PET: comparison with 18F-FDG PET," *European Journal of Nuclear Medicine and Molecular Imaging*, vol. 36, no. 3, pp. 382–388, 2009.

Hindawi Publishing Corporation
Gastroenterology Research and Practice
Volume 2013, Article ID 512483, 6 pages
http://dx.doi.org/10.1155/2013/512483

Research Article

Preliminary Study on Hepatocyte-Targeted Phosphorus-31 MRS Using ATP-Loaded Galactosylated Chitosan Oligosaccharide Nanoparticles

Ri-Sheng Yu,[1] Xiu-Liang Zhu,[1] Jian-Zhong Sun,[1] Dan Shi,[1] Ying Chen,[1] Zhi-Kang Wang,[1] Ke-Zhong Tang,[1] and Yong-Zhong Du[2]

[1] *Department of Radiology, The Second Affiliated Hospital, Zhejiang University School of Medicine, No. 88 Jiefang Road, Hangzhou 310009, China*
[2] *Department of Pharmaceutics, College of Pharmaceutical Sciences, Zhejiang University, No. 866 Yuhangtang Road, Hangzhou 310058, China*

Correspondence should be addressed to Xiu-Liang Zhu; zhuxiul@yeah.net and Yong-Zhong Du; duyongzhong01@126.com

Received 22 September 2013; Accepted 8 November 2013

Academic Editor: Horia Stefãnescu

Copyright © 2013 Ri-Sheng Yu et al. This is an open access article distributed under the Creative Commons Attribution License, which permits unrestricted use, distribution, and reproduction in any medium, provided the original work is properly cited.

Background. The clinical applications of hepatic phosphorus-31 magnetic resonance spectroscopy (31P MRS) remain to be difficult because the changes of phosphates between normal hepatic tissues and pathological tissues are not so obvious, and furthermore, up to now there is few literature on hepatocyte-targeted 31P MRS. *Materials and Methods*. The ATP-loaded Gal-CSO (Gal-CSO/ATP) nanoparticles were prepared and the special cellular uptake of them as evaluated by using HepG-2 tumor cells and A549 tumor cells, respectively. Two kinds of cells were incubated with the nanoparticles suspension, respectively. Then were prepared the cell samples and the enhancement efficiency of ATP peaks detected by 31P MRS was evaluated. *Results*. The cellular uptake rate of Gal-CSO/ATP nanoparticles in HepG-2 cells was higher than that in A549 cells. Furthermore, the enlarged ATP peaks of Gal-CSO/ATP nanoparticles in HepG-2 cells were higher than those in A549 cells *in vitro* detected by 31P MRS. *Conclusions*. Gal-CSO/ATP nanoparticles have significant targeting efficiency in hepatic cells *in vitro* and enhancement efficiency of ATP peaks in HepG-2 cells. Furthermore, 31P MRS could be applied in the research of hepatic molecular imaging.

1. Introduction

Recent progress of magnetic resonance spectroscopy (MRS) technology has great potential in many biomedical research areas. Due to the ubiquity of phosphorus-containing moieties in energy metabolism, phosphorus-31 MRS (31P MRS) has been utilized to assess energy states in living systems [1]. This technique permits simultaneous detection and quantitation of several cytosolic phosphorus-containing compounds involved in energy metabolism (adenosine triphosphate (ATP), including γ, α, and β signals resolved sequentially, and inorganic phosphate (Pi)) and membrane phospholipid metabolism (phosphomonoesters (PME) and phosphodiesters (PDE)) [2, 3]. These important phosphorus-containing molecules are intricately involved in the cellular processes linked to cellular destruction, turnover, and malignant transformation.

Although it holds promise as a noninvasive means of documenting the extent and progression of liver disease [4, 5] and it has been used to improve the level of diagnosis and treatment response in patients with cancer [6], the clinical applications of hepatic 31P MRS remain to be difficult because there was no significant difference of the content of phosphorus compounds between normal hepatic tissue and hepatopathy tissue *in vivo*; the 31P MRS was only used *in vitro* [3, 5]. Furthermore, to our knowledge, there are no published results on hepatocyte-targeted 31P MRS.

In recent years, nanoparticles have been extensively used to deliver drugs, genes, diagnostics, and vaccines into specific cells or tissues [7–10]. Chitosan is a naturally occurring polysaccharide obtained by deacetylation of chitin, which is a polycationic polymer comprised of mainly glucosamine units [11]. It has good biocompatibility, biodegradability, and

low toxicity. The water-soluble chitosan with lower molecular weight, chitosan oligosaccharide (CSO), was obtained by enzymatic degradation in our lab [12], and like some other polycations it is known to interact with ATP by electrostatic forces of attraction to form CSO/ATP nanoparticles.

Mammalian hepatocytes possess large numbers of high-affinity, cell-surface receptors (asialoglycoprotein receptor, ASGP-R) that can bind asialoglycoproteins [13–15]. It can specifically recognize ligands with terminal galactose residues. Once a ligand binds to the ASGP-R, the ligand-receptor complex is rapidly internalized by hepatocytes, and the receptor recycled back to the surface of hepatocytes and is reutilized [15, 16], allowing high binding capacity and efficient uptake of galactosylated ligands by hepatocytes. Taking into account, we attempted to integrate a novel hepatocyte targeting carrier with multiple galactose residues.

The main goal of this study was to examine the Gal-CSO/ATP nanoparticles for hepatocyte-targeted imaging and to evaluate their targeting efficiency and the enhancement efficiency of ATP peaks detected by 31P MRS.

2. Materials and Methods

2.1. Preparation of Gal-CSO/ATP Nanoparticles. Nanoparticles were prepared successfully in our earlier research [17]. Briefly, 0.01 g Gal-CSO and 0.01 g ATP were first dissolved in 10 mL deionized water, respectively, and the mixture was stirred for 10 min by magnetic stirrer (400 rpm). Subsequently, ATP solution was dropwise mingled with the stirred Gal-CSO solution. When the transparency of the solution decreased accompanying an apparent Tyndall effect, this meant that the nanoparticles were obtained.

2.2. Cell Culture. Two cell lines were investigated in this study, and they are commercially available from Institute of Biochemistry and Cell Biology (Shanghai, China). HepG-2 (human hepatocellular carcinoma cell line) cells and A549 (human lung carcinoma cell line) cells were incubated in Dulbecco's Modified Eagle's Medium low glucose (DMEM), supplemented with 10% fetal bovine serum (FBS) under generally established cell culture conditions in 5% CO_2 at 37°C. HepG-2 and A549 cells were seeded in a 24-well culture plate (Nalge Nunc International, Naperville, IL, USA), respectively, at a density of 50,000 cells per well and incubated for 24 h.

2.3. Nanoparticle Labeling. Synthesis of the FITC-labeled chitosan was based on the reaction between the isothiocyanate group of FITC and the primary amino group of the D-glucosamine residue as reported in the literature [18]. Briefly, 2 mg of FITC was dissolved in 1 mL of dehydrated alcohol. 0.5 mL of Gal-CSO/ATP nanoparticles were dispersed in 2 mL distilled water, respectively. After then, they were treated by ultrasonication for 20 circulations (400 W, working for 2 s following stopping for 3 s). Two of them were mixed with 100 μL of FITC-alcohol solution (2.0 mg/mL), and the reaction was performed for 6 h under magnetic stirring (400 rpm) in darkness at room temperature. The FITC-labeled nanoparticles were dehydrated with pure carbinol and freeze-dried in a dark room. The nanoparticle suspension was stored in the dark room for further use.

2.4. Cellular Uptake. The A549 cells were used as a control. After the HepG-2 and A549 cells were cultured in 24-well plate adherent to the flask, they were then incubated with FITC-labeled Gal-CSO/ATP nanoparticles dispersion in growth medium for 24 h, respectively. Cell nuclei were stained with Hoechst for 30 min. Following the incubation, cells were washed thrice with PBS and then fixed with fresh 4% paraformaldehyde at 4°C for 20 min. The coverslips were observed by a confocal laser scanning microscope (LSM-510 META, ZEISS, Germany).

2.5. Quantitative Determination of Intracellular ATP Content. Two kinds of cells were seeded in a 24-well plate, respectively, at a density of 10,000 cells per well and incubated for 24 h. After then, 20 μL of Gal-CSO/ATP nanoparticles suspension was added (the actual content of ATP was 1.27 mg/mL in nanoparticles) to the cells, respectively, and then further incubated for 12 h and 24 h, respectively.

After the predetermined uptake time, removed the supernatant fluid and washed the cells thrice with PBS (pH 7.4). After trypsin digestion for one minute, HCl buffer solution (pH 1.0) was added. Cells were collected in a 5 mL PB pipe at the dedicated time, respectively. The cells were stored at −80°C for 2 h and placed at room temperature; then using freeze-thaw method was used three times. After 24 h, the intracellular ATP content was determined by ultraviolet spectrophotometry. The UV wavelength was set at 259 nm. The ATP loading efficiency was then calculated from the ATP content in the water phase (PBS) during the separation process of nanoparticles and the charged amount of ATP.

2.6. Gal-CSO/ATP Nanoparticles on HepG-2 Cells Targeted MRS Imaging In Vitro. Taking A549 cells as contrast agents, we added 0.4 mL Gal-CSO/ATP nanoparticles suspension to HepG-2 cell culture solution to obtain the cell sample for MRS detection. The methods were as follows: 30 mL cell sample was placed into the cell culture bottles, followed by being put into a plastic cup (without phosphorus compounds) containing a certain amount of distilled water, and then 2 mL, 4 mL, 6 mL, 8 mL, and 10 mL ATP solutions (10 mg/mL, Beijing Double-crane Pharmaceutical LTD. Co., China) were added into the bottles, respectively. Subsequently, they were detected by 31P MRS.

All 31P MRS examinations were performed with a 1.5 T imager (Siemens, Sonata, Germany), which is equipped with a commercial dual 1H/31P surface coil for imaging of cell samples. The basic MR images in all orientations were obtained with true fast imaging with steady precession (true FISP) sequence for the localization of voxels. 31P MR spectra were measured using a standard 2-dimensional chemical shift imaging (CSI) technique in the transverse plane with the following parameters: TR = 1000 ms, TE = 2.3 ms, matrix 8 × 8, viewing interpolation 16 × 16, field of view = 200 mm,

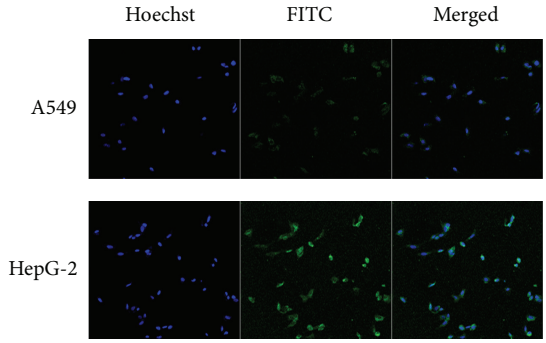

Figure 1: Fluorescence images of HepG-2 cells and A549 cells after the cells were incubated with FITC labeled Gal-CSO/ATP nanoparticles for 24 h, respectively. It is shown that the Gal-CSO/ATP nanoparticles could be uptaken by HepG-2 cells, and the fluorescence intensity in HepG-2 cells was stronger than that in A549 cells.

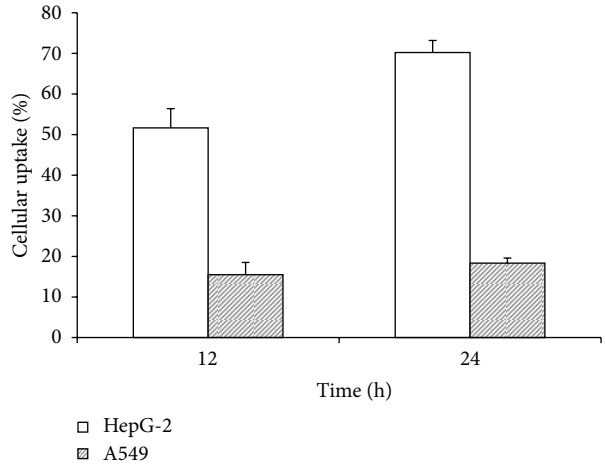

Figure 2: Cellular uptake percentage of Gal-CSO/ATP nanoparticles in different cell lines for 12 and 24 h, respectively. It is showen that HepG-2 cells were significantly higher than A549 cells in the cellular uptake percentage of the Gal-CSO/ATP nanoparticles.

flip angle = 90 degrees, thickness = 4 cm, and voxel volume 2.5 cm × 2.5 cm × 4 cm. Spectra were evaluated using Siemens syngo 2004B software.

3. Results

3.1. Cellular Uptake Tests. Figure 1 showed the fluorescence images of HepG-2 and A549 cells after the cells were incubated with FITC-labeled Gal-CSO/ATP nanoparticles for 24 h, respectively. It showed that the Gal-CSO/ATP nanoparticles could be uptaken by HepG-2 cells, and the fluorescence intensity in HepG-2 cells was stronger than in A549 cells. It further demonstrated that, under identical conditions, the cellular uptake capability of the Gal-CSO/ATP nanoparticles in HepG-2 cells was higher than in A549 cells.

3.2. Quantitative Determination of Intracellular ATP Content. The results of quantitative cellular uptake for FITC labeled Gal-CSO/ATP nanoparticles were presented in Figure 2 after the nanoparticles were incubated with HepG-2 and A549 cells, respectively. It was clear that HepG-2 cells were significantly higher than A549 cells in the cellular uptake percentage of the Gal-CSO/ATP nanoparticles. About 50% and 70% nanoparticles could be uptaken by HepG-2 cells in 12 and 24 h, respectively. However, the uptaken amounts of the nanoparticles by A549 cells were lower than 20% in 24 h.

3.3. Gal-CSO/ATP Nanoparticles on HepG-2 Cells Targeted MRS Imaging In Vitro. There was no significant MRS peaks of phosphorus compounds (ATP, PME, PDE and Pi) in solution containing HepG-2 cells when added into the 2 mL ATP solution mentioned above. Peaks of phosphorus compounds were detected when added into 4 mL ATP solution, but the MRS peaks were not ideal (see Figure 3(a)), while there were no peaks of phosphorus compounds detected in A549 cells solution. It was exciting that the ideal peaks of phosphorus compounds could be obtained in the solution containing HepG-2 cells by adding 6 mL ATP solution into the bottle (see Figure 3(b)), while it was quite hard for us to get peaks of phosphorus compounds in a solution containing A549 cells (see Figure 3(c)). When we added 8 mL ATP solution into the bottle, ideal peaks of phosphorus compounds emerged in solution containing HepG-2 cells, but the peaks of phosphorus compounds in the solution containing A549 cells were not so good as those of HepG-2 cells (see Figure 3(d)). And both of two bottles could get perfect MRS peaks when added 10 mL ATP to the solution.

4. Discussion

31P MRS imaging diagnoses the disease of liver through the peak signal intensity, which reflects the content levels of the specific phosphorylated compounds. We can achieve the purpose of MRS targeted molecular imaging by incorporation of measurable phosphide into the hepatic tissue to enlarge differences of peaks from one or more phosphorylated compounds.

One promising prospect for human hepatic 31P MRS is the measurement of hepatic energy homeostasis through the measurement of ATP, the well-known universal energy currency [19]. Previous studies have demonstrated that the measurement of hepatic ATP levels correlates with biochemical evidence of hepatic dysfunction, and histological evidence of loss of functioning hepatocytes and progressive disease, and animal models of acute liver disease [20–22]. Previous studies in our earlier research have demonstrated that Gal-CSO/ATP nanoparticles showed high encapsulation efficiency, sustained release of ATP, and efficiently delivered it to HepG-2 cells [17]. In addition, galactosylated chitosan was found to be a suitable material for liver-targeting drug/gene delivery or liver tissue engineering [23, 24], and as a hepatocyte-targeting carrier, Gal-CSO nanoparticles have a great promising potential for clinical applications due to their active liver-targeting characteristics and more than satisfactory compatibility with hepatoma cells [8]. For these

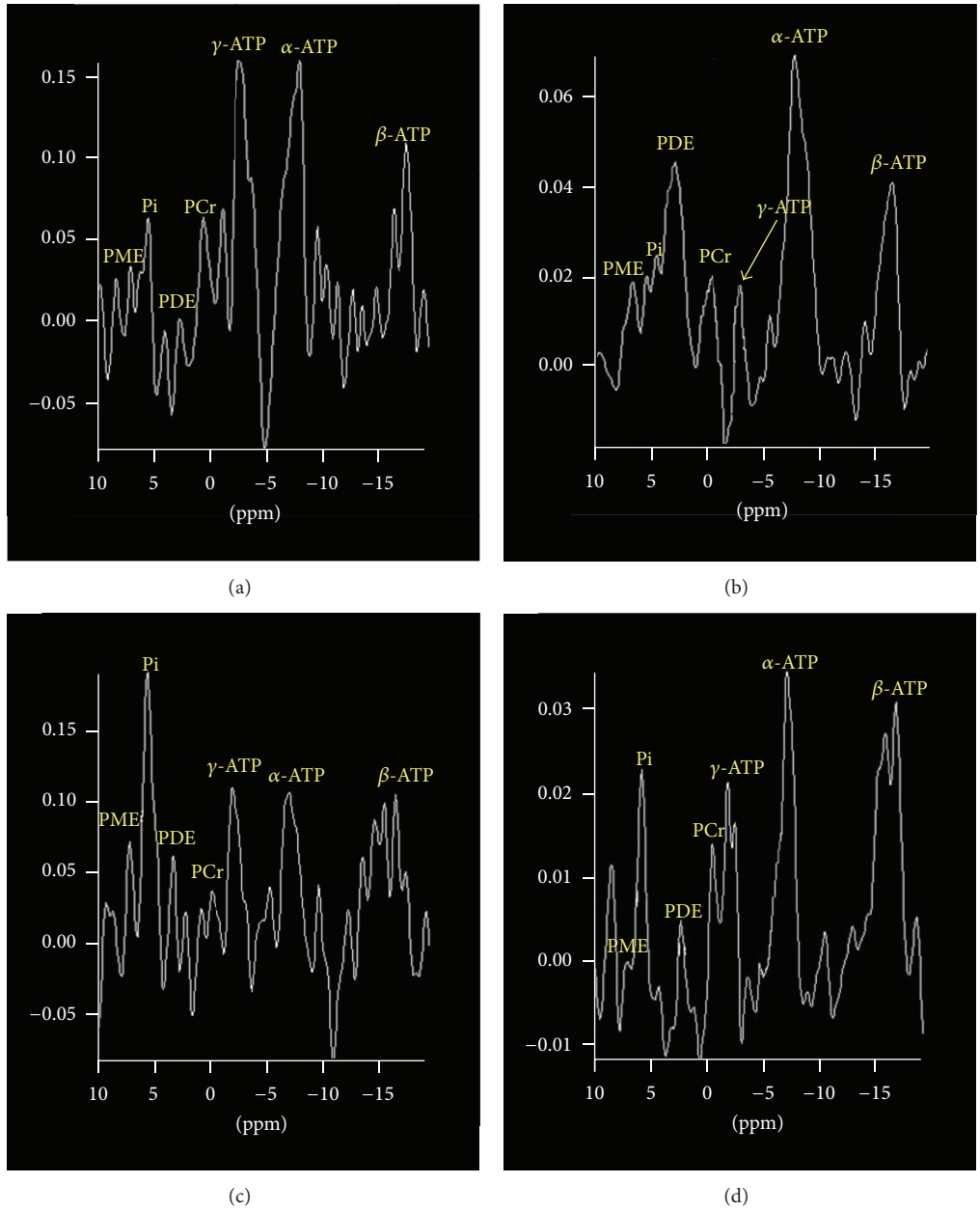

Figure 3: Peaks of phosphorus compounds were obtained from a solution containing HepG-2 cells. (a) MRS peaks were not ideal when adding 4 mL ATP solution; (b) MRS peaks were ideal when adding 6 mL ATP solution; (c) MRS peaks were in disorder when adding 6 mL ATP solution into the bottle containing A549 cells; and (d) MRS peaks were ideal when adding 8 mL ATP solution.

reasons, in order to achieve the targeted imaging of hepatic 31P MRS and change the ATP peaks, we have synthesized novel nanoparticles, Gal-CSO/ATP nanoparticles, to improve the ATP content in the hepatic cells and to be tested as a hepatocyte-targeted carrier to evaluate its targeting efficiency and the enhancement efficiency of ATP peaks detected by 31P MRS.

In this study, Gal-CSO/ATP nanoparticles were prepared, and a fluorescent marker molecule called FITC, was encapsulated in these nanoparticles, so the qualitative study of cellular uptake of nanoparticles by HepG-2 and A549 cells could be detected by fluorescence microscope. The cell lines HepG-2 and A549 have been selected as models, because the former is well known for expressing ASGP-R [25, 26], which is present only on hepatocytes at a high density and retained on several human hepatoma cell lines, that binds and internalizes galactose-terminal (asialo)glycoprotein [27–29], and the latter one was taken as contrast agent which has no ASGP-R. The ASGP-R has been exploited as a hepatocyte-specific targeting marker for drug and gene delivery [30, 31]. To enhance the ligand-mediated endocytosis and nanoparticles uptake by the targeted cells, active targeting can be

integrated with the passive targeting to enhance hepatocyte-specific delivery [32].

31P MRS findings were as follows: (1) the quantity of phosphorus compounds in solutions with different cells had no significant difference, because the similar MRS and ATP peaks were obtained from solutions with different cells added with the same ATP solution; (2) the ideal ATP peaks could be obtained by artificially increasing a certain quantity of ATP solution in the targeted cells. Furthermore, we had realized that the targeted imaging of 31P MRS by using ATP-loaded Gal-CSO nanoparticles and this work is ongoing in our lab.

5. Conclusions

The aforementioned results of the present study demonstrated that the Gal-CSO/ATP nanoparticles have significant targeting efficiency in liver cells *in vitro* and enhancement efficiency of ATP peaks in HepG-2 cells, and it further demonstrated that 31P MRS could be applied in the research of hepatocyte-targeted imaging. This preliminary study may be helpful to open up the field of hepatic molecular imaging and increase the clinical applications in the field of liver diseases in future.

Conflict of Interests

The authors declare that there is no conflict of interests regarding the publication of this paper.

Disclosure

There was no financial disclosure for the research.

Authors' Contribution

Xiu-Liang Zhu and Yong-Zhong Du contributed equally to this work.

Acknowledgments

The authors would like to thank Dr. XiaoYing Ying and Mr. LiYong Jie for their kindly assistance in their experiments. This study was supported by the National Nature Science Foundation of China (nos. 81171334 and 30770626).

References

[1] Z. Zhang, J. Li, S. Wu et al., "Cine-MRI and 31P-MRS for evaluation of myocardial energy metabolism and function following coronary artery bypass graft," *Magnetic Resonance Imaging*, vol. 28, no. 7, pp. 936–942, 2010.

[2] H. Kugel, H.-J. Wittsack, F. Wenzel, D. Stippel, W. Heindel, and K. Lackner, "Non-invasive determination of metabolite concentrations in human transplanted kidney in vivo by 31P MR spectroscopy," *Acta Radiologica*, vol. 41, no. 6, pp. 634–641, 2000.

[3] I. R. Corbin, L. N. Ryner, H. Singh, and G. Y. Minuk, "Quantitative hepatic phosphorus-31 magnetic resonance spectroscopy in compensated and decompensated cirrhosis," *The American Journal of Physiology: Gastrointestinal and Liver Physiology*, vol. 287, no. 2, pp. 379–384, 2004.

[4] A. K. P. Lim, N. Patel, G. Hamilton, J. V. Hajnal, R. D. Goldin, and S. D. Taylor-Robinson, "The relationship of in vivo 31P MR spectroscopy to histology in chronic hepatitis C," *Hepatology*, vol. 37, no. 4, pp. 788–794, 2003.

[5] I. R. Corbin, R. Buist, J. Peeling, M. Zhang, J. Uhanova, and G. Y. Minuk, "Hepatic 31P MRS in rat models of chronic liver disease: assessing the extent and progression of disease," *Gut*, vol. 52, no. 7, pp. 1046–1053, 2003.

[6] D. L. Morse, D. Carroll, S. Day et al., "Characterization of Breast cancers and therapy response by MRS and quantitative gene expression profiling in the choline pathway," *NMR in Biomedicine*, vol. 22, no. 1, pp. 114–127, 2009.

[7] M. O. Oyewumi and R. J. Mumper, "Influence of formulation parameters on gadolinium entrapment and tumor cell uptake using folate-coated nanoparticles," *International Journal of Pharmaceutics*, vol. 251, no. 1-2, pp. 85–97, 2003.

[8] Q. Wang, L. Zhang, W. Hu et al., "Norcantharidin-associated galactosylated chitosan nanoparticles for hepatocyte-targeted delivery," *Nanomedicine*, vol. 6, no. 2, pp. 371–381, 2010.

[9] F.-L. Mi, Y.-Y. Wu, Y.-L. Chiu et al., "Synthesis of a novel glyco-conjugated chitosan and preparation of its derived nanoparticles for targeting HepG2 cells," *Biomacromolecules*, vol. 8, no. 3, pp. 892–898, 2007.

[10] J. Zhang, X. G. Chen, W. B. Peng, and C. S. Liu, "Uptake of oleoyl-chitosan nanoparticles by A549 cells," *Nanomedicine*, vol. 4, no. 3, pp. 208–214, 2008.

[11] T. Kean, S. Roth, and M. Thanou, "Trimethylated chitosans as non-viral gene delivery vectors: cytotoxicity and transfection efficiency," *Journal of Controlled Release*, vol. 103, no. 3, pp. 643–653, 2005.

[12] F.-Q. Hu, M.-D. Zhao, H. Yuan, J. You, Y.-Z. Du, and S. Zeng, "A novel chitosan oligosaccharide-stearic acid micelles for gene delivery: properties and in vitro transfection studies," *International Journal of Pharmaceutics*, vol. 315, no. 1-2, pp. 158–166, 2006.

[13] G. Y. Wu and C. H. Wu, "Receptor-mediated delivery of foreign genes to hepatocytes," *Advanced Drug Delivery Reviews*, vol. 29, no. 3, pp. 243–248, 1998.

[14] E. I. Rigopoulou, D. Roggenbuck, D. S. Smyk et al., "Asialoglycoprotein receptor (ASGPR) as target autoantigen in liver autoimmunity: lost and found," *Autoimmunity Reviews*, vol. 12, no. 2, pp. 260–269, 2012.

[15] T. Ishihara, A. Kano, K. Obara et al., "Nuclear localization and antisense effect of PNA internalized by ASGP-R-mediated endocytosis with protein/DNA conjugates," *Journal of Controlled Release*, vol. 155, no. 1, pp. 34–39, 2011.

[16] J. H. N. Yik, A. Saxena, J. A. Weigel, and P. H. Weigel, "Nonpalmitoylated human asialoglycoprotein receptors recycle constitutively but are defective in coated pit-mediated endocytosis, dissociation, and delivery of ligand to lysosomes," *The Journal of Biological Chemistry*, vol. 277, no. 43, pp. 40844–40852, 2002.

[17] X. L. Zhu, Y. Z. Du, R. S. Yu et al., "Galactosylated chitosan oligosaccharide nanoparticles for hepatocellular carcinoma cell-targeted delivery of adenosine triphosphate," *International Journal of Molecular Sciences*, vol. 14, no. 8, pp. 15755–15766, 2013.

[18] Z. Ma and L.-Y. Lim, "Uptake of chitosan and associated insulin in Caco-2 cell monolayers: a comparison between chitosan molecules and chitosan nanoparticles," *Pharmaceutical Research*, vol. 20, no. 11, pp. 1812–1819, 2003.

[19] S. F. Solga, A. Horska, J. M. Clark, and A. M. Diehl, "Hepatic 31P magnetic resonance spectroscopy: a hepatologist's user guide," *Liver International*, vol. 25, no. 3, pp. 490–500, 2005.

[20] I. R. Corbin, R. Buist, V. Volotovskyy, J. Peeling, M. Zhang, and G. Y. Minuk, "Regenerative activity and liver function following partial hepatectomy in the rat using 31P-MR spectroscopy," *Hepatology*, vol. 36, no. 2, pp. 345–353, 2002.

[21] I. R. Corbin, R. Buist, J. Peeling, M. Zhang, J. Uhanova, and G. Y. Minuk, "Utility of hepatic phosphorus-31 magnetic resonance spectroscopy in a rat model of acute liver failure," *Journal of Investigative Medicine*, vol. 51, no. 1, pp. 42–49, 2003.

[22] R.-S. Yu, L. Hao, F. Dong et al., "Biochemical metabolic changes assessed by 31P magnetic resonance spectroscopy after radiation-induced hepatic injury in rabbits," *World Journal of Gastroenterology*, vol. 15, no. 22, pp. 2723–2730, 2009.

[23] S.-J. Seo, I.-Y. Kim, Y.-J. Choi, T. Akaike, and C.-S. Cho, "Enhanced liver functions of hepatocytes cocultured with NIH 3T3 in the alginate/galactosylated chitosan scaffold," *Biomaterials*, vol. 27, no. 8, pp. 1487–1495, 2006.

[24] T. H. Kim, I. K. Park, J. W. Nah, Y. J. Choi, and C. S. Cho, "Galactosylated chitosan/DNA nanoparticles prepared using water-soluble chitosan as a gene carrier," *Biomaterials*, vol. 25, no. 17, pp. 3783–3792, 2004.

[25] Y. Maitani, K. Kawano, K. Yamada, T. Nagai, and K. Takayama, "Efficiency of liposomes surface-modified with soybean-derived sterylglucoside as a liver targeting carrier in HepG2 cells," *Journal of Controlled Release*, vol. 75, no. 3, pp. 381–389, 2001.

[26] S. Gao, J. Chen, X. Xu et al., "Galactosylated low molecular weight chitosan as DNA carrier for hepatocyte-targeting," *International Journal of Pharmaceutics*, vol. 255, no. 1-2, pp. 57–68, 2003.

[27] C. Yin, L. Ying, P.-C. Zhang et al., "High density of immobilized galactose ligand enhances hepatocyte attachment and function," *Journal of Biomedical Materials Research A*, vol. 67, no. 4, pp. 1093–1104, 2003.

[28] K. Leung, *Molecular Imaging and Contrast Agent Database (MICAD)*, National Center for Biotechnology Information (US), Bethesda (MD), 2004–2013, http://www.ncbi.nlm.nih.gov/books/NBK5330/.

[29] A. Akinc, W. Querbes, S. De et al., "Targeted delivery of RNAi therapeutics with endogenous and exogenous ligand-based mechanisms," *Molecular Therapy*, vol. 18, no. 7, pp. 1357–1364, 2010.

[30] E. B. Dizhe, B. N. Akifiev, B. V. Missul et al., "Receptor-mediated transfer of DNA-galactosylated poly-L-lysine complexes into mammalian cells in vitro and in vivo," *Biochemistry*, vol. 66, no. 1, pp. 55–61, 2001.

[31] A. Murao, M. Nishikawa, C. Managit et al., "Targeting efficiency of galactosylated liposomes to hepatocytes in vivo: effect of lipid composition," *Pharmaceutical Research*, vol. 19, no. 12, pp. 1808–1814, 2002.

[32] Z. Xu, L. Chen, W. Gu et al., "The performance of docetaxel-loaded solid lipid nanoparticles targeted to hepatocellular carcinoma," *Biomaterials*, vol. 30, no. 2, pp. 226–232, 2009.

Hindawi Publishing Corporation
Gastroenterology Research and Practice
Volume 2013, Article ID 617967, 8 pages
http://dx.doi.org/10.1155/2013/617967

Review Article

Enterovesical Fistulae: Aetiology, Imaging, and Management

Tomasz Golabek,[1] Anna Szymanska,[2] Tomasz Szopinski,[1] Jakub Bukowczan,[3] Mariusz Furmanek,[4] Jan Powroznik,[5] and Piotr Chlosta[1]

[1] *Department of Urology, Collegium Medicum of the Jagiellonian University, Ulica Grzegorzecka 18, 31-531 Cracow, Poland*
[2] *Department of Interventional Radiology and Neuroradiology, Medical University of Lublin, Ulica Jaczewskiego 8, 20-954 Lublin, Poland*
[3] *Department of Endocrinology and Diabetes, Royal Victoria Infirmary, Queen Victoria Road, Newcastle upon Tyne NE1 4LP, UK*
[4] *Department of Radiology, Central Clinical Hospital Ministry of Interior in Warsaw, ul. Wolowska 137, 02-507 Warsaw, Poland*
[5] *The 1st Department of Urology, Postgraduate Medical Education Centre, European Health Centre in Otwock, ul. Borowa 14/18, 05-400 Otwock, Poland*

Correspondence should be addressed to Tomasz Golabek; elementare@op.pl

Received 3 September 2013; Accepted 29 October 2013

Academic Editor: Iwona Sudoł-Szopinska

Copyright © 2013 Tomasz Golabek et al. This is an open access article distributed under the Creative Commons Attribution License, which permits unrestricted use, distribution, and reproduction in any medium, provided the original work is properly cited.

Background and Study Objectives. Enterovesical fistula (EVF) is a devastating complication of a variety of inflammatory and neoplastic diseases. Radiological imaging plays a vital role in the diagnosis of EVF and is indispensable to gastroenterologists and surgeons for choosing the correct therapeutic option. This paper provides an overview of the diagnosis of enterovesical fistulae. The treatment of fistulae is also briefly discussed. *Material and Methods*. We performed a literature review by searching the Medline database for articles published from its inception until September 2013 based on clinical relevance. Electronic searches were limited to the keywords: "enterovesical fistula," "colovesical fistula" (CVF), "pelvic fistula", and "urinary fistula". *Results*. EVF is a rare pathology. Diverticulitis is the commonest aetiology. Over two-thirds of affected patients describe pathognomonic features of pneumaturia, fecaluria, and recurrent urinary tract infections. Computed tomography is the modality of choice for the diagnosis of enterovesical fistulae as not only does it detect a fistula, but it also provides information about the surrounding anatomical structures. *Conclusions*. In the vast majority of cases, this condition is diagnosed because of unremitting urinary symptoms after gastroenterologist follow-up procedures for a diverticulitis or bowel inflammatory disease. Computed tomography is the most sensitive test for enterovesical fistula.

1. Introduction

Enterovesical fistula (EVF) represents an abnormal communication between the intestine and the bladder. Although EVF are uncommon, they cause significant morbidity and may markedly affect patient's quality of life. Enterovesical fistulae most frequently occur as a consequence of advanced-stage disease or due to traumatic or iatrogenic injuries. The diagnosis of EVF can be challenging and is often delayed for several months after symptoms begin. Radiological imaging plays a vital role in establishing the site, course, and complexity of fistulae and in identifying an aetiological factor. This paper describes the imaging appearances of enterovesical fistulae and the option for their management.

2. Material and Methods

A comprehensive search strategy was applied for Medline/PubMed electronic database from its inception until September 2013. We selected all human research articles published in English, not classified as case report, editorial, comment, letter, or news. The search strategy included the following terms: "enterovesical fistula," "colovesical fistula", "pelvic fistula" and "urinary fistula".

3. Results and Discussion

We found a total of 274 papers about urinary tract fistulae and a total of 75 articles specifically related to EVF. Among these, 70 were original articles and 5 were reviews.

3.1. Aetiology of Enterovesical Fistulae. It is estimated that enterovesical fistulae account for 1 in every 3,000 surgical hospital admissions [1]. EVF most frequently occur in a setting of inflammatory bowel disease. Diverticulitis is the commonest aetiology accounting for approximately 65–79% of cases, which are almost exclusively colovesical [2–5]. The relative risk for developing enterovesical fistula in the presence of diverticular disease is between 1 and 4% [4, 6]. The underlying mechanism of it is a direct extension of ruptured diverticulum or erosion of a peridiverticular abscess, into the bladder, and a phlegmon and abscess are the risk factors for subsequent fistula formation [4, 5, 7]. The second most common cause of EVF is cancer (10–20% of cases), followed by Crohn's disease (5–7%) [4, 8, 9]. While only approximately 2% of patients with Crohn's disease develop EVF, ileovesical fistula remains the most common type [8, 10]. Regional enteritis, secondary to the transmural inflammation characteristic of Crohn's colitis, may result in adherence to the bladder with subsequent erosion into the organ and further fistula formation [8, 9]. The mean duration of Crohn's disease at the time of onset of EVF-related symptoms is 10 years and an average patient's age is 30 [9]. Less-common inflammatory causes of EVF include Meckel's diverticulum, genitourinary coccidioidomycosis, pelvic actinomycosis, and appendicitis [11–14]. Advanced-stage colon and bladder malignancies account for up to one-fifth of all cases, with the latter being extremely rare [4, 15]. Other urogenital malignancies, as well as lymphoma, cause EVF only occasionally [16, 17]. The iatrogenic aetiology of enterovesical fistulae may occur as a consequence of general surgical procedures (particularly for colorectal cancer, diverticulitis, or inflammatory bowel disease), as well as vascular and urological interventions [18, 19]. Fistulae may also develop as a complication of both chemo- and radiation therapy. External beam radiation or brachytherapy to the bowel in the treatment field can precipitate fistula formation by inducing progressive endarteritis obliterans, which subsequently may result in necrosis and breakdown of mucosal surfaces [20]. Radiation-associated fistulae usually develop years after radiation therapy for gynaecological or urological malignancies [20, 21]. Enterovesical fistulae, secondary to cytotoxic therapy, are extremely rare and have been previously reported in a patient undergoing chemotherapy for non-Hodgkin's lymphoma [22]. Other uncommon causes of EVF include penetrating abdominal or pelvic injuries and foreign bodies in the bowel and peritoneum [5, 23].

3.2. Types of Enterovesical Fistulae. Classification of enterovesical fistulae is based on the bowel segment involved. All EVF can be divided into the following 4 primary categories: (i) colovesical, (ii) rectovesical (including rectourethral), (iii) ileovesical, and (iv) appendicovesical fistulae. While colovesical fistula is the most common form of vesicointestinal fistula and is most frequently located between the sigmoid colon and the dome of the bladder, rectovesical fistulae are observed in the postoperative setting (i.e., after prostatectomy) [24]. A key consideration in determining optimal management of EVF is not only the termination point of the fistula tract but also the complexity of the fistula itself. Simple enterovesical fistulae are usually small and single and occur in nonradiated tissue. Complex EVF are larger, have multiple tracts, often develop in a previously irradiated tissue, and are commonly accompanied by a pelvic abscess or a colonic obstruction [2, 21].

3.3. Clinical Manifestations and Diagnosis. Symptoms of vesicoenteric fistulae may originate from both the urinary and the gastrointestinal tracts. However, patients with EVF usually present with lower urinary tract symptoms, which include pneumaturia (the most common symptom present in 50–70% of cases), fecaluria (reported in up to 51%), frequency, urgency, suprapubic pain, recurrent urinary tract infections (UTIs), and haematuria [5, 8, 21, 25]. Over 75% of affected patients describe pathognomonic features of pneumaturia, fecaluria, and recurrent UTIs due to *Escherichia coli*, coliform bacteria, mixed growth, or enterococci [4, 5, 21]. The hallmark of enterovesical fistulae is Gouverneur's syndrome characterised by suprapubic pain, frequency, dysuria and tenesmus [26]. Physical signs include malodorous urine and debris in the urine, as well as less commonly reported fever. Additionally, symptoms of an underlying disease causing the fistula may be present. In patients with fistulating Crohn's disease, abdominal pain, abdominal mass, and abscess are more common [27].

3.4. Diagnostic Algorithm. The diagnosis of an enterovesical fistula poses a significant challenge as there is no consensus on any clear gold standard for EVF workup. A review of the literature showed that enterovesical fistulae are most commonly diagnosed based on clinical evidence. Nevertheless, diagnostic verification of EVF is necessary not only to establish the presence of a fistula but also to exclude stricture of the bowel and presence of abscess and to evaluate the anatomical region of involved intestine to guide the subsequent surgery [28]. Although cystoscopy, with the highest yield in identifying a potential lesion, is an essential component of the entire investigation process, its findings are usually nonspecific and include erythema, oedema, and congestion. Endoscopic evaluation of the urinary bladder fails to identify EVF in 54–65% of cases [4, 25, 28]. Colonoscopy is not particularly valuable in detecting fistulae. A detection rate for EVF can be as low as 8.5% and does not usually exceed 55% [25, 29, 30]. However, as 10%–15% of colovesical fistulae are secondary to neoplasms, endoscopic examination of the large bowel should be an integral part of CVF workup. It is helpful in determining the nature of the bowel pathology responsible for the fistula formation [4, 5, 25].

The poppy seed test involves oral intake of 50 mg of poppy seeds mixed in beverage or yoghurt. Since seeds remain largely undigested through the gastrointestinal tract, they may appear in urine within 48 hours following intake which is considered a positive confirmatory test for enterovesical fistula. Kwon et al. compared the accuracy of the poppy seed

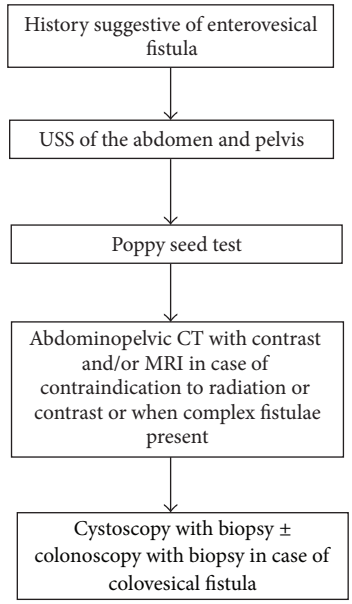

Figure 1: Diagnostic imaging and procedures algorithm for enterovesical fistulae.

test with CT scanning and nuclear cystography in 20 patients with surgically confirmed fistulae. The poppy seed test yielded a 100% detection rate, whereas CT scanning and nuclear cystography yielded rates of 70% and 80%, respectively. The poppy seeds test is inexpensive and easy to perform; however, it provides little detail regarding the location and type of fistula present [29].

The proposed algorithm for diagnosis of enterovesical fistula is presented in Figure 1.

4. Imaging Techniques and Appearances

4.1. Ultrasonographic Examination. Ultrasonography (USS) may be useful in the diagnosis of colovesical fistulae. In some instances, the fistula is easily identified, with no additional manoeuvers needed [31]. Its detection rate in small series reached 100% [32]. The yield of the transabdominal ultrasonographic examination for suspected fistula can be enhanced by the use of abdominal compression, which reveals an echogenic "beak sign" connecting the peristaltic bowel lumen and the urinary bladder [33]. The identification of the ureteric orifices with their associated urinary jets and the use of lower abdominal compression are essential components of this technique.

Anorectal, transrectal, and transvaginal ultrasonography can help to identify a fistulous tract, as well as its relation to the adjacent anatomical structures (Figures 2(a), 2(b), and 2(c)) [34, 35].

4.2. Computed Tomography Examination. Computed tomography (CT) is the modality of choice for the diagnosis of enterovesical fistulae due to its high sensitivity for the detection of EVF, but more importantly it provides essential additional information about the adjacent anatomical structures [5, 25, 36]. Moreover, the underlying pathology of colovesical fistulae is, in the majority of cases, an extraluminal disease process, and CT scanning is an optimal modality to detect pericolic complications of the diverticular disease [2–5, 7]. The diagnostic accuracy of computed tomography for detecting colovesical fistulae is up to 90–100% [5, 36–38]. CT scanning should be performed following oral administration of contrast but prior to intravenous administration of contrast, in order to permit detection of Gastrografin or other diluted iodinated contrast agents within the bladder. The findings on CT, which are suggestive of enterovesical fistula include (i) air in the bladder (in the absence of previous lower urinary tract instrumentation), (ii) oral contrast medium in the bladder on nonintravenous contrast enhanced scans, (iii) presence of colonic diverticula, and (iv) bladder wall thickening adjacent to a loop of thickened intestine (Figures 3, 4(a), and 4(b)) [4, 5, 37, 39]. The pathognomonic finding of air within the urinary bladder contributes to the high diagnostic accuracy of CT in detecting EVF; however, false positives may occur following recent lower urinary tract instrumentation or due to active urinary tract infection with a gas-forming organism.

Compared with conventional axial CT imaging, 3-dimensional CT provides better visualisation of the anatomical relationship of the bladder and EVF to adjacent structures [40, 41]. Majority of modern CT scanners can acquire a raw data volume enabling almost immediate three planar reconstruction without additional cost.

4.3. Magnetic Resonance Imaging. Although computed tomography is the modality of choice in evaluation of colovesical fistulae, the actual fistulous tract is identified on CT only occasionally [36, 37]. Magnetic resonance imaging (MRI) has excellent intrinsic soft tissue resolution together with its multiplanar imagining capability. Moreover, MRI allows accurate depiction of fistulous tract without the necessity of direct opacification required in CT scanning. Its use in colovesical fistulae is well established and its sensitivity and specificity reach up to 100% [25, 42–44]. The appearance of a fistula on MRI depends whether it is filled with fluid, air, or a combination of both. Therefore, the use of combined sequences is ideal. T1-weighted images delineate the extension of the fistula relative to sphincters and adjacent hollow viscera and show inflammatory changes in fat planes. On T2-weighted images, the fistula typically produces a high-signal-intensity, fluid-filled communication, whereas the air-filled fistulous tract is seen as a low signal intensity, regardless of the pulse sequence used [43, 44]. In cases of fistulae due to diverticulitis, abscess (containing high-signal fluid on T2-weighted images) is commonly seen lying between the inferior wall of the sigmoid colon and the superior bladder wall (which is thickened and inflamed) [42].

Use of intravenous gadolinium enhancement significantly improves the detection of bladder fistulae. Early postgadolinium T1-weighted images show enhancement of tract walls and signal void fluid centrally [44]. Both axial and sagittal planes are useful for the detection of enterovesical fistulae [42–44]. Use of short tau inversion-recovery (STIR) images has not been established in the literature yet. Although

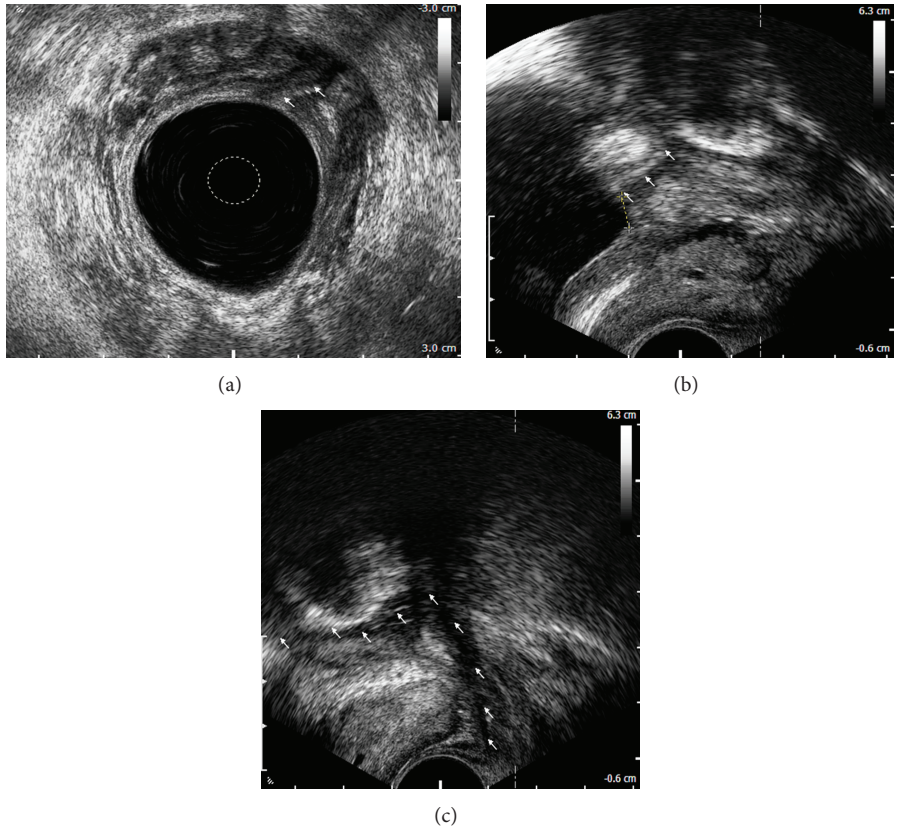

(a) (b)

(c)

Figure 2: Rectovesical fistula: anorectal endosonographic view of a fistulous orifice in the urinary bladder (arrows) (a), transrectal ultrasonographic view of a fistulous orifice (arrows) located 6 mm from the internal outlet of the bladder (crosses) (b), and transrectal ultrasonographic view of a fistulous tract adjacent to the left lobe of the prostate (arrows) (c).

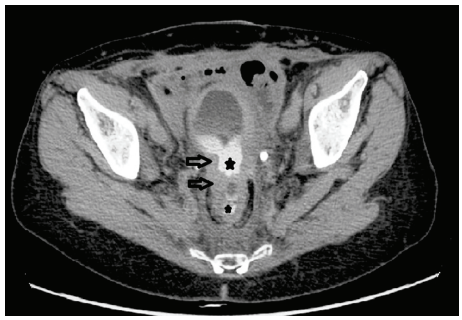

Figure 3: Colovesical fistula: axial image in the delayed phase of CT urogram demonstrates bladder and rectal wall thickening (arrows) with contrast present in both (∗).

MRI allows for a precise delineation of fistulous tracts, its high cost and the common lack of MRI access within the emergency room limit its use to more complex elective cases.

4.4. Radiographic Examinations. A plain abdominal X-ray is not generally helpful, although when taken with the patient standing may show an air-fluid level within the bladder. Similarly, intravenous urography fails to demonstrate the fistula, unless the patient has severe outlet obstruction [45].

Barium enemas (BE) have a limited role in the diagnosis of enterovesical fistulae due to a low sensitivity of approximately 30% [29, 46]. However, it may be useful in differentiating diverticular disease from colonic cancer as a cause of EVF. Radiographic examination of centrifuged first urine sample obtained immediately after a nondiagnostic BE, called the Bourne test, may significantly enhance the yield of the barium study [46, 47]. Radiodense particles detected in the urine sediment confirm the presence of a fistula [40, 41]. A detection rate for colovesical fistulae can even reach 90% [46]. However, currently its role in an enterovesical fistula workup is marginal since CT and other more advanced studies provide explicit information regarding not only the presence or absence of a fistula but more importantly about its location, complexity, and surrounding anatomical structures.

Enterovesical fistulae may be evaluated with cystography which may demonstrate contrast outside the bladder; however, it is less likely to demonstrate a fistula [25]. A detection rate for enterovesical fistula ranges between 20% and 30% [29]. The herald sign is a crescentic defect on the upper margin of the bladder and it represents a perivesical abscess. The pathognomonic finding of colovesical fistula is the "beehive" sign caused by the elevation of the bladder wall at the vesical end of the fistulous tract [5, 48].

The use of Tc-99 m DTPA as a valuable method in diagnosis of enterovesical fistula has been reported [49, 50].

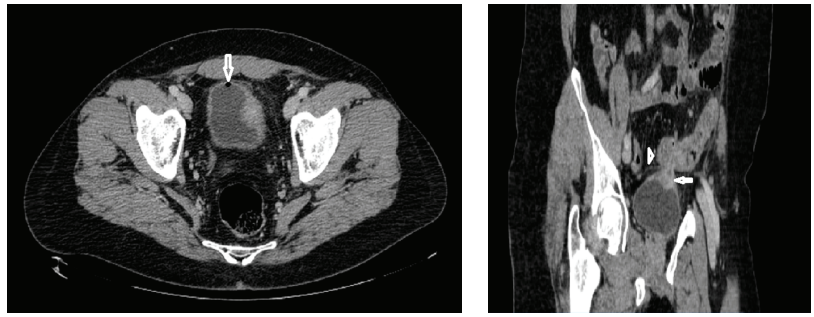

(a) (b)

Figure 4: Colovesical fistula: axial image of contrast enhanced CT of the abdomen and pelvis demonstrates air in the bladder (arrow) and thickened left bladder wall (a); sagittal image shows bladder wall thickening (arrow) adjacent to a loop of thickened sigmoid colon (arrow head) (b).

It is a simple and readily available tool, which provides anatomic as well as functional information about the urinary tract. Moreover, it may demonstrate the presence and location of a fistula indicated by the passing of the radioactive urine from the urinary system into the bowel. The severity of EVF can be determined by assessing the urine flow rate that passes through the fistula [51].

Because of the superiority of CT scanning, as a tool for diagnosis and treatment planning, plain cystography, and radionuclide renography are only occasionally used in the evaluation of enterovesical fistulae.

Advantages and disadvantages of diagnostic tests and procedures used for detection of enterovesical fistulae are presented in Table 1.

5. Management of Enterovesical Fistulae

5.1. Conservative Management. Nonoperative treatment of enterovesical fistulae may be an option in nontoxic, minimally symptomatic patients with nonmalignant EVF origin, particularly in those with Crohn's disease. A trial of medical therapy including bowel rest, total parenteral nutrition, antibiotics, steroids, immunomodulatory drugs, and urethral catheter drainage may be warranted [52]. In patients with colovesical fistulae, conservative management has been reported to be associated with the same disease-specific mortality as with the surgical treatment [28, 53]. However, others have found significantly more deaths related to poor physical condition, progression of malignant disease, and the septic effect of the EVF [30, 54]. Therefore, nonsurgical management of colovesical fistulae is generally reserved for patients unfit for major intervention or with extensive unresectable neoplastic process. In those cases, medical therapy with catheter drainage of the bladder alone or supravesical percutaneous diversion could be beneficial. However, most patients will require a diverting stoma in due course of a disease.

5.2. Surgical Repair. Endoscopic, open, and laparoscopic approaches have all been used in surgical treatment of enterovesical fistulae [2, 8, 52, 55–59]. Colonoscopic closure of iatrogenic perforations <1 cm is a valuable option of a minimally invasive treatment. In such cases, repair of the perforation can be achieved using the TriClip device [55]. Endoscopic treatment of enterovesical fistulae due to colorectal cancer is commonly associated with bowel stenosis and requires the use of covered self-expanding metal stents. This technique allows for the application of stents within the stenotic bowel segment, even in the presence of a neoplastic, fragile tissue, without further narrowing of its lumen. However, this method is contraindicated in the management of enterovesical fistula caused by diverticulitis as stent placement is associated with high risk of the colon perforation [60].

Operative management of enterovesical fistulae is mainly dependent on the underlying pathology, site of the bowel lesion, and patient's preoperative status. Both open and laparoscopic approaches have been used for the treatment of enterovesical fistula [2, 8, 57, 58]. The aim of operative management is to resect and reanastomose the offending bowel segment and to close the bladder. The treatment may involve single-stage or multistage procedures [2, 52]. The former involves resection and primary anastomosis without a protective colostomy, whereas, during the latter, resection and primary anastomosis with colostomy and/or Hartmann procedure are performed (two-stage procedure) with later closure of the stoma (three-stage approach). Staged procedures have been advocated in patients with gross faecal contamination and large intervening pelvic abscesses or in those with advanced malignancy or radiation changes [2, 8]. Historically, proximal defunctioning procedures as sole interventions have been recommended in the management of EVF [61]. Although they are associated with low surgical trauma, they are unlikely to result in a fistula tract closure. Moreover, a fistula often recurs following reversal of a colostomy and patients may still remain prone to urinary sepsis [53].

Bowel resection with primary anastomosis is advocated in the majority of EVF cases [2, 25]. Successful one-stage resections have been reported in 18% to 92% of EVF cases [54, 62]. Surgical technique involves blunt dissection of the bowel from the bladder, resection of the intestine, and primary anastomosis. As an opening of a fistulous tract in the bladder may not be directly visible, distention of the bladder with methylene blue solution instilled through a catheter may

Table 1: Advantages and disadvantages of diagnostic tests and procedures used for the detection of enterovesical fistulae.

Modality	Advantages	Disadvantages
Cystoscopy	Direct visualisation of the bladder Allows for the biopsy of a lesion	Invasive test Visualises only intraluminal content Success rate of 35%–46%
Colonoscopy	Helps to identify bowel pathology that caused a colovesical fistula	Invasive test Visualises only intraluminal content Success rate of 8.5%–55%
Poppy seed test	Noninvasive Inexpensive Convenient to perform Accuracy of up to 100%	Does not provide information on fistula location and type
Transabdominal ultrasonography	No X-ray exposure Inexpensive and available Success rate of up to 100%	Does not provide more detailed information regarding complexity of a fistula
Abdominopelvic CT	Modality of choice Diagnostic accuracy between 30 and 100% Provides information about the complexity of a fistula and the surrounding anatomical structures	X-ray exposure Expensive Often fails to identify fistulous tract
MRI	No X-ray exposure Helpful in complex cases Success rate of up to 100%	Expensive Limited availability
Barium enema	Useful in differentiating diverticular disease from colonic cancer Low perforation rates (<1%)	X-ray exposure Barium peritonitis Visualises only intraluminal content Detection rate of approximately 30%
Bourne test	Inexpensive Detection rate for colovesical fistulae of up to 90%	Does not provide information on fistula location and type
Cystogram	Easy to perform Available	X-ray exposure Low detection rate Does not provide information on fistula location Not helpful in case of a complex fistula

be helpful. The type of bladder repair, whether excision or oversewing, is not of critical importance since small defects do not require closure and may be left to heal spontaneously [63]. Although no strong evidence is available, if technically possible, interposition of the omental flap between the bladder and intestine may be employed. Such maneuver might improve healing process and reduce the fistula recurrence rate due to high vascularity and immunological properties of the omentum [64].

Surgical management of radiation-induced enterovesical fistulae is challenging and in severe cases impossible as no clear planes between the anatomical structures can be identified. Moreover, radiation-induced fistulae are more likely to recur. Hence, in such patients, a proximal defunctioning stoma may be an option as it can improve their quality of life.

The outcome of enterovesical fistulae management is, in the majority of cases, excellent. Postoperative recurrence of EVF is uncommon in patients with benign and nonradiation-induced fistulae. Persistence of a fistula after presumably definitive treatment may also be related to malignancy, nutritional issues, unrecognised foreign body, or surgical factors.

6. Conclusions

Enterovesical fistulae are an uncommon complication of both benign and malignant processes. The diagnosis of EVF may, however, be challenging. With a high index of suspicion for fistula formation in patients presenting with symptoms suggestive of abnormal communication between the intestine and the bladder, appropriate radiological investigation can lead to a significant reduction in morbidity. Recognition of a fistulous tract, delineation of its course, and characterisation of its complexity affect the EVF management. In this respect, cross-sectional imaging with CT and MRI remains an ideal modality option in patients with enterovesical fistulae. Management of EVF is mainly dependent on the underlying pathology, site of the bowel lesion, and patient's preoperative performance status. Surgical one-stage strategy is a preferred option in most of the cases.

References

[1] J. I. Pugh, "On the pathology and behaviour of acquired non-traumatic vesico-intestinal fistula," *The British Journal of Surgery*, vol. 51, pp. 644–657, 1964.

[2] W. J. Mileski, R. J. Joehl, R. V. Rege, and D. L. Nahrwold, "One-stage resection and anastomosis in the management of colovesical fistula," *American Journal of Surgery*, vol. 153, no. 1, pp. 75–79, 1987.

[3] S. G. Pollard, R. Macfarlane, and R. Greatorex, "Colovesical fistula," *Annals of the Royal College of Surgeons of England*, vol. 69, no. 4, pp. 163–165, 1987.

[4] I. R. Daniels, B. Bekdash, H. J. Scott, C. G. Marks, and D. R. Donaldson, "Diagnostic lessons learnt from a series of enterovesical fistulae," *Colorectal Disease*, vol. 4, no. 6, pp. 459–462, 2002.

[5] S. F. Najjar, M. K. Jamal, J. F. Savas, and T. A. Miller, "The spectrum of colovesical fistula and diagnostic paradigm," *American Journal of Surgery*, vol. 188, no. 5, pp. 617–621, 2004.

[6] A. M. Bahadursingh, K. S. Virgo, D. L. Kaminski, and W. E. Longo, "Spectrum of disease and outcome of complicated diverticular disease," *American Journal of Surgery*, vol. 186, no. 6, pp. 696–701, 2003.

[7] K. P. Balsara and C. Dubash, "Complicated sigmoid diverticulosis," *Indian Journal of Gastroenterology*, vol. 17, no. 2, pp. 46–47, 1998.

[8] D. Randall, V. Tittle, G. Wright, and C. Blanshard, "Crohn's disease and enterovesical fistulae: common things are common," *British Journal of Hospital Medicine*, vol. 71, no. 9, pp. 530–531, 2010.

[9] G. Gatta, G. Di Grezia, V. Di Mizio et al., "Crohn's disease imaging: a review," *Gastroenterology Research and Practice*, vol. 2012, Article ID 816920, 15 pages, 2012.

[10] J. S. Gruner, J. K. Sehon, and L. W. Johnson, "Diagnosis and management of enterovesical fistulas in patients with Crohn's disease," *American Surgeon*, vol. 68, no. 8, pp. 714–719, 2002.

[11] M. Bouassida, M. M. Mighri, K. Trigui et al., "Meckel's diverticulum: an exceptional cause of vesicoenteric fistula: case report and literature review," *The Pan African Medical Journal* , vol. 15, p. 9, 2013.

[12] J. R. Kuntze, M. H. Herman, and S. G. Evans, "Genitourinary coccidioidomycosis," *The Journal of Urology*, vol. 140, no. 2, pp. 370–374, 1988.

[13] J. V. Piper, B. A. Stoner, S. K. Mitra, and A. Talerman, "Ileovesical fistula associated with pelvic actinomycosis," *British Journal of Clinical Practice*, vol. 23, no. 8, pp. 341–343, 1969.

[14] A. Athanassopoulos and M. J. Speakman, "Appendicovesical fistula," *International Urology and Nephrology*, vol. 27, no. 6, pp. 705–708, 1995.

[15] C.-H. Yang, K.-H. Liu, T.-C. Chen, P.-L. Chang, and T.-S. Yeh, "Enterovesical fistula caused by a bladder squamous cell carcinoma," *World Journal of Gastroenterology*, vol. 15, no. 33, pp. 4215–4217, 2009.

[16] A. B. Paul and J. Thomas StJ., "Enterovesical fistual caused by small bowel lymphoma," *British Journal of Urology*, vol. 71, no. 1, pp. 101–102, 1993.

[17] D. H. Patel, S. Dang, F. R. Bentley, R. N. Julka, K. W. Olden, and F. Aduli, "Carcinosarcoma of the colon: a rare cause of colovesical fistula," *American Surgeon*, vol. 75, no. 4, pp. 335–337, 2009.

[18] N. A. Armenakas, G. Pareek, and J. A. Fracchia, "Iatrogenic bladder perforations: longterm followup of 65 patients," *Journal of the American College of Surgeons*, vol. 198, no. 1, pp. 78–82, 2004.

[19] M. Y. Lind, E. J. Hazebroek, W. J. Kirkels, W. C. J. Hop, W. Weimar, and J. N. M. Ijzermans, "Laparoscopic versus open donor nephrectomy: ureteral complications in recipients," *Urology*, vol. 63, no. 1, pp. 36–39, 2004.

[20] G. S. Gerber and H. W. Schoenberg, "Female urinary tract fistulas," *The Journal of Urology*, vol. 149, no. 2, pp. 229–236, 1993.

[21] R. B. McBeath, M. Schiff Jr., V. Allen, M. R. Bottaccini, J. I. Miller, and J. T. Ehreth, "A 12-year experience with enterovesical fistulas," *Urology*, vol. 44, no. 5, pp. 661–665, 1994.

[22] M. S. Ansari, G. Nabi, I. Singh, A. K. Hemal, and G. Pandey, "Colovesical fistula an unusual complication of cytotoxic therapy in a case of non-Hodgkin's lymphoma," *International Urology and Nephrology*, vol. 33, no. 2, pp. 373–374, 2001.

[23] P. L. Crispen, B. T. Kansas, P. G. Pieri et al., "Immediate postoperative complications of combined penetrating rectal and bladder injuries," *Journal of Trauma*, vol. 62, no. 2, pp. 325–329, 2007.

[24] M. Tonolini and R. Bianco, "Multidetector CT cystography for imaging colovesical fistulas and iatrogenic bladder leaks," *Insights Imaging*, vol. 3, no. 2, pp. 181–187, 2012.

[25] S. Melchior, D. Cudovic, J. Jones, C. Thomas, R. Gillitzer, and J. Thüroff, "Diagnosis and surgical management of colovesical fistulas due to sigmoid diverticulitis," *The Journal of Urology*, vol. 182, no. 3, pp. 978–982, 2009.

[26] J. Vidal Sans, J. Pradell Teigell, and J. Palou Redorta, "Review of 31 vesicointestinal fistulas: diagnosis and management," *European Urology*, vol. 12, no. 1, pp. 21–27, 1986.

[27] M. A. Pontari, M. A. McMillen, R. H. Garvey, and G. H. Ballantyne, "Diagnosis and treatment of enterovesical fistulae," *American Surgeon*, vol. 58, no. 4, pp. 258–263, 1992.

[28] M. H. Solkar, M. J. Forshaw, D. Sankararajah, M. Stewart, and M. C. Parker, "Colovesical fistula—is a surgical approach always justified?" *Colorectal Disease*, vol. 7, no. 5, pp. 467–471, 2005.

[29] E. O. Kwon, N. A. Armenakas, S. C. Scharf, G. Panagopoulos, and J. A. Fracchia, "The poppy seed test for colovesical fistula: big bang, little bucks!," *The Journal of Urology*, vol. 179, no. 4, pp. 1425–1427, 2008.

[30] D. Kavanagh, P. Neary, J. D. Dodd, K. M. Sheahan, D. O'Donoghue, and J. M. P. Hyland, "Diagnosis and treatment of enterovesical fistulae," *Colorectal Disease*, vol. 7, no. 3, pp. 286–291, 2005.

[31] M. A. Long and J. E. Boultbee, "The transabdominal ultrasound appearances of a colovesical fistula," *British Journal of Radiology*, vol. 66, no. 785, pp. 465–467, 1993.

[32] G. Maconi, G. M. Sampietro, F. Parente et al., "Contrast radiology, computed tomography and ultrasonography in detecting internal fistulas and intra-abdominal abscesses in Crohn's disease: a prospective comparative study," *American Journal of Gastroenterology*, vol. 98, no. 7, pp. 1545–1555, 2003.

[33] D. Sutijono, "Point-of-care sonographic diagnosis of an enterovesical fistula," *Journal of Ultrasound in Medicine*, vol. 32, no. 5, pp. 883–885, 2013.

[34] I. Sudoł-szopińska, "Progress in ano-rectal endosonography," *Ultrasonografia*, vol. 40, pp. 80–89, 2010.

[35] J. Tyloch, "The ultrasound in diagnostics and the treatment the diseases of prostate gland," *Ultrasonografia*, vol. 40, pp. 90–108, 2010.

[36] S. M. Goldman, E. K. Fishman, and O. M. B. Gatewood, "CT in the diagnosis of enterovesical fistulae," *American Journal of Roentgenology*, vol. 144, no. 6, pp. 1229–1233, 1985.

[37] M. G. Sarr, E. K. Fishman, and S. M. Goldman, "Enterovesical fistula," *Surgery Gynecology and Obstetrics*, vol. 164, no. 1, pp. 41–48, 1987.

[38] T. W. Jarrett and E. D. Vaughan Jr., "Accuracy of computerized tomography in the diagnosis of colovesical fistula secondary to diverticular disease," *The Journal of Urology*, vol. 153, no. 1, pp. 44–46, 1995.

[39] J. D. Labs, M. G. Sarr, E. K. Fishman, S. S. Siegelman, and J. L. Cameron, "Complications of acute diverticulitis of the colon: improved early diagnosis with computerized tomography," *The American Journal of Surgery*, vol. 155, no. 2, pp. 331–335, 1988.

[40] G. A. Anderson, I. L. Goldman, and G. W. Mulligan, "3-dimensional computerized tomographic reconstruction of colovesical fistulas," *The Journal of Urology*, vol. 158, no. 3, pp. 795–797, 1997.

[41] T. Shinojima, F. Nakajima, and J. Koizumi, "Efficacy of 3-D computed tomographic reconstruction in evaluating anatomical relationships of colovesical fistula," *International Journal of Urology*, vol. 9, no. 4, pp. 230–232, 2002.

[42] S. Ravichandran, H. U. Ahmed, S. S. Matanhelia, and M. Dobson, "Is there a role for magnetic resonance imaging in diagnosing colovesical fistulas?" *Urology*, vol. 72, no. 4, pp. 832–837, 2008.

[43] Y. Z. Tang, T. C. Booth, D. Swallow et al., "Imaging features of colovesical fistulae on MRI," *British Journal of Radiology*, vol. 85, pp. 1371–1375, 2012.

[44] R. C. Semelka, H. Hricak, B. Kim et al., "Pelvic fistulas: appearances on MR images," *Abdominal Imaging*, vol. 22, no. 1, pp. 91–95, 1997.

[45] G. M. Kirsh, N. Hampel, J. M. Shuck, and M. I. Resnick, "Diagnosis and management of vesicoenteric fistulas," *Surgery, Gynecology and Obstetrics*, vol. 173, no. 2, pp. 91–97, 1991.

[46] M. A. Amendola, F. P. Agha, and T. L. Dent, "Detection of occult colovesical fistula by the Bourne test," *American Journal of Roentgenology*, vol. 142, no. 4, pp. 715–718, 1984.

[47] R. B. Bourne, "New aid in the diagnosis of vesicoenteric fistula," *The Journal of Urology*, vol. 91, pp. 340–342, 1964.

[48] A. V. Kaisary and R. W. Grant, "'Beehive on the bladder': a sign of colovesical fistula," *Annals of the Royal College of Surgeons of England*, vol. 63, no. 3, pp. 195–197, 1981.

[49] R. Sadeghi, M. Hiradfar, V. R. D. Kakhki, and M. Kajbafzadeh, "Radionuclide renography: a seldom used test for the detection of vesicoenteric fistula," *Hellenic Journal of Nuclear Medicine*, vol. 10, no. 3, pp. 185–186, 2007.

[50] G. Buyukdereli and I. B. Guney, "Demonstration of vesicorectal fistula on renal scan," *Clinical Nuclear Medicine*, vol. 30, no. 7, pp. 510–511, 2005.

[51] P.-F. Kao, K.-Y. Tzen, P.-L. Chang, C. R. Chang-Chien, M.-F. Tsai, and D.-L. You, "Diuretic renography findings in enterovesical fistula," *British Journal of Radiology*, vol. 70, pp. 421–423, 1997.

[52] T. Yamamoto and M. R. B. Keighley, "Enterovesical fistulas complicating Crohn's disease: clinicopathological features and management," *International Journal of Colorectal Disease*, vol. 15, no. 4, pp. 211–215, 2000.

[53] M. Amin, R. Nallinger, and H. C. Polk Jr., "Conservative treatment of selected patients with colovesical fistula due to diverticulitis," *Surgery Gynecology and Obstetrics*, vol. 159, no. 5, pp. 442–444, 1984.

[54] G. Garcea, I. Majid, C. D. Sutton, C. J. Pattenden, and W. M. Thomas, "Diagnosis and management of colovesical fistulae; six-year experience of 90 consecutive cases," *Colorectal Disease*, vol. 8, no. 4, pp. 347–352, 2006.

[55] A. Trecca, F. Gaj, and G. Gagliardi, "Our experience with endoscopic repair of large colonoscopic perforations and review of the literature," *Techniques in Coloproctology*, vol. 12, no. 4, pp. 315–321, 2008.

[56] A. Arezzo, A. Miegge, A. Garbarini, and M. Morino, "Endoluminal vacuum therapy for anastomotic leaks after rectal surgery," *Techniques in Coloproctology*, vol. 14, no. 3, pp. 279–281, 2010.

[57] J. S. Joo, F. Agachan, and S. D. Wexner, "Laparoscopic surgery for lower gastrointestinal fistulas," *Surgical Endoscopy*, vol. 11, no. 2, pp. 116–118, 1997.

[58] A. Spinelli, M. Sacchi, P. Bazzi, N. Leone, S. Danese, and M. Montorsi, "Laparoscopic surgery for recurrent Crohn's disease," *Gastroenterology Research and Practice*, vol. 2012, Article ID 381017, 6 pages, 2012.

[59] C. Giovanni, C. Emanuele, C. Roberto et al., "Laparoscopic conservative surgery of colovesical fistula: is it the right way?" *Wideochirurgia i Inne Techniki Mało Inwazyjne*, vol. 8, no. 2, pp. 162–165, 2013.

[60] T. H. Baron, "Colonic stenting: technique, technology, and outcomes for malignant and benign disease," *Gastrointestinal Endoscopy Clinics of North America*, vol. 15, no. 4, pp. 757–771, 2005.

[61] C. W. Mayo and J. M. Miller, "Surgical treatment of sigmoidovesical fistulas," *Archives of Surgery*, vol. 40, no. 5, pp. 897–891, 1940.

[62] M. J. Krco, M. A. Malangoni, S. C. Jacobs, and R. K. Lawson, "Colovesical fistulas," *Urology*, vol. 23, no. 4, pp. 340–342, 1984.

[63] G. Scozzari, A. Arezzo, and M. Morino, "Enterovesical fistulas: diagnosis and management," *Techniques in Coloproctology*, vol. 14, no. 4, pp. 293–300, 2010.

[64] D. P. O'Leary, "Use of the greater omentum in colorectal surgery," *Diseases of the Colon and Rectum*, vol. 42, no. 4, pp. 533–539, 1999.

Hindawi Publishing Corporation
Gastroenterology Research and Practice
Volume 2013, Article ID 469097, 9 pages
http://dx.doi.org/10.1155/2013/469097

Clinical Study

Surveillance of HCC Patients after Liver RFA: Role of MRI with Hepatospecific Contrast versus Three-Phase CT Scan—Experience of High Volume Oncologic Institute

Vincenza Granata,[1] Mario Petrillo,[1] Roberta Fusco,[1] Sergio Venanzio Setola,[1] Elisabetta de Lutio di Castelguidone,[1] Orlando Catalano,[1] Mauro Piccirillo,[2] Vittorio Albino,[2] Francesco Izzo,[2] and Antonella Petrillo[1]

[1] *Division of Radiology, Department of Diagnostic Imaging, Radiant and Metabolic Therapy, "Istituto Nazionale Tumori Fondazione Giovanni Pascale-IRCCS", Via Mariano Semmola, 80131 Naples, Italy*
[2] *Division of Hepato-Biliary Surgery, Department of Abdominal Oncology, "Istituto Nazionale Tumori Fondazione Giovanni Pascale-IRCCS", Via Mariano Semmola, 80131 Naples, Italy*

Correspondence should be addressed to Antonella Petrillo; antonellapetrillo2@gmail.com

Received 29 August 2013; Accepted 3 October 2013

Academic Editor: Monica Lupsor Platon

Copyright © 2013 Vincenza Granata et al. This is an open access article distributed under the Creative Commons Attribution License, which permits unrestricted use, distribution, and reproduction in any medium, provided the original work is properly cited.

Purpose. To compare the diagnostic accuracy of hepatospecific contrast-enhanced MRI versus triple-phase CT scan after radiofrequency ablation (RFA) in hepatocellular carcinoma (HCC) patients. *Methods*. Thirty-four consecutive HCC patients (42 hepatic nodules) were treated with percutaneous RFA and underwent MR and CT scans. All patients were enrolled in a research protocol that included CT with iodized contrast medium injection and MR with hepatospecific contrast medium injection. All patients were restaged within four weeks and at 3 months from ablation. The images were reviewed by four different radiologists to evaluate tumor necrosis, residual or recurrence disease, and evidence of new foci. *Results*. Thirty-two nodules were necrotic after treatment; 10 showed residual disease. Six new HCCs were identified. At first month followup CT has identified 34 necrotic lesions and 8 residual diseases; no new foci were recognized. At MRI instead, 32 complete necrotic lesions were identified, 10 lesions showed residual disease, and 2 new HCCs were found. At three months, CT demonstrated 33 completely necrotic lesions, 9 residual diseases, and 2 new HCCs. MR showed 31 complete necrotic lesions, 11 cases of residual disease, and 6 new HCCs. *Conclusions*. Hepatospecific contrast-enhanced MRI is more effective than multiphase CT in assessment of HCC treated with RFA.

1. Introduction

Hepatocellular carcinoma (HCC) is one of the most common causes of cancer death worldwide [1]. Although surgical resection offers a better curative option than nonsurgical treatments, it is not an option for the majority of patients because of the presence of poor hepatic function and the typically advanced nature of the disease at presentation [2].

Effective nonsurgical treatment of HCC includes radiofrequency ablation (RFA). Several randomized controlled trials have demonstrated that RFA is able to achieve higher rates of complete tumor ablation using fewer sessions, with tumor necrosis rates of 90–95% in solitary HCC under 4 cm [3–7]. Assessing the effectiveness of RFA is critical in determining the success of treatment and in guiding future therapy. However, current imaging modalities and imaging response criteria are limited in their ability to provide clinically satisfactory information about the extent of tumor necrosis, which is essential in determining patient prognosis [8].

In 2000, have been established common parameters to define cancer response to therapy by means of the introduction of the Response Evaluation Criteria in Solid Tumors (RECIST). RECIST 1.1, published in January 2009, was an update to the original criteria [3]. Both criteria were based on decrease in tumor size as evidence of successful therapy

[9] resulting inadequate when new antcancer therapies are considered, being the response, quantified in terms of tumor necrosis, and not often correctly evaluated through the "one-dimensional assessment" of treated tumors. Such difficulties emerged with the introduction of regional therapies, leading to the development of new imaging evaluation criteria focused on tumor vascularization assessment, cell necrosis, mobility of water molecules, and concentration of particular metabolites in the context of tumor, pointing to a multiparametric evaluation that could add more accurate data than "one-dimensional" assessment. European Association for the Study of the Liver (EASL), in accordance with the guidelines of the American Association for the Study Liver Diseases (AASLD), recommended the assessment of lesion contrast enhancement through an MDCT examination, as "standard approach" to evaluate HCC response to therapy after local regional therapies.

The decrease in viable cell mass is not necessarily reflected by changes in tumor size, and tumors may not decrease in size after RFA despite the fact that they are nonviable [10, 11]. Tumors may apparently increase in size, and this is caused by inclusion around the treated lesion of a safety margin to improve clinical ablation success [11]. CT is the most widely used modality to confirm the technical success of RFA [12] even if MRI due to its intrinsic imaging capabilities and the absence of radiation exposure has been well shown as an alternative candidate to MDCT examination. The availability of biphasic contrast media, such as gadoxetate disodium, with a combined vascular and an elective hepatocytic uptake, is potentially able to offer more chance to standardize HCC followup after treatment, offering at the same time a morphological imaging combined with a purely functional imaging [4]. Gadoxetate disodium is a gadolinium-based liver specific MR contrast agent that differs from most of other gadolinium agents in possessing substantially increased r1 relaxivity in blood, which can be used to either reduce the dose of contrast medium or increase the degree of both vascular and parenchymal contrast enhancement. Furthermore, since about half of the gadoxetate disodium amount is eliminated through the hepatobiliary pathway, liver-specific imaging during the delayed hepatobiliary phase can be performed to improve both lesion detection and lesion characterization.

Moreover, according to EASL criteria, MRI for its intrinsic contrast resolution is particularly suitable in "identification" and "quantization" of the necrosis induced by ablative therapies. Liver-specific MR contrast agents having different pharmacokinetics, compared to traditional gadolinium chelates, opened new interesting perspectives in terms of diagnostic accuracy particularly when residual active tumor, "benign enhancement," and perilesion tissue must be differentiated; in the context of a cirrhotic liver new malignant nodules can develop. MRI with liver-specific contrast agent can be used to confirm the technical success of RFA [13].

Aim of this study was to evaluate the diagnostic accuracy of magnetic resonance imaging (MRI) by liver-specific contrast agent, gadoxetic acid (Gd-EOB-DTPA, Primovist), when compared with multidetector computed tomography (MDCT) after radiofrequency ablation (RFA), to assess the evidence of residual tumor tissue.

Table 1: Demographics, etiology of cirrhosis, and clinical stage of the 34 patients.

Patients	Score
Age (mean ± standard deviation)	60 ± 10
Sex (male/female)	2/1
Aetiology	
Virus B	14
Virus C	10
Alcohol	6
Others	4
Child-pugh	
A	8
B	25
C	1
Alpha-fetoprotein (ng/mL)	40–100

2. Materials and Methods

2.1. Patients. This study was approved by our institutional review board, and written informed consent was obtained from all patients. Between March 2009 and May 2010, 34 consecutive patients with 42 pathologically proven HCCs (diameter between 16 and 40 mm) were treated with RFA under sonography guide (Table 1).

All RFA treatments were carried out with the patient under general anesthesia and tracheal intubation, in the operating room, under sonographic guidance. One grounding pad was placed on the posterior surface of each thigh. A 250 W monopolar instrument (Radiotherapeutics, Mountain View, CA, USA), with a 12-hook 14 G electrode (LeVeen needle electrode) generating a 4 cm array diameter, was used. RFA treatment consisted typically of two phases with a one-minute cooling interval. The first RFA application lasted about 7 minutes while the second lasted about 2 minutes.

2.2. Imaging Technique. All patients underwent both a triple-phase MDCT and MR examinations, before RFA, at 1 M and at 3 M after RFA. Contrast-enhanced triple-phase helical MDCT was performed with a 16-detector row scanner (Brilliance 16, Philips Medical Systems, Eindhoven, the Netherlands). MDCT scanning parameters were 120 kVp, 189–200 mAs, 5 mm slice thickness with an increment (overlap) of 2.5 mm, and table speed of 18.75–26.75 mm/rotation (pitch 0.828–1.07). Scans were performed in craniocaudal direction. Scans were carried out including a region encompassing liver from diaphragm dome to iliac crests as follows: hepatic arterial phase scanning began 30–40 s after injection of 120 mL of a nonionic iodinated contrast media (CM, iomeprol, Iomeron 400, Bracco, Italy) at a rate of 4 mL/s with a bolus-triggered technique (120 kVp; 40–60 mA; monitoring frequency from 12 seconds after the contrast injection; trigger threshold, 100 HUs in descending aorta; delay from trigger to initiation of scan, 18 seconds); portal and equilibrium phases were obtained scanning the same region respectively 70 seconds and 180 seconds after CM injection. CM was administered

through antecubital vein with an automated injector system (Empower CTA, E-Z-EM Inc., New York, NY).

MRI examination was performed with a 1.5-T MR system (Magnetom Symphony, upgraded to Total Imaging Matrix Package, Siemens, Erlangen, Germany) with an eighteen-channel body surface phased-array coil. The liver was imaged in the axial plane in all patients both before and after administration of gadoxetic acid (Primovist, Bayer Schering Pharma, Germany) at a dose of 0.1 mL/kg (0.25 mmol/mL). The contrast agent was administered IV at a rate of 2 mL/s followed by a 20 mL saline flush through the antecubital vein with a power injector (Spectris Solaris EP MR; MEDRAD, Inc., Indianola, PA).

The MRI protocol included a respiration triggered T1-weighted turbo field-echo in-phase and out-of-phase acquisition (TR/TE 160/2.35–4.87 ms, flip angle 70°, slice thickness 5 mm, gap 20%, base resolution 256 mm, phase resolution 90%, and parallel imaging using Generalized autocalibrating partially parallel acquisition (GRAPPA) with acceleration factor 2, acquisition time 33 s) and a breath-hold multi-shot T2-weighted acquisition with and without fat suppression (TR/TE 1500/90 ms, flip angle 170°, slice thickness 5 mm, gap 0 mm, base resolution 320 mm, phase resolution 78%, and GRAPPA with acceleration factor 2, acquisition time 45 s). For gadoxetic acid-enhanced MRI, unenhanced, arterial phase (20–35 s), portal phase (70 s), equilibrium phase (3 min.), and delayed hepatobiliary phase (20 min.) images were obtained with a T1-weighted 3D turbo-field-echo sequence (T1 high-resolution isotropic volume examination, Vibe, Siemens Healthcare) (TR/TE 4.80/1.76 ms, flip angle 12°, slice thickness 3 mm, gap 20%, base resolution 320 mm, phase resolution 70%, and GRAPPA with acceleration factor 2, acquisition time 18 s).

2.3. Images Review. Four blinded observers with at least 7 years' experience in interpretation of MR and CT images of the liver independently and randomly reviewed the CT and MR images acquired at one and at three months after RFA. The four reviewers had all been involved in the original studies. The interval between reviews of the CT and MR images was at least 15 days. The observers recorded in consensus the presence and segmental location of the treated lesions, using a 4-point confidence scale (score) based on published studies on HCC [14]: 1, no residual HCC; 2, probably no residual HCC; 3, probable residual HCC; 4, definite residual HCC. They also evaluated the presence of new HCC using the same 4-point confidence scale both for arterial phase, portal phase, and hepatobiliary phase. In clinical practice at our institution, nodules that become enhanced in the arterial phase and show a washout pattern in the portal or equilibrium phase with or without capsular enhancement at triple-phase MDCT are considered HCC. So treated lesions that show an area that becomes enhanced in the arterial phase and have a washout pattern in the portal or equilibrium phase are considered still active lesions. Completely ablated lesions appear as a hypoattenuating area with no foci of contrast enhancement either within the lesion or at its periphery. Moreover, for RF ablation to be complete, the entire tumor as well as a peripheral safety margin of 0.5–1 cm of normal hepatic tissue must be ablated.

The criteria for residual HCC and new foci of HCC on gadoxetic acid-enhanced MR images were similar to the criteria for the triple-phase CT pattern. In addition, a hypointense nodule seen on gadoxetic acid-enhanced hepatobiliary phase MR images was considered HCC on the basis of previous findings [15]. A hypervascular nodule seen on gadoxetic acid-enhanced arterial phase MR images with a washout pattern was considered HCC even though the nodule appeared isointense or hyperintense relative to the surrounding liver parenchyma on hepatobiliary phase images [15]. On unenhanced T1- and T2-weighted MR imaging, the signal intensity within the ablated lesion was reported too.

The standard reference for diagnosis of complete necrosis was considered the subsequent CT and MR imaging, showing persistent absence of contrast enhancement. All cases with residual tumor tissue or with new nodules underwent biopsy.

2.4. Statistical Analysis. Sensitivity, specificity, negative predictive value and positive predictive value were reported for both imaging techniques. Fischer tests were used in order to evaluate statistical significance of table 2×2 for CT and MRI [16]. Statistical analyses for the differences of calculated sensitivity and specificity values of TC and RM were performed using McNemar test [17]. Statistical analyses for the differences of calculated positive and negative predictive values for each observer and technique were performed as previous report [17]. An analysis of all false positive and falsenegative observations was also undertaken.

The alternative free-response receiver operating characteristic (ROC) analysis of all lesions was performed tumor by tumor [18]. The area under the ROC curve, computed using trapezoid rule integration, was used to assess the diagnostic accuracy of each technique. A P value < 0.05 was considered to indicate a statistically significant difference. Statistical analysis was performed using statistic toolbox of Matlab R2007a (Matworks, Natick, MA).

3. Results

At one month, CT detected 34 necrotic lesions, including 30 true necrotic lesions and 4 false negatives. Additionally, there were 8 residual tumors detected by CT, including 6 true residual tumors (Figure 1(a)) and 2 false positives. CT failed to recognize 2 new HCCs. At 1-month followup, MR detected 32 necrotic lesions, with 31 true necrotic lesions (Figure 2) and 1 false negative. Additionally, there were 10 residual tumor diagnoses, with 9 true residual tumors (Figure 1(b)) and one false positive. MR detected 2 new HCCs. MRI had a higher sensitivity and specificity (McNemar test) than CT, at one month, and the differences between the two techniques were statistically significant ($P < 0.05$) (Table 2). Regarding the positive and negative predictive values, significant differences were seen between the two techniques with $P < 0.05$.

At 3-month followup, CT detected 33 necrotic lesions with 30 true necrotic lesions and 3 false negatives. There were also 9 residual tumors, with 7 being true residual

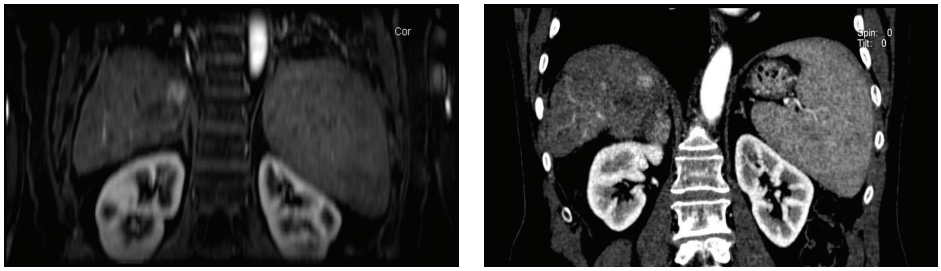

(a) (b)

Figure 1: 77-year-old man treated with RFA for HCC. (a) Arterial-phase, coronal Vibe T1-W FS at 1-month followup. Residual tumor tissue in the cephalad portion of the treated area. (b) Coronal reformatted, artery-phase CT at 1-month followup. Residual tumor tissue in the cephalad portion of the treated area.

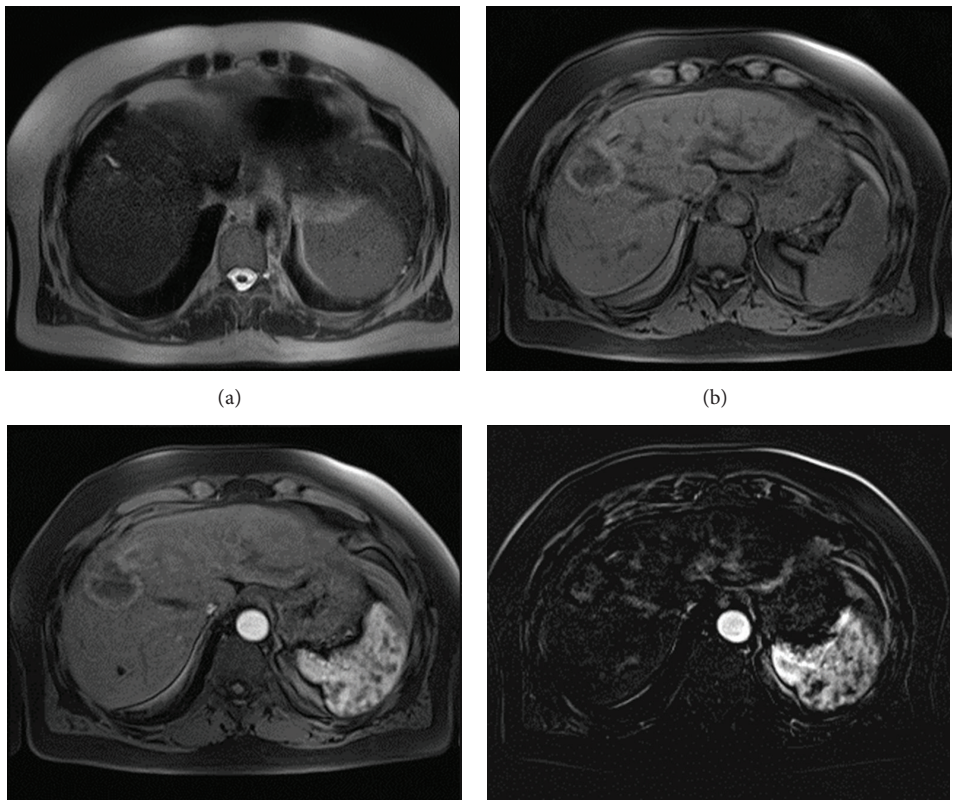

(a) (b)

(c) (d)

Figure 2: 69-year-old woman treated with RFA for HCC. (a) Axial Haste T2-W, at 1-month followup; treated necrotic nodule, heterogeneously isointense to hypointense. A dilatation of an intrahepatic biliary branch, as a complication of RFA, is recognizable. (b) Axial Vibe T1-w FS, at 1 month followup: treated necrotic nodule, heterogeneously isointense to hyperintense, with peripheral hypointense rim. (c) At 1-month followup arterial-phase scan MR image showing no contrast enhancement. (d) At 1-month followup postprocessing subtract image (arterial phase and no contrast phase) showing no contrast enhancement.

Table 2: One-month followup results.

	Sensitivity	Specificity	Positive predictive value	Negative predictive value	*P* value
CT	6/12 (50%)	30/32 (94%)	6/8 (75%)	30/36 (83%)	<0.01
MRI	11/12 (92%)	31/32 (97%)	11/12 (92%)	31/32 (97%)	<0.001

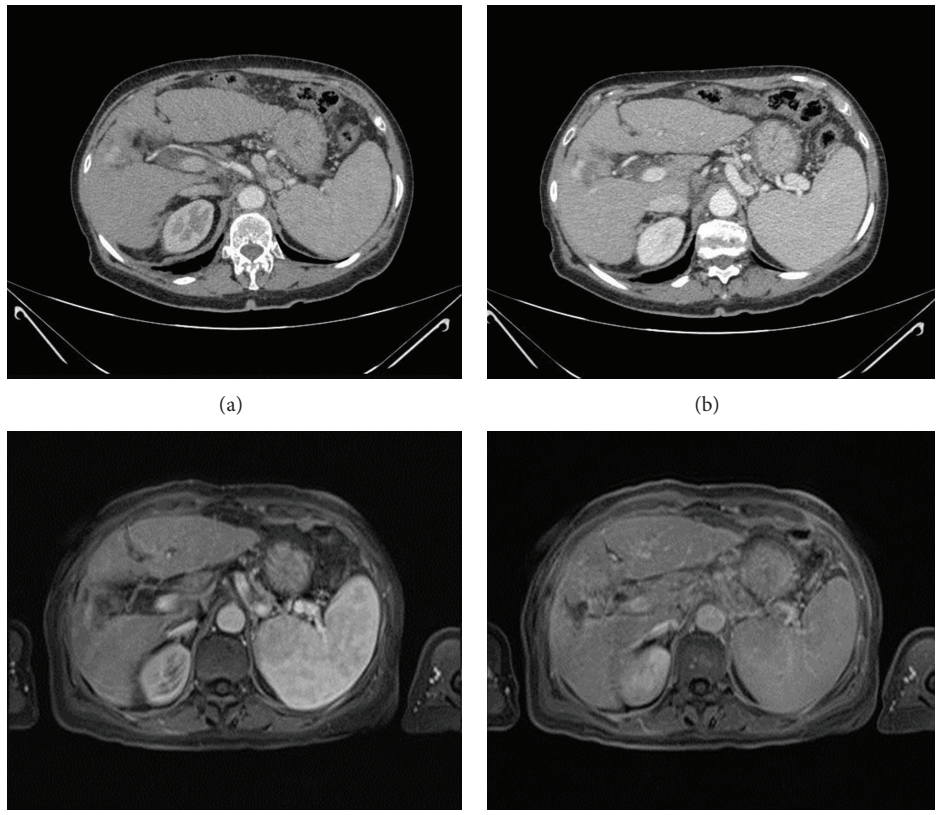

Figure 3: 66-year-old woman with an arteriovenous shunt after RFA for HCC. (a) Arterial-phase CT scan at 3-month followup. Enhancing tissue close to the ablated area, incorrectly diagnosed as residual tumor. (b) Portal-phase CT scan at 3-month followup. Enhancing tissue close to the ablated area, incorrectly diagnosed as residual tumor. The lack of washout should have raised the suspicion of a benign finding. (c) Arterial-phase MR image at 3-month followup. Enhancing tissue close to the ablated area, incorrectly diagnosed as residual tumor. (d) Portal-phase MR image at 3-month followup. The lack of wash-out and the same parenchymal enhancement identify the lesion as benign.

tumors and 2 being false positive diagnoses (Figure 3). CT recognized 2 new HCC nodules, confirmed at biopsy. At 3-month followup, MR detected 31 necrotic lesions, all being true necrotic lesions with no false negative diagnosis. There were 11 residual tumors with 10 being true residual tumors (Figure 4) and one being a false positive. MRI detected 6 new HCCs, all confirmed at biopsy. The size of these new nodules was 6–12 mm (mean, 10 mm). MRI showed a higher sensitivity and specificity (McNemar test) than CT at three months, and the difference between the two techniques was statistically significant ($P < 0.05$) (Table 3). Regarding the positive and negative predictive values, significant differences were seen between the two techniques with $P < 0.05$.

In Table 4, the CT score was reported to identify the false positive at first and three months at arterial phase and portal phase. At arterial phase CT characterizes both at first and three months all lesions as residual diseases while at portal phase only at three months seen the two lesions as probably residual diseases.

In Table 5, the MR score were reported to identify the false positive at first and three months at arterial phase, portal phase, and hepatobiliary phase. At arterial phase MR characterizes both at first and three months all lesions as residual diseases, at portal phase only one lesion as probably residuals at three months, and at hepatobiliary phase one lesion as probably residual at one month and as probably necrotic area at three months.

The gadoxetic acid-enhanced hepatobiliary phase MR images allowed identifying false positive better than arterial phase.

The area under curves calculated by ROC analysis were, respectively, for the CT followup at one month 0.98, for the CT followup at 3 months 0.99, for the MR followup at one month 0.99, and for the MR followup at 3 months 1.

MR showed a major accuracy in the identification of necrotic or residual lesions after RFA having a major area under curve.

In Table 6, the CT and MR scores were reported to identify new HCC at first months at arterial phase, portal phase, and hepatobiliary phase. CT did not see any lesions both at arterial than portal phase. MR characterized one lesion probably as new HCC at arterial phase and two lesions probably as new HCC at portal phase, while at hepatobiliary phase MR characterized both lesions as HCCs.

In Table 7, the CT and MR scores were reported at three months at arterial phase, portal phase, and hepatobiliary phase. CT seen only two lesions (2/6; 33.3%) both at arterial than portal phase. At arterial phase MR did not see two

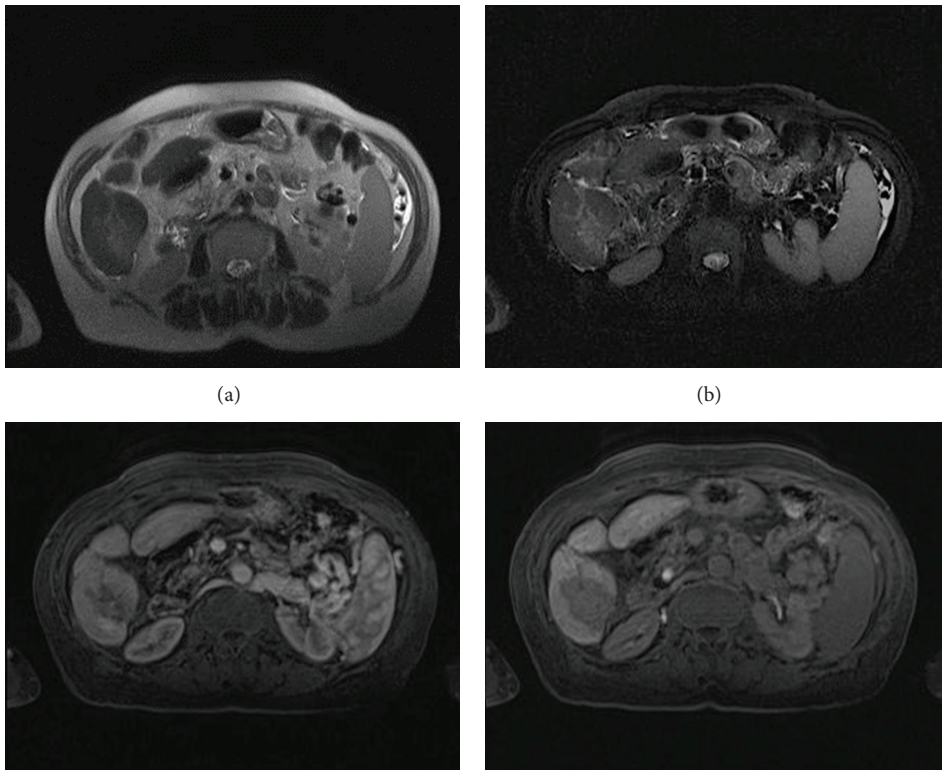

(a) (b) (c) (d)

Figure 4: 50-year-old man with an ablated HCC at segment 6. At three months, MRI showed that at T2-W (a) and T2-W FS (b) there was no inflammatory reactions while during arterial (c) and hepatospecific phase (d) residual disease was evident.

Table 3: Three-month followup results.

	Sensitivity	Specificity	Positive predictive value	Negative predictive value	*P* value
CT	9/16 (56%)	30/32 (94%)	9/11 (82%)	30/37 (81%)	<0.01
MRI	16/16 (100%)	31/32 (97%)	16/17 (94%)	31/31 (100%)	<0.001

Table 4: CT score at first (1 M) and three months (3 M) in arterial phase (AP) and portal phase (PP) for false positive.

False positive	AP CT score	PP CT score
1 M	4	4
	4	4
3 M	4	3
	4	3

Table 5: MR score at first (1 M) and three months (3 M) in arterial phase (AP), portal phase (PP), and hepatobiliary phase (HP) for false positive.

False positive	AP MR score	PP MR score	HP MR score
1 M	4	4	3
3 M	4	3	2

lesions while it characterized one lesions as probably new HCC and three lesions as new HCCs (3/6; 50%). At portal phase MR characterized three lesions as probably new HCC and three lesions as new HCCs (3/6; 50%). At hepatobiliary phase MR characterized each lesion as new HCC (6/6; 100%).

The gadoxetic acid-enhanced hepatobiliary phase MR images allowed identifying new small HCCs better than arterial phase (Figure 5).

4. Discussion

Accurate imaging evaluation is important in determining whether a tumor is completely treated or needs additional treatment. Early detection of residual or locally recurrent tumor after RF ablation of HCC is critical and can facilitate successful retreatment at an early stage. Late diagnosis results in peripheral regrowth and makes retreatment difficult owing to limited access [19].

Our study demonstrates that gadoxetate disodium-enhanced MR imaging with combined interpretation of dynamic and delayed hepatobiliary phase images significantly improves the sensitivity in the detection of residual HCC compared to multidetector CT. The diagnostic accuracy improved accordingly due to combined analysis of dynamic

Table 6: CT and MR score at first months (1 M) at arterial phase (AP), portal phase (PP), and hepatobiliary phase (HP) for new HCCs.

New HCC 1 M	AP CT score	PP CT score	AP MR score	PP MR score	HP MR score
1	1	1	3	3	4
2	1	1	2	3	4

Table 7: CT and MR score at three months (3 M) at arterial phase (AP), portal phase (PP), and hepatobiliary phase (HP) for new HCCs.

New HCC 3 M	AP CT score	PP CT score	AP MR score	PP MR score	HP MR score
1	4	4	4	4	4
2	4	4	4	4	4
3	1	1	2	3	4
4	1	1	2	3	4
5	1	1	4	4	4
6	1	2	3	3	4

and hepatobiliary phase compared to dynamic MR imaging alone and significant improvement for the combined analysis compared with multidetector CT alone.

In our study, at followup CT, all completely ablated lesions appear as a hypoattenuating area with no foci of contrast enhancement either within the lesion or at its periphery; treated areas with focal enhancement during arterial phase and wash-out during portal and equilibrium phase were considered still active tumors.

Unenhanced T1-W and T2-W MR imaging demonstrates markedly heterogeneous signal intensity within the ablated lesion. This variability in signal intensity, according to previous study, is caused by an uneven evolution of coagulation necrosis and the host response to thermal injury over time [20]. Gadolinium-enhanced dynamic MR imaging is known to be a useful diagnostic method for evaluating therapeutic response after RF ablation of HCC [21]. As at CT, the presence or absence of contrast enhancement in the treated lesion is instructive. A tumor that has been completely treated no longer enhances on gadolinium-enhanced dynamic MR images. When a tumor is not completely treated, residual or recurrent tumor is usually seen as focal and nodular enhancement at the margin of the ablated lesion. During the delayed hepatobiliary phase the residual tumor and the ablated lesion appear as a hypointense area.

In our experience, the residual HCCs were detected and assigned a high confidence score by all readers with the inclusion of delayed hepatobiliary phase MR images.

Along with improvement in sensitivity and diagnostic accuracy, a further advantage of the combined interpretation of dynamic and hepatobiliary phase MR images was the lower number of false positive findings compared with those using dynamic MR or CT image sets, with a consequent increase in positive predictive value. In agreement with previously published findings [22], most of our false positive results were small arteriovenous shunts that were misinterpreted as residual HCC because of their nodular appearance and unequivocal arterial phase enhancement at either multidetector CT or dynamic MR imaging.

With combined interpretation of dynamic and delayed hepatobiliary phase MR images, all arterial-portal venous shunts were correctly assessed by each reader, including two lesions that were prospectively misinterpreted by two readers as residual tumor on dynamic CT images alone.

The advances in imaging technology may also come at the cost of detection of an increased number of hypervascular liver lesions deemed too small to characterize, lesions that might have gone unnoticed in the past. Although most of these small undetermined lesions are nonneoplastic even in patients with pathologically proved HCC [22], in the clinical practice of radiology, any new hepatic lesion discovered at followup imaging in a cirrhotic liver must be assumed to represent an HCC until proved otherwise. On the basis of our findings and similar results [22], we believe that, as an adjunct to dynamic MR imaging, hepatobiliary phase MR images can improve the characterization of most of these undetermined, diminutive lesions.

The four false negative CT examinations were attributed to the reactive hyperemia in tissue surrounding the ablated lesion that hides the residual tumor. The combined interpretation of T2-W, dynamic and hepatobiliary phase MR images has made it possible to identify residual tumor.

Peripheral rim enhancement resulting from reactive hyperemia is usually uniform in thickness and envelops the ablated lesion, whereas residual tumor demonstrates focal and irregular peripheral enhancement. In addition, peripheral rim enhancement representing reactive hyperemia is high or isoattenuating during the portal venous and equilibrium phases. Such reactive hyperemia in tissue surrounding the ablated lesion may make accurate assessment of therapeutic response difficult [21].

Moreover, for RF ablation to be complete, the entire tumor as well as a peripheral safety margin of normal hepatic tissue must be ablated. In all ablated lesions, in our study, CT and MRI showed the ablated lesion to be larger than the preablation tumor, while nine residual HCCs had equal size preablation tumors. In only one case residual tumor was placed at the edge of a large treated area.

The results of our study demonstrate also that, compared with multiphasic 16-section multidetector CT, gadoxetate disodium-enhanced MR imaging yields significantly higher diagnostic accuracy and sensitivity for the detection of new HCC in treated patients. Our data corroborate the results of a recent study by Di Martino et al. [23], which showed a

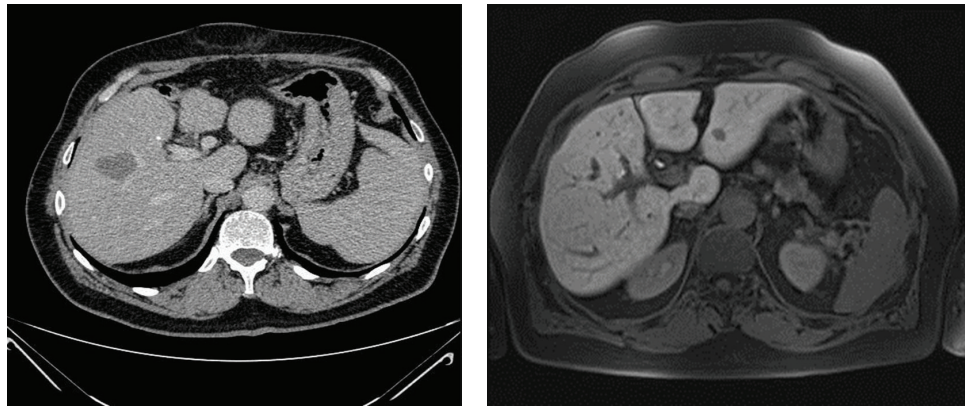

(a) (b)

Figure 5: 63-year-old man with an ablated HCC at segment 5–8. (a) Portal-phase CT scan at 1-month followup. The necrotic lesion is recognizable. (b) Hepatospecific phase MR image at 1-month followup. A new HCC is evident in the left lobe.

trend, although not statistically significant, toward improved diagnostic accuracy with gadoxetate disodium-enhanced MR imaging compared with multidetector CT for the detection of HCC particularly for smaller lesions, particularly those less than 2 cm. In particular, our data showed that 4 HCCs (mean size, 10 mm) were detected, correctly, only with gadoxetate disodium-enhanced MR imaging.

Our results are in opposition with findings of [24, 25]. In fact, Watanabe et al. [24] report in the conclusion that the incorporation of hepatocyte phase images did not improve the diagnostic accuracy of gadoxetate disodium-enhanced MRI for locally recurrent HCCs after RFA because the reactive therapeutic response induced pseudolesions with similar findings; the possible presence of these pseudolesions should be recognized by radiologists as a pitfall when interpreting gadoxetate disodium-enhanced MR images after RFA, especially by inexperienced radiologists. Motosugi et al. [25] mentioned that over 10% of vascular pseudolesions, such as arteriovenous shunts, show hypointensity in the hepatocyte phase and can be misinterpreted as HCC even with the combined interpretation of hepatobiliary and dynamic contrast enhanced MRI.

These findings can be explained because in this study the interpretation of radiological data (residual tumor or necrosis) is the result of a combined assessment of the different vascular phases with the addition of the hepatospecific phase; therefore, an arterio-venous shunt or a vascular pseudolesion presents a similar signal to vessels, easily recognizable by an expert radiologist. The arteriovenous shunt or a vascular pseudolesion show a different signal from the residual tumor and tissue necrosis: in our series the residual of HCC shows a washin and wash-out with constant hypointense signal in the hepatospecific phase; an area of necrosis shows constant hypointense signal in the different phases of the study including hepato-specific phase; arteriovenous shunt or a vascular pseudolesion shows isointense signal compared to the vessels.

Our study has a number of limitations. The reviewers had been involved in the original studies, and this may have determined a recall bias. However, given the long time interval between the exams and the revision sessions, we believe that this recall bias was minimized. No correlation was obtained with diffusion-weighted MR data. This was done to compare the dynamic phases of CT and MRI. Diffusion MRI offers relevant additional information, and now we have started correlating the diffusion imaging with the dynamic imaging of MRI.

In summary, the results of our study indicate that combined interpretation of dynamic and hepatobiliary phase MR images improves the diagnostic accuracy of gadoxetate disodium-enhanced MR imaging for the detection of residual HCC and new HCC in treated patients compared with either dynamic MR or CT alone.

References

[1] J. Bruix and M. Sherman, "Management of hepatocellular carcinoma," *Hepatology*, vol. 42, no. 5, pp. 1208–1236, 2005.

[2] T. Unek, S. Karademir, N. C. Arslan et al., "Comparison of Milan and UCSF criteria for liver transplantation to treat hepatocellular carcinoma," *World Journal of Gastroenterology*, vol. 17, no. 37, pp. 4206–4212, 2011.

[3] S. A. Curley and F. Izzo, "Radiofrequency ablation of primary and metastatic hepatic malignancies," *International Journal of Clinical Oncology*, vol. 7, no. 2, pp. 72–81, 2002.

[4] S. A. Curley and F. Izzo, "Radiofrequency ablation of hepatocellular carcinoma," *Minerva Chirurgica*, vol. 57, no. 2, pp. 165–176, 2002.

[5] S. A. Curley, F. Izzo, L. M. Ellis, J. N. Vauthey, and P. Vallone, "Radiofrequency ablation of hepatocellular cancer in 110 patients with cirrhosis," *Annals of Surgery*, vol. 232, no. 3, pp. 381–391, 2000.

[6] T. M. Pawlik, F. Izzo, D. S. Cohen, J. S. Morris, and S. A. Curley, "Combined resection and radiofrequency ablation for advanced hepatic malignancies: results in 172 patients," *Annals of Surgical Oncology*, vol. 10, no. 9, pp. 1059–1069, 2003.

[7] S. A. Curley, P. Marra, K. Beaty et al., "Early and late complications after radiofrequency ablation of malignant liver tumors

in 608 patients," *Annals of Surgery*, vol. 239, no. 4, pp. 450–458, 2004.

[8] A. Corner, C. Ayuso, M. Varala et al., "Evaluation of tumor response after locoregional therapies in hepatocellular carcinoma. are response evaluation criteria in solid tumors reliable?" *Cancer*, vol. 115, no. 3, pp. 616–623, 2009.

[9] P. Therasse, S. G. Arbuck, E. A. Eisenhauer et al., "New guidelines to evaluate the response to treatment in solid tumors," *Journal of the National Cancer Institute*, vol. 92, no. 3, pp. 205–216, 2000.

[10] S. K. Kim, H. K. Lim, Y. H. Kim et al., "Hepatocellular carcinoma treated with radio-frequency ablation: spectrum of imaging findings," *Radiographics*, vol. 23, no. 1, pp. 107–121, 2003.

[11] A. S. Kierans, M. Elazzazi, L. Braga et al., "Thermoablative treatments for malignant liver lesions: 10-Year experience of MRI appearances of treatment response," *American Journal of Roentgenology*, vol. 194, no. 2, pp. 523–529, 2010.

[12] H. K. Lim, D. Choi, W. J. L. Won Jae Lee et al., "Hepatocellular carcinoma treated with percutaneous radio-frequency ablation: evaluation with follow-up multiphase helical CT," *Radiology*, vol. 221, no. 2, pp. 447–454, 2001.

[13] T. J. Vogl, S. Kümmel, R. Hammerstingl et al., "Liver tumors: comparison of MR imaging with Gd-EOB-DTPA and Gd-DTPA," *Radiology*, vol. 200, no. 1, pp. 59–67, 1996.

[14] L. Bolondi, S. Gaiani, N. Celli et al., "Characterization of small nodules in cirrhosis by assessment of vascularity: the problem of hypovascular hepatocellular carcinoma," *Hepatology*, vol. 42, no. 1, pp. 27–34, 2005.

[15] A. Huppertz, S. Haralda, A. Kraus et al., "Enhancement of focal liver lesions at gadoxetic acid-enhanced MR imaging: correlation with histopathologic findings and spiral CT-initial observations," *Radiology*, vol. 234, no. 2, pp. 468–478, 2005.

[16] L. Joseph and C. Reinhold, "Statistical inference for proportions," *American Journal of Roentgenology*, vol. 184, no. 4, pp. 1057–1064, 2005.

[17] N. E. D. Hawass, "Comparing the sensitivities and specificities of two diagnostic procedures performed on the same group of patients," *British Journal of Radiology*, vol. 70, pp. 360–366, 1997.

[18] N. A. Obuchowski, "ROC analysis," *American Journal of Roentgenology*, vol. 184, pp. 364–372, 2005.

[19] F. S. Ferrari, A. Megliola, A. Scorzelli et al., "Treatment of small HCC through radiofrequency ablation and laser ablation. Comparison of techniques and long-term results," *Radiologia Medica*, vol. 112, no. 3, pp. 377–393, 2007.

[20] R. Stoffner, P. Schullian, G. Widmann, R. Bale, and C. Kremser, "Magnetic resonance imaging of radiofrequency current-induced coagulation zones in the EX vivo bovine liver," *RöFo*, vol. 182, no. 8, pp. 690–697, 2010.

[21] S. K. Kim, H. K. Lim, Y. H. Kim et al., "Hepatocellular carcinoma treated with radio-frequency ablation: spectrum of imaging findings," *Radiographics*, vol. 23, no. 1, pp. 107–121, 2003.

[22] U. Motosugi, T. Ichikawa, H. Sou et al., "Distinguishing hypervascular pseudolesions of the liver from hypervascular hepatocellular carcinomas with gadoxetic acid-enhanced MR imaging," *Radiology*, vol. 256, no. 1, pp. 151–158, 2010.

[23] M. Di Martino, D. Marin, A. Guerrisi et al., "Intraindividual comparison of gadoxetate disodium—enhanced MR imaging and 64-section multidetector CT in the detection of hepatocellular carcinoma in patients with cirrhosis," *Radiology*, vol. 256, no. 3, pp. 806–816, 2010.

[24] H. Watanabe, M. Kanematsu, S. Goshima et al., "Is gadoxetate disodium-enhanced MRI useful for detecting local recurrence of hepatocellular carcinoma after radiofrequency ablation therapy?" *American Journal of Roentgenology*, vol. 198, no. 3, pp. 589–595, 2012.

[25] U. Motosugi, T. Ichikawa, H. Sou et al., "Distinguishing hypervascular pseudolesions of the liver from hypervascular hepatocellular carcinomas with gadoxetic acid-enhanced MR imaging," *Radiology*, vol. 256, no. 1, pp. 151–158, 2010.

Hindawi Publishing Corporation
Gastroenterology Research and Practice
Volume 2013, Article ID 729279, 7 pages
http://dx.doi.org/10.1155/2013/729279

Research Article

Bile Duct Strictures Caused by Solid Masses: MR in Differential Diagnosis and as a Prognostic Tool to Plan the Endoscopic Treatment

Tomasz Gorycki and Michał Studniarek

Department of Radiology, Medical University of Gdańsk, 7 Dębinki Street, 80-950 Gdańsk, Poland

Correspondence should be addressed to Tomasz Gorycki; tgor@gumed.edu.pl

Received 24 August 2013; Accepted 24 September 2013

Academic Editor: Iwona Sudoł-Szopinska

Copyright © 2013 T. Gorycki and M. Studniarek. This is an open access article distributed under the Creative Commons Attribution License, which permits unrestricted use, distribution, and reproduction in any medium, provided the original work is properly cited.

The aim of the study was to assess how realiable is differential diagnosis and prognosis for endoscopic treatment with MR signal characteristics as the qualitative parameter and magnetic resonance cholangiopancreatography (MRCP) images in cases of bile duct obstructions caused by solid masses. *Material and Methods*. Retrospective study of MR and MRCP images in 80 patients (mean age 58 ys) was conducted. Mean signal intensity ratio (SIR) from planar MR images and MRCP linear measurements were compared between benign and malignant lesions and in groups including the size and number of stents placed during ERCP (< 10 F <) in 51 cases in which ERCP was performed. *Results*. Significantly higher SIR values were encountered in malignant lesions in T2W images ($r = 0,0003$) and STIR T2W images ($r = 0,0002$). Malignant lesions were characterised by longer strictures ($r = 0,0071$) and greater proximal biliary duct dilatation ($r = 0,0024$). High significance for predicting ERCP conditions was found with mean SIR in STIR T2W images and stricture length. *Conclusion*. Probability of malignancy of solid lesions obstructing biliary duct increased with higher SIR in T2W images and with longer strictures. Passing the stricture during ERCP treatment was easier and more probable in cases of shorter strictures caused by lesions with higher SIR in STIR T2W images.

1. Introduction

There is an increase of number of patients undergoing magnetic resonance (MR) prior to endoscopic retrograde cholangiopancreatography (ERCP) [1, 2]. MR with magnetic resonance cholangiopancreatography (MRCP) offers wide range of qualitative and quantitative parameters characterising solid lesions resulting in biliary strictures allowing for better planning of intervention methods to reduce number of complications [1, 2].

Magnetic resonance imaging (MRI) plays an important role in evaluation of hepatobiliary system in all hepatic, suprapancreatic, and pancreatic segments. In many comparative imaging studies MRI shows similar or even higher diagnostic accuracy in focal hepatic lesions detection than multidetector computed tomography (MDCT, CT) [3–5]. When surroundings of the biliary tree in hepatic segment are concerned, MRI appears to have higher ability of precise characterization of observed hepatic lesions [3–5]. Also in the imaging of the pancreatic region of biliary duct MRI is significantly superior to CT in both detecting and excluding malignant conditions [4]. Conventional T1-weighted and T2-weighted images allow the evaluation of extraductal soft tissues with increasing diagnostic accuracy by demonstrating the extension of masses surrounding biliary duct [6–8].

Usually the value of differential diagnosis based on T1- and T2-weighted images and Gd-DTPA enhanced T1-weighted images, and MR cholangiographic images were determined for each of these techniques alone. Until now many authors have analysed the technique of examination, diagnostic features of benign versus malignant lesions in parenchymal regions around biliary ducts, focusing on qualitative analysis of signal intensity [4–8]. Others used semiquantitative scales in order to establish certain features of MR sequences including liver signal-to-noise ratio, contrast-to-noise ratio or lesionliver contrast-to-noise ratio

[9]. Kim et al. have undertaken a trial to determine the value of conventional T1- and T2-weighted images and Gd-DTPA enhanced MR images as a supplement to MR cholangiographic images in differentiation of benign from malignant lesions that cause biliary dilatation asking the observers to review the images using a point scale and assign a confidence level to their evaluation of the cause of biliary abnormality [6]. Although MRCP provides the same imaging information as direct cholangiography, used alone it has limited specificity for the diagnosis of malignant strictures [10]. In everyday practice a combination of MRCP and cross-sectional MRI should be performed in assessment of pancreatobiliary disorders [1, 6, 7, 10–12].

The purpose of this study was to assess how realiable is the differential diagnosis and prognosis for endoscopic treatment on the basis of signal characteristics from plane MR images and MRCP images in cases of bile duct obstructions caused by solid masses.

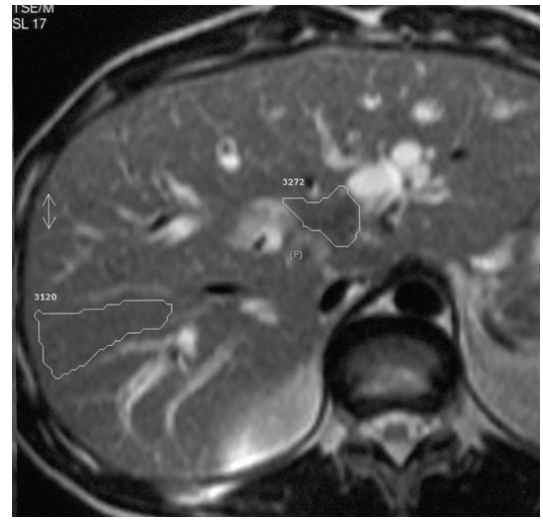

Figure 1: Axial plane scan for ROIs drawings. A case of hilar cholangio cell carcinoma.

2. Materials and Methods

T1W (SE 500/10), T2W (UTSE/RC 2500/100), STIR T2W (TSE 2500/100), and T1W (SE 500/10) contrast-enhanced (Gd-DTPA) nonbreathhold, respiratory gated MR images including the entire hepato-pancreatic region as well as cholangiopancreatographic MR images (3DTSE 1800/700) were acquired in axial and coronal planes in 80 patients (mean age 58,3) directed to MR examination after ultrasonography disclosing cholestasis. In 51 patients endoscopic retrograde cholangiopancreatography (ERCP) was performed with Pentax ED-3440T, and stents to provide the optimal conditions of biliary drainage have been placed. The aid was to insert two or one at least of 10 F size. However, in 14 cases of tight biliary strictures only single 7 F stents were successfully inserted. All ERCP procedures were performed by experienced interventional gastroenterologists.

In 53 cases malignant lesions have been confirmed in surgery and biopsy to be a reason of biliary obstruction. There were as follows: 25 cases of pancreatic cancer, 11 cases of hepatic metastases, 9 cases of cholangiocarcinoma, 3 cases of metastatic nodules in the hilar region, 3 cases of carcinoma of the gall bladder, and 2 cases of hepatocellular carcinoma. Among 27 cases of benign conditions of inflammatory origin, 21 patients underwent follow-up MRI examinations for a 2 year period, and therapeutic procedures both endoscopic or during open surgery were performed in cases of biliary ducts dilatation or when anastomosis was required.

In 6 patients the benign origin has been proved in 2-year period of clinical observation.

Mean signal intensity ratio (SIR) of benign versus malignant lesions when countable area of mass was detected around bile duct strictures as well as the linear measurements covering stricture morphology from MRCP images has been compared. Also a correlation with size of stents inserted during endoscopy was analysed.

Images subjected to analysis represented strictly the same plane with well-defined lesion and corresponded to the level of biliary obstruction observed on MRCP images.

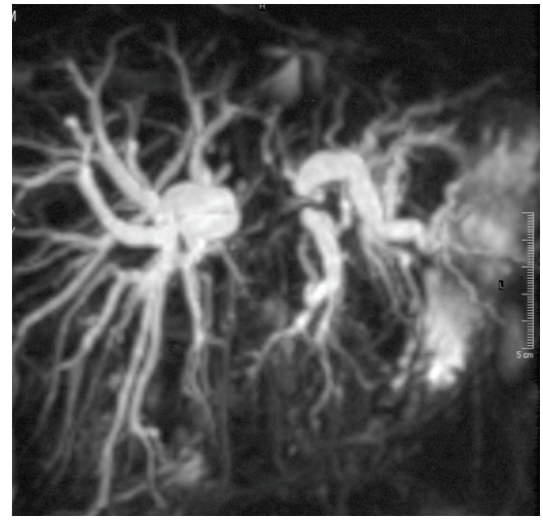

Figure 2: Corresponding MRCP image describing stricture morphology.

Quantitative analysis was performed with both operator-defined region of interest (ROI) measurements of mean signal intensity of lesion and its background and linear measurements from MRCP images concerning morphology of the biliary stricture a.i. stricture length, stricture width, proximal ductal dilatation, and distance from stricture to hepatic ducts junction. For the liver and pancreatic lesions ROIs for measuring SI of background were put in areas devoid cystic structures, large vessels, and inhomogeneities in organs of their origin accordingly (Figures 1 and 2). For lesions causing strictures of hilar and suprapancreatic segments of biliary ducts ROIs for background SI were taken like for hepatic lesions. Signal intensity ratio (SIR) calculated from these measurements as well as MRCP linear measurements were compared in two groups including benign and malignant

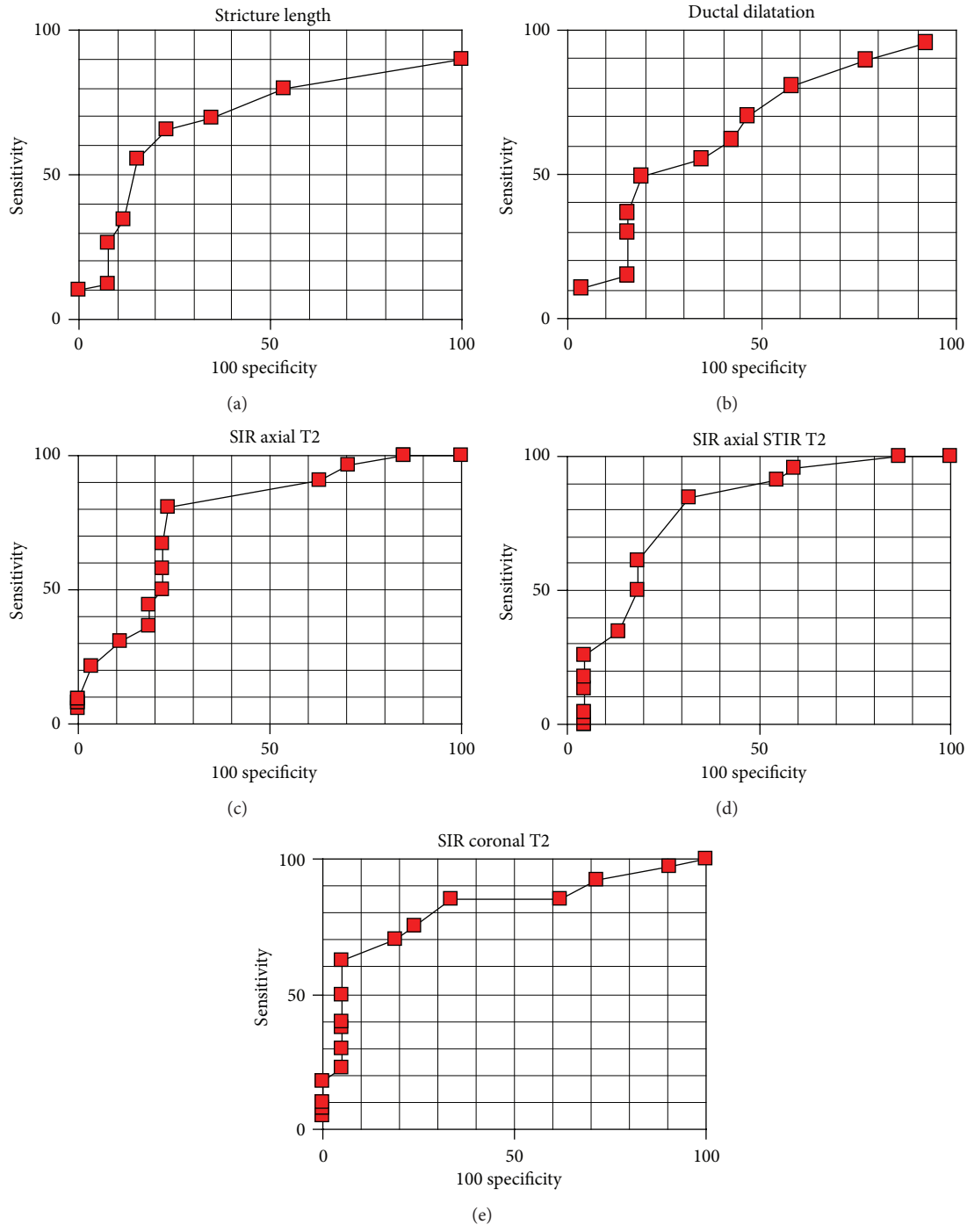

Figure 3: ROC curves for differential diagnosis between benign and malignant lesions with MRCP stricture morphology and SIR.

lesions as well as in two groups with the inclusion of the size of stents (one stent size less than 10 F versus 10 F or more than one stent placed) in 51 cases in which stents have been inserted. Statistical analysis of the obtained data was performed with the use of Kruskal Wallis test. The usefulness of the tests for purposes of differential diagnosis, accuracy, and predictive values was established based on analysis of receiver operating curves (ROC) counted for every feature.

3. Results

Significantly higher mean SIR was encountered in malignant lesions in T2W ($r = 0,0003$) and STIR T2W images ($r = 0,0002$). Malignant lesions were also characterised by longer strictures ($r = 0,0071$) and larger diameter of biliary ducts proximatly to obstruction ($r = 0,0024$), whereas SIR counted from T1W images with and without contrast enhancement

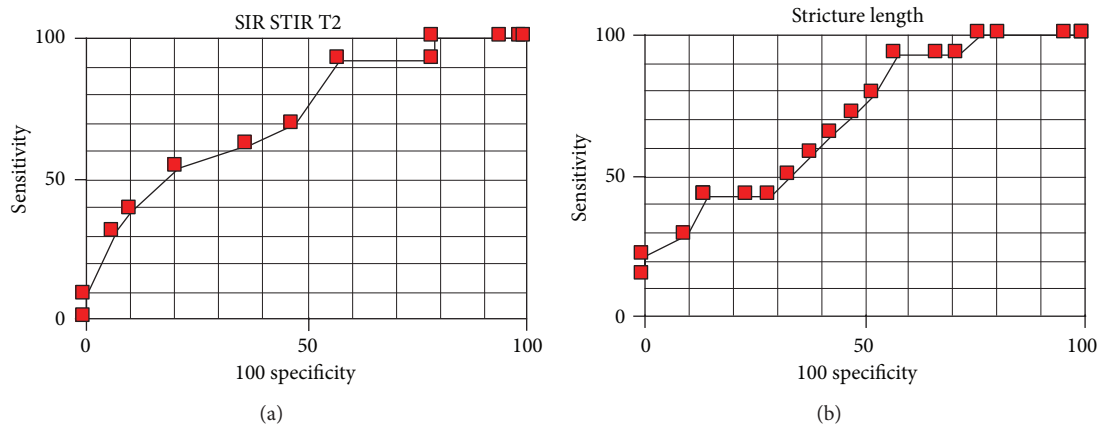

Figure 4: ROC curves for prognosis of endoscopic treatment based on SIR from STIR T2W images and stricture length.

Table 1: PPV and NPV in detecting the malignancy with SIR calculated for cut-off levels.

Image	ROC level	Accuracy %	PPV %	NPV %
Axial T2W	1,1006	79,7	87,5	67,7
Axial STIR T2W	1,1010	79,4	84,8	65,2
Coronal T2W	1,1173	75,4	85,7	61,5

($P = 0,4395$, $P = 0,6163$) and stricture thickness ($P = 0,4266$) did not differ significantly between benign and malignant lesions.

When the size and number of stents were taken into account significantly distinguishing features were—mean SIR in STIR T2W ($P = 0,0224$) images and stricture length in MRCP images ($P = 0,0312$). Therefore it was easier to pass a stricture during ERCP when the lesion leading to the stricture showed higher SIR in STIR T2W images and in cases of shorter strictures. SIR counted from T1W images ($P = 0,7121$), T1W images with contrast enhancement ($P = 0,4502$), and T2W images without fat saturation ($P = 0,7121$) did not differ significantly between groups of lesions around strictures treated with ERCP procedure. These relations were also described by ROC curves—Figures 3 and 4. Account of results obtained including predictive values is presented in Tables 1, 2, and 3.

4. Discussion

For the lesions associated with obturation of the bile duct reference standards used to prove the etiology and for comparison were surgery, a biopsy confirming malignancy, or the clinical course during followup (at least 12 months) in cases without histopathologic proof of malignancy [13–15]. In this study in 53 cases malignant lesions have been confirmed in surgery and biopsy to be a reason of biliary obstruction. Among 24 cases of benign conditions, mostly of inflammatory origin, 21 patients underwent follow-up MRI examinations for a 2-year period, and therapeutic procedures both endoscopic or during open surgery were performed in cases of biliary ducts dilatation or when anastomosis was required. In 6 patients the course of the disease proved the benign origin in 2-year period of clinical observation.

The sensitivity, specificity, and accuracy of MRCP for detecting and locating bile duct strictures were 85–100%, 71–100%, and 70–100% among the studies [12–18]. However, MRCP alone had a limited ability to reveal concurrent intraductal cholangiocarcinoma associated with hepatolithiasis. Also nondilated poorly visualised bile ducts distally from strictures can lead to misdiagnosis [13, 16–18]. In 3D MRCP the use of water as a natural contrast in duodenum and evaluation of both (maximum intensity projection) MIP and source cholangiopancreatographic images are the simplest methods to decrease the number of misdiagnoses in these cases [16, 18]. The influence of bile duct dilatation and presence of gas and fluid in the duodenum on sensitivity in the diagnosis of localization and cause of biliary duct pathologies are also common in ultrasonography performed in most cases prior to magnetic resonance [19, 20].

Analysis of imaging variables at MR images with characteristics at MRCP images together was found to be the best predictor of malignancy of the bile duct stricture [6, 7, 18]. MR with MRCP proved the same diagnostic value as ERCP for visualizing the bile ducts, replacing ERCP as the primary investigation in patients with multiple risk factors; this would reduce the numbers of patients exposed to the risks of ERCP [14, 15, 21].

In this study SIR was counted on the basic MR images (T1W, T2W, STIR T2W) which proved similar diagnostic value between different MR systems whereas modified T2W images could represent different diagnostic value strongly dependent on the MR system and kind of sequence used in the study [6–8].

Among different factors used to describe signal characteristics of lesions in liver and pancreas the most accurate for the purposes of differential diagnostics is signal intensity ratio based on mean signal intensity (SIR) measurements

Table 2: PPV and NPV in detecting the malignancy with MRCP morphology calculated for cut-off levels.

	ROC level	Accuracy %	PPV %	NPV %
Stricture length (mm)	21,3	69,3	84,2	54,1
Ductal dilatation (mm)	12,3	58,9	74,3	60,7

Table 3: PPV and NPV when stricture length and SIR STIR T2 were used to forecast the conditions for biliary stenting.

	ROC level	Accuracy %	PPV %	NPV %
Stricture length (mm)	22,1	60	50	70,6
SIR STIR T2	1,244	68,8	63,6	71,4

performed in operator's dependent regions of interest [6, 8, 9]. Minimum pixels number covered with ROI enough to avoid stronger influence of the partial volume effect differs between studies from 25 to 100 [2, 11]. In this study mean SI of the smallest lesion was counted from ROI consisting of 92 pixels (197 mm^2). In the study no significant differences in SIR values between malignant and benign lesions counted from T1-weighted and Gd-enhanced T1-weighted images were found. The use of fast spin echo sequences allowed the increase of TR which has strong influence on T2W contrast and with only slight prolongation of time of acquisition. These sequences allow better tissue separation within T2 contrast area [6, 7, 9]. In fast spin echo sequences transfer of magnetization has strong influence on solid tissue areas and minimal influence on fluid-reach areas like poorly drained or edematous areas and with blood plasma leakage from vessels gathered around lesion causing them to present as areas of relatively high signal intensity [22–24]. This phenomenon is also easily observed, for example, in renal parenchyma built with tubular fluid-filled structures. In this way, it is possible mechanism for relative signal intensity increase measured with SIR in areas of malignant infiltration near tubular structures like biliary or pancreatic ducts. It was observed in all T2-weighted images as a difference between groups of malignant versus benign conditions in this study (P: 0,0002-0,0003). Also the relative signal intensity of malignant metastatic lesions in the area of hepatoduodenal ligament was higher than that of surrounding tissues in T2-weighted images because of the long T2 especially in sequences with fat saturation [22]. Assessment of ROC curves concerning T2-weighted sequences (with or without fat saturation and in both planes) shows that the cut-off levels are very similar (1,1006–1,1173) with similar accuracy counted for their values (75,4–79,7%). Therefore, no significant differences in information supplied by presented T2-weighted images have been stated.

Also submitted to analysis were MRCP MIP and source images. Besides the fact that MRCP requires neither contrast medium administration nor biliary and pancreatic intervention, this technique presents further important advantages. The biliary tree is shown without dilatation effect due to pressure and choleretic effect of contrast medium used for ERCP or percutaneous cholangiography, and it is also possible to obtain images of the whole biliary tree even in cases of critically tight strictures or complete obstruction that would prevent passing them with leaders during endoscopy or percutaneous cholangiography as carrying a high risk of perforation [2, 14, 15, 17, 22]. MRCP not being the therapeutic procedure itself allows to plan the optimal way of drainage. The message of these relativities follows the general tendency to decrease the number of diagnostic ERCP and to perform ERCP as therapeutic procedure only [2, 14, 15, 17, 22].

It is worth mentioning that presumably there are two factors changing the accuracy rate of MRCP images in determining the nature of biliary obstruction: the biliary duct dilatation and the use of cross-sectional scans for analysis [16–18, 23], what corresponds to the results obtained by Pamos et al. [24]. In his study higher sensitivity and specificity in the diagnosis of malignancy were obtained with MRCP in cases of dilated biliary ducts. As shown in this study SIR counted from T2W images could increase to some extent the accuracy of diagnosis of malignant lesion causing the biliary obstruction, acting as additional factor to be assessed together with MRCP images.

STIR T2-weighted images had the highest predictive value when assessing the conditions for endoscopic treatment, when the size and number of stents were taken into account. Masses causing biliary strictures characterised by higher SI in STIR T2-weighted images proved to be easier to pass with stents during endoscopic procedures. Tight strictures associated with the presence of dense fibrous tissues show as low intensity areas in T2-weighted images especially when fat saturation sequence was applied. From morphologic measurements analysed in MRCP images only the stricture length was associated with the size of stents with which the stricture was passed. As one could expect longer strictures caused more difficulties during endoscopy. However the stronger feature as shown on ROC curves for the purposes of the evaluation of stenting conditions seems to be SIR measured in STIR T2-weighted images as shown in Table 3.

Three limitations of this study must be considered. First, no diffusion weighted images (DWI) were performed in the group taken to analysis, so in order to establish the relationship between signal profile in DWI and conditions during ERCP the study should be continued. Second, there were analysed less cases of benign lesions (27/80) versus malignant (53/80). Presumably, it was caused by the fact that some of the cases were diagnosed with CT following ultrasound without MRI. The third limitation of the work was that no 2D MRCP images were used for analysis; however, they are used in every day practice to the same extent of those of 3D MRCP, but in many cases better understanding of the

complex biliary strictures is possible due to analysis of both source images and the reconstructions, and this is possible only with 3D MRCP technique.

5. Conclusions

Probability of malignancy of solid lesions obstructing biliary duct increased with higher SIR in T2W images and with longer strictures observed in MRCP images. Introducing a larger size stents was more probable in cases of lesions showing higher SIR in STIR T2W images and in case of shorter strictures. These features could be additional parameters taken into consideration when conditions for endoscopic treatment are being discussed in order to reduce complications during ERCP.

Conflict of Interests

The authors declare that there is no conflict of interests regarding the publication of this paper.

Acknowledgment

Special thanks are due to Professor Marian Smoczyński from the Department of Gastroenterology and Hepatology, Medical University of Gdańsk.

References

[1] K. Hekimoglu, Y. Ustundag, A. Dusak et al., "MRCP vs ERCP in the evaluation of biliary pathologies: review of current literature," *Journal of Digestive Diseases*, vol. 9, no. 3, pp. 162–169, 2008.

[2] R. Trap, S. Adamsen, O. Hart-Hansen, and M. Henriksen, "Severe and fatal complications after diagnostic and therapeutic ERCP: a prospective series of claims to insurance covering public hospitals," *Endoscopy*, vol. 31, no. 2, pp. 125–130, 1999.

[3] S. W. Anderson, E. Rho, and J. A. Soto, "Detection of biliary duct narrowing and choledocholithiasis: accuracy of portal venous phase multidetector CT," *Radiology*, vol. 247, no. 2, pp. 418–427, 2008.

[4] H. Saisho and T. Yamaguchi, "Diagnostic imaging for pancreatic cancer: computed tomography, magnetic resonance imaging, and positron emission tomography," *Pancreas*, vol. 28, no. 3, pp. 273–278, 2004.

[5] C. D. Becker, "Multidetector CT and MRI of biliary diseases," *Journal de Radiologie*, vol. 84, no. 4, pp. 473–479, 2003.

[6] M.-J. Kim, D. C. Mitchell, K. Ito, and E. K. Outwater, "Biliary dilatation: differentiation of benign from malignant causes—value of adding conventional MR imaging to MR cholangiopancreatography," *Radiology*, vol. 214, no. 1, pp. 173–181, 2000.

[7] L. Zhong, L. Li, and Q. Y. Yao, "Preoperative evaluation of pancreaticobiliary tumor using MR multi-imaging techniques," *World Journal of Gastroenterology*, vol. 11, no. 24, pp. 3756–3761, 2005.

[8] C. C. Denoiseux, I. Boulay-Coletta, J. P. Nakache, I. D. Claude, and M. Zins, "Liver T2-weighted MR imaging: assessment of a three-dimensional fast spin-echo with extended echo train acquisition sequence at 1.5 Tesla," *Journal of Magnetic Resonance Imaging*, vol. 38, no. 2, pp. 336–343, 2013.

[9] J. Gaa, H. Fischer, G. Laub, and M. Georgi, "Breath-hold MR imaging of focal liver lesions: comparison of fast and ultrafast techniques," *European Radiology*, vol. 6, no. 6, pp. 838–843, 1996.

[10] T. Rösch, A. Meining, S. Frühmorgen et al., "A prospective comparison of the diagnostic accuracy of ERCP, MRCP, CT, and EUS in biliary strictures," *Gastrointestinal Endoscopy*, vol. 55, no. 7, pp. 870–876, 2002.

[11] I. Rogoveanu, D. I. Gheonea, A. Saftoiu, and T. Ciurea, "The role of imaging methods in identifying the causes of extrahepatic cholestasis," *Journal of Gastrointestinal and Liver Diseases*, vol. 15, no. 3, pp. 265–271, 2006.

[12] A. C. F. Taylor, A. F. Little, O. F. Hennessy, S. W. Banting, P. J. Smith, and P. V. Desmond, "Prospective assessment of magnetic resonance cholangiopancreatography for noninvasive imaging of the biliary tree," *Gastrointestinal Endoscopy*, vol. 55, no. 1, pp. 17–22, 2002.

[13] G. Masselli, R. Manfredi, A. Vecchioli, and G. Gualdi, "MR imaging and MR cholangiopancreatography in the preoperative evaluation of hilar cholangiocarcinoma: correlation with surgical and pathologic findings," *European Radiology*, vol. 18, no. 10, pp. 2213–2221, 2008.

[14] P. A. Testoni, A. Mariani, A. Giussani et al., "Risk factors for post-ERCP pancreatitis in high-and low-volume centers and among expert and non-expert operators: a prospective multicenter study," *American Journal of Gastroenterology*, vol. 105, no. 8, pp. 1753–1761, 2010.

[15] P. A. Testoni, "Preventing post-ERCP pancreatitis: where are we?" *Journal of the Pancreas*, vol. 4, no. 1, pp. 22–32, 2003.

[16] F. Maccioni, M. Martinelli, N. Al Ansari et al., "Magnetic resonance cholangiography: past, present and future: a review," *European Review for Medical and Pharmacological Sciences*, vol. 14, no. 8, pp. 721–725, 2010.

[17] K. Hekimoglu, Y. Ustundag, A. Dusak et al., "MRCP vs ERCP in the evaluation of biliary pathologies: review of current literature," *Journal of Digestive Diseases*, vol. 9, no. 3, pp. 162–169, 2008.

[18] T. Hyodo, S. Kumano, F. Kushihata et al., "CT and MR cholangiography: advantages and pitfalls in perioperative evaluation of biliary tree," *British Journal of Radiology*, vol. 85, pp. 887–896, 2012.

[19] M. K. Walas, K. Skoczylas, and I. Ireneusz Gierbliński, "Errors and mistakes in the ultrasound diagnostics of the liver, gallbladder and bile ducts," *Journal of Ultrasonography*, vol. 12, pp. 446–462, 2012.

[20] M. K. Walas, K. Skoczylas, and I. Ireneusz Gierbliński, "Standards of the Polish Ultrasound Society—update. The liver, gallbladder and bile ducts examinations," *Journal of Ultrasonography*, vol. 12, no. 51, pp. 428–445, 2012.

[21] J. Vandervoort, R. M. Soetikno, T. C. K. Tham et al., "Risk factors for complications after performance of ERCP," *Gastrointestinal Endoscopy*, vol. 56, no. 5, pp. 652–656, 2002.

[22] P. J. Mergo, P. R. Ros, P. C. Buetow, and J. L. Buck, "Diffuse disease of the liver: radiologic-pathologic correlation," *Radiographics*, vol. 14, no. 6, pp. 1291–1307, 1994.

[23] L. Kaufman, D. M. Kramer, L. E. Crooks, and D. A. Ortendahl, "Measuring signal-to-noise ratios in MR imaging," *Radiology*, vol. 173, no. 1, pp. 265–267, 1989.

[24] S. Pamos, A. Benages, E. Medina, and V. Martinez Sanjuan, "Prospective evaluation of magnetic resonance cholangiopancreatography in patients with biliary disease: comparative study with conventional ultrasonography and endoscopic retrograde cholangiopancreatography: diagnostic algorithm," *Digestive and Liver Disease*, vol. 35, no. 3, pp. 186–192, 2003.

Hindawi Publishing Corporation
Gastroenterology Research and Practice
Volume 2013, Article ID 248625, 3 pages
http://dx.doi.org/10.1155/2013/248625

Research Article

Importance of the Ultrasonography in Diagnosis of Ileal Duplication Cyst

Arzu Gebesce,[1] Mevlit Korkmaz,[2] Esengul Keles,[1] Feride Korkmaz,[3] Kamran Mahmutyazıcıoglu,[4] and Hamza Yazgan[1]

[1] *Department of Pediatrics, Fatih University, Istanbul, Turkey*
[2] *Department of Pediatrics Surgery, Fatih University, Istanbul, Turkey*
[3] *Department of Anesthesiology, Fatih University, Istanbul, Turkey*
[4] *Department of Radiology, Fatih University, Istanbul, Turkey*

Correspondence should be addressed to Arzu Gebesce; agebesce@fatih.edu.tr

Received 12 July 2013; Revised 1 October 2013; Accepted 2 October 2013

Academic Editor: Horia Stefãnescu

Copyright © 2013 Arzu Gebesce et al. This is an open access article distributed under the Creative Commons Attribution License, which permits unrestricted use, distribution, and reproduction in any medium, provided the original work is properly cited.

Gastrointestinal duplication cysts are rare congenital anomalies that can be seen in anywhere of the gastrointestinal system from the mouth to the anus. These are prenatally diagnosed through antenatal ultrasonography. However, attention must be paid since these formations might be confused with ovarian or mesenteric cysts. Our patient, who had been diagnosed with ovarian cyst on the ultrasonography performed in another center and with mesenteric cyst based on the abdominal MRI carried out at fifth month of life, presented to our clinic with the only complaint of constipation at 9th month of life. The diagnosis was set through double wall appearance of duplication cyst on the abdominal ultrasonography. The patient's cyst was resected.

1. Introduction

Gastrointestinal duplication cysts are rare congenital anomalies that can be seen in anywhere of the gastrointestinal system with a prevalence between 1 : 4500 and 1 : 10000. The most common location is ileum. Signs and symptoms differ based on the location, although mostly it manifests as acute abdominal or intestinal obstruction before 2 years of life. More rarely serious complications such as gastrointestinal bleeding or malignant degeneration may also occur. Colonic duplication cysts are further rare. Gastrointestinal duplication cysts are usually seen as two different forms as lumen-communicating and noncommunicating types. The most common form is cystic and noncommunicating type [1–3]. The treatment is surgery and total excision is the method of choice. In this report, our patient, who had been diagnosed with ovarian cyst on the ultrasonography (USG) performed in another center and with mesenteric cyst based on the abdominal MRI carried out at fifth month of life, presented to our clinic with the only complaint of constipation at 9th month of life. The diagnosis was set in our clinic through double wall appearance on the abdominal ultrasonography. The patient's cyst was resected.

2. Case Report

On the second-level USG ordered at 23rd gestational week of a healthy mother aged 32, a hypoechoic formation with 5 mm and 9 mm in size which was observed at the right side of the bladder in the pelvis was considered and followed up as ovarian cystic formation.

The patient was born by normal vaginal route at term, weight of 3000 gr. The patient's Apgar score was found 8 in minute 1 and 9 in minute 5. No pathologic finding was found at the physical examination of the patient. On the contrast enhanced abdominal MRI performed in a different center when the patient was five months old showed simple cyst. It also revealed two lobule-contoured, thick-walled cystic lesion with diameters of 19 mm, 12 mm, and 5 mm in the right lateral part of the abdomen. The mass was diagnosed as mesenteric cyst, and the patient was followed up for this diagnosis.

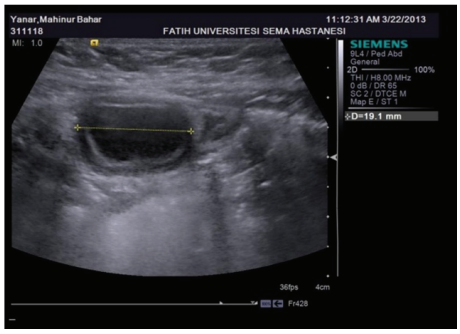

Figure 1: On sonography, we found that the hypoechoic outer wall of the cystic structure was continuous with the hypoechoic outer wall of the adjacent ileal bowel, and the hypoechoic outer wall of the cystic structure was continuous with the hypoechoic outer wall of the adjacent ileal bowel.

Figure 2: On exploration, a duplication cyst of 19 mm, 12 mm, and 5 mm in size was found at the ileal level at an approximate distance of 45 cm from the ileocecal valve.

Our patient presented to our clinic at her 9th month of life with only complaint of constipation. On physical examination, biochemical and hematological values were found normal in the patient who had a growth and development of 50 percentile. On her USG performed in our clinic, 19 mm, 12 mm, and 5 mm in size the duplication cyst having double wall appearance was observed in the right lower quadrant. On sonography, we found that the hypoechoic outer wall of the cystic structure was continuous with the hypoechoic outer wall of the adjacent ileal bowel, and the hypoechoic outer wall of the cystic structure was continuous with the hypoechoic outer wall of the adjacent ileal bowel (Figure 1).

An exploratory laparotomy was performed. On the exploration, a duplication cyst of 19 mm, 12 mm, and 5 mm in size was found at the ileal level at an approximate distance of 45 cm from the ileocecal valve (Figure 2). About 7 cm ileal segment involving the cyst was resected through distal and proximal bowel clamps. No complication was observed in postnatal followups of the patient. Histopathological examination of the piece was consisted with intestinal duplication cyst.

3. Discussion

Alimentary tract duplications are uncommon congenital anomalies that occur mostly in paediatric patients. The first reported case was made by Calder in 1733 [4]. Duplications arise from disturbances in the embryonic development of the gastrointestinal tract. Several major theories have been proposed for the formation of duplications at various sites, including the aberrant luminal recanalisation theory and the diverticular theory [5]. Others include the split notochord theory which explains the formation of neurenteric duplications and associated vertebral anomalies. Recently, Bishop and Koop suggested that environmental factors such as trauma or hypoxia in early foetal development were likely to be responsible when multiple duplications are found in association with anomalies such as malrotation or atresia [6].

Primary cystic lesions seen in the fetal and neonatal periods include renal, choledochal ovarian, mesenteric, duplication cysts, or Meckel's diverticulum. Double wall appearance of duplication is monitored on USG as a hyperechoic edge surrounding the mucosal wall inside and a hypoechoic wall surrounding the smooth muscular layer outside. However, the double wall sign can also be a characteristic of Meckel's diverticulum or sonographic artifacts. Furthermore, Meckel's diverticulum can have a spherically shaped cystlike appearance, which is similar to an enteric duplication cyst, on sonography [7–9]. Although Meckel's diverticulum is located on the antimesenteric border and communicates with the adjacent bowel lumen, in contrast to the duplication cyst, these differentiating features are often not visible on USG or CT [10, 11].

Presentation of intestinal duplications is variable depending on size, shape, and type of mucosa. They may be asymptomatic and discovered accidentally at surgery. They may be minimally symptomatic and associated with vague abdominal pain, constipation, or failure to thrive [12]. Our patient presented to our clinic at her 9th month of life with only complaint of constipation.

The enteric duplication cyst can be associated with malrotation. In half of the cases, there are associated malformations, the most frequent of these being esophageal duplications, followed by vertebral abnormalities [13]. No malrotation and malformations as esophageal duplications and vertebral abnormalities were seen in our case.

Our patient, who had been diagnosed with ovarian cyst on the ultrasonography (USG) performed in another center and with mesenteric cyst based on the abdominal MRI carried out at fifth month of life, presented to our clinic with the only complaint of constipation at 9th month of life. On USG duplication cyst was diagnosed through the double wall appearance which is specific for duplication cyst. The treatment option proposed for duplication cysts is surgery and the surgery of choice is excision because of the potential complications [14]. In our patient also we performed surgical excision under general anesthesia.

4. Conclusion

In conclusion, ultrasonography is an inexpensive and practicable imaging modality in evaluation of intra-abdominal cystic lesions. Although it seems asymptomatic and rare, this type of cyst must be surgically excised because of the potential complications and malignant degeneration.

Conflict of Interests

The authors declare that they have no conflict of interests.

References

[1] J. Schalamon, J. Schleef, and M. E. Höllwarth, "Experience with gastro-intestinal duplications in childhood," *Langenbeck's Archives of Surgery*, vol. 385, no. 6, pp. 402–405, 2000.

[2] P. S. Puligandla, L. T. Nguyen, D. St-Vil et al., "Gastrointestinal duplications," *Journal of Pediatric Surgery*, vol. 38, no. 5, pp. 740–744, 2003.

[3] A. Geller, K. K. Wang, and E. P. DiMagno, "Diagnosis of foregut duplication cysts by endoscopic ultrasonography," *Gastroenterology*, vol. 109, no. 3, pp. 838–842, 1995.

[4] S. J. Keckler and G. W. Holcomb, "Alimentary tract duplications," in *Ashcrafts's Paediatric Surgery*, G. W. Holcomb and J. P. Murphy, Eds., pp. 517–525, Sanders Elsevier, Philadelphia, Pa, USA, 5 edition, 2010.

[5] G. W. Holcomb III, A. Gheissari, J. A. O'Neill Jr., N. A. Shorter, and H. C. Bishop, "Surgical management of alimentary tract duplications," *Annals of Surgery*, vol. 209, no. 2, pp. 167–174, 1989.

[6] H. C. Bishop and C. E. Koop, "Surgical management of duplications of the alimentary tract," *The American Journal of Surgery*, vol. 107, no. 3, pp. 434–442, 1964.

[7] S. R. Shankar, S. V. Parelkar, S. A. Das, and A. B. Mathure, "An antenatally-diagnosed solitary, non-parasitic hepatic cyst with duodenal obstruction," *Pediatric Surgery International*, vol. 16, no. 3, pp. 214–215, 2000.

[8] B. Matteo, R. M. Deise, and D. D. Marcelo, "Sonographic findings of Meckel's diverticulitis in children," *The American Journal of Roentgenology*, vol. 180, no. 2, pp. 425–428, 2003.

[9] M. M. Ferro, R. Milner, L. Voto et al., "Intrathoracic alimentary tract duplication cysts treated in utero by thoracoamniotic shunting," *Fetal Diagnosis and Therapy*, vol. 13, no. 6, pp. 343–347, 1998.

[10] A. M. Fink, E. Alexopoulou, and H. Carty, "Bleeding Meckel's diverticulum in infancy: Unusual scintigraphic and ultrasound appearances," *Pediatric Radiology*, vol. 25, no. 2, pp. 155–156, 1995.

[11] G. Cheng, D. Soboleski, A. Daneman, D. Poenaru, and D. Hurlbut, "Sonographic pitfalls in the diagnosis of enteric duplication cysts," *The American Journal of Roentgenology*, vol. 184, no. 2, pp. 521–525, 2005.

[12] D. L. Angela and M. H. Christine, "From the archives of the AFIP. Meckel diverticulum: radiologic features with pathologic correlation," *Radiographics*, vol. 24, no. 2, pp. 565–587, 2004.

[13] P. Srivastava, A. N. Gangopadhyay, V. kumar et al., "Non-communicating isolated enteric duplication cyst in childhood," *Journal of Pediatric Surgery*, vol. 44, no. 7, pp. e9–e10, 2009.

[14] E. L. Wrenn Jr., "Alimentary tract duplications," in *Pediatric Surgery*, K. W. Ashcraft, Ed., pp. 527–539, Elsevier Saunders, New York, NY, USA, 2th edition, 2000.